Dissecting the molecular function and regulation of the meiotic α-kleisins REC8 and RAD21.2 in *Arabidopsis thaliana*

Dissertation with the aim of achieving a doctoral degree at the Faculty of Mathematics, Informatics and Natural Sciences
Department of Biology
of Universität Hamburg

Submitted by
Viola Kuttig

2021 in Hamburg, Germany

Supervisior: Prof. Dr. Arp Schnittger

1st Examiner: Prof. Dr. Arp Schnittger

2nd Examiner: Prof. Dr. Stefan Hoth

Datum der Disputation: 31.08.2021

INDEX

List of Figures

List of Tables

List of Abbreviation

A	ampere
aa	amino acids
AB	Antibody
ACT	ACTIN
AE	Axial element
AFD1	KLEISIN of maize
AM1	AMEIOTIC 1
AP1	APETALA 1
APC/C	ANAPHASE PROMOTIN COMPLEX
ASK1	ARABIDOPSIS SERINE/THREONINE KINASE 1
ASY1, 3, 4	ASYNAPTIC 1, 3, 4
bp	base pair
CAF-1	CHROMATIN ASSEMBLY FACTOR
CAL	CAULIFLOWER
CaMV	Cauliflower Mosaic Virus
CDC5, 7	CELL DIVISION CYCLE 5, 7
CDKA;1	CYCLIN DEPENDENT KINASE A;1
cDNA	complementary DNA
CENH3	CENTROMERE HISTON
ChIP	Chromatin Immunoprecipitation
CK1	CASEIN KINASE 1
CO	crossover
COH	KLEISIN of *C.elegans*
COX11	CYTOCHROME OXIDASE 11
CTF7	CHROMOSOME FIDELITY 7
DEK15	DEFECTIVE KERNEL 15
DMC1	DISRUPTION OF MEIOTIC CONTROL
DNA	Desoxyribonucleic acid
DSB	Double Strand Break
ESP	SEPARASE
FAS1	FASCINATA 1
FIB2	FIBRILLARIN
FISH	Fluorescence in situ hybridization
FTSH7	FTSH PROTEASE7
g	gram
GAL4	GALACTOSE 4
GFP	GREEN FLUORESCENT PROTEIN
GR	Glucocorticoid receptor
H2A.W6	HISTONE 2 VARIANT A.W6
H3K27me3	Histone 3 lysine 27 trimethylation

H3K4me3	histone3 Lys-4 trimethylation
HDA	Histone deacytelase
HMT	Histone methyltransferase
HP	HETEROCHROMATIN PROTEIN 1
HR	homologous recombination
HTA7	HISTONE 2 VARAINAT A.W7
HXK1	HEXOKINASE
IgG	IMMUNGLOBULIN G
MBD6	Methyl Binding Domain 6
min	minutes
MRE11	MEIOTIC RECOMBINATION 11
MSH	MUTS HOMOLOG
MTOPIVB	TOPOISOMERASE IV subunit B
NASC	Nottingham Arabidopsis Stock Center
NBS1	NIJMEGEN BREAKAGE SYNDROME
NCO	Non-crossover
NOR	Nucleolus Organizer Region
PANS	PATROUNUS
PCNA1	PROLIFERATING CELLULAR NUCLEAR ANTIGEN1
PCR	Polymerase chain reaction
PDS5	PRECOCIOUS DISSOCIATION OF SISTER
PMC	Pollen Mother Cell
PP2A	SERINE/THREONINE PHOSPHATASE 2A
Pro	Promoter
qPCR	quantitative PCR
qRT-PCR	quantitative Realtime PCR
RAD21.1/.2/.3	RAD21 cohesin complex component 1, 2, 3
RAD50, 51	DNA REPAIR PROTEIN 50, 51
RAD51	RAS ASSOCIATED WITH DIABETES PROTEIN
rDNA	ribosomal DNA
REC8	RECOMBINATION PROTEIN 8
RFP	RED FLUORESCENT Protein
RNA	Ribonucleic acid
RNAi	Ribonucleic acid interference
rpm	rounds per minute
RPS5	RIBOSOMAL PROTEIN S5 A
RT	room temperature
s	seconds
SAC	SPINDLE ASSEMBLY
SC	Synaptonemal Complex
SCC1	Sister chromatid cohesion 1
SCC2, 3, 4	SISTERCHROMATID COHESION

SGO	SHUGOSHIN
SLiCE	Seamless Ligation Cloning Extract
SMC1, 3	Structural maintenance Protein1, 3
SPO11	DNA topoisomerase VI
SWI1	SWITCH 1
SYN/2/3/4	RAD21 cohesin complex component 1, 2, 3
TFP	Turquoise Fluorescent Protein
TTN	Titan, synonymous for smc1 and 3 mutants
TUA5	TUBULIN ALPHA 5
UEVC1	UBIQUITIN E2 VARIANT 1C
V	volt
WAPL	WINGS APART LIKE
WT	wild-type
Y2H	Yeast two hybrid

Abstract

The faithful transmission of chromosomes during cell divisions is essential for the survival of eukaryotic organisms. Aside from mitosis, which leads to two genetically identical daughter cells, meiosis is required for sexual reproduction and ensures biodiversity via the formation of haploid gametes with newly assorted allelic combinations. Essential for a proper chromosome segregation during both cell divisions is the chromosomally bound multi-subunit complex called cohesin. The mitotic and meiotic complexes are formed by the heterodimer of the STRUCTURAL MAINTENANCE proteins SMC1 and SMC3. The binding of a α-kleisin protein to SMC1 and SMC3 closes and forms a ring shaped complex, keeping sister chromatids together. In *Arabidopsis thaliana,* four α-kleisins (RAD21.1, RAD21.2, RAD21.3 and REC8) have been identified so far. Although a function in vegetative cells has been postulated for the three RAD21 proteins, less is known about their exact roles. In contrast, the meiotic specific α-kleisin REC8 has been intensively studied revealing its requirement for proper chromosome segregation via its stepwise loss during meiosis. This was found to be dependent on a tightly controlled phosphorylation status of REC8 in organisms like yeast. However, the kinase responsible for the REC8 phosphorylation remains unknown *in planta*. A previous *in vitro* analysis identified CDKA;1 as a possible candidate kinase for REC8 phosphorylation in Arabidopsis. Therefore, I mutagenized the CDKA;1 phosphorylation sites identified *in vitro* and analyzed their impact on meiosis by complementation assays of the *rec8* mutant phenotype. The simulations dephospho-mutation of seven sites resulted in a partial *rec8* like phenotype indicating the general importance of REC8 phosphorylation. By the subsequent analysis of single mutants, I could identify one site for which a single dephospho-mutation led to aberrant meiotic procedure as well.

Interestingly, *rec8* mutant plants show severe defects in chromosome cohesion that leads to complete sterile plants. However, these plants are able to partially maintain centromeric cohesion almost until the end of meiosis I, leading to the question if another cohesin complex mediates sister chromatid cohesion in meiosis like it was shown for other organisms like mammals,

worms and flies. Therefore, I systematically re-investigated the localization of the α-kleisins in meiosis. While RAD21.1 and RAD21.3 were only found to be expressed in vegetative cells, I found that RAD21.2, contrasting previous reports, showed a chromosomal localization during both cell divisions. Interestingly, an enrichment of RAD21.2 at heterochromatic repetitive DNA elements like ribosomal DNA (rDNA) was found. In many species, meiotic recombination in these regions is blocked by a poorly understood mechanism. The analysis of *RAD21.2 RNAi* knock down plants that exhibit an increase of non-homologous recombination in rDNA regions inducing genome instability, leads to the hypothesis that RAD21.2 is required for the repression of recombination at heterochromatin. Since an appearance of REC8 at rDNA regions was found in *RAD21.2 RNAi* knock down plants, we hypothesize that the distribution of REC8 and RAD21.2 containing cohesin complexes shape the recombination landscape in Arabidopsis meiosis.

Zusammenfassung

Die korrekte Weitergabe von Chromosomen während der Zellteilung ist essentiell für das Überleben eukaryotischer Organismen. Neben der mitotischen Zellteilung, die zwei identische Tochterzellen hervorbringt, wird die meiotische Zellteilung für die sexuelle Reproduktion benötigt und erhält darüberhinaus die Biodiversität durch die Bildung haploider Gameten mit neuen allelischen Kombinationen aufrecht.

Essentiell für die mitotische und meiotische Zellteilung sind die Cohesin Komplexe. Sowohl der mitotische als auch der meiotische Cohesin Komplex wird durch ein Hetrodimer aus den Proteinen SMC1 und SMC3 gebildet. Der Komplex wird durch die Bindung eines α-Kleisins geschlossen. In *Arabidopsis thaliana* wurden vier unterschiedliche α-Kleisine (RAD21.1, RAD21.2, RAD21.3 und REC8) beschrieben. Auch wenn eine Rolle in vegetativen Zellen für die drei RAD21 Proteine vermutet wird, fehlen genaue Analysen zu ihrer Funktion. Im Gegensatz dazu gibt es viele Daten zu dem Meiose-spezifischen Protein REC8. Während der Meiose ist REC8 besonders für die schrittweise Dissoziation des Cohesin Komplexes relevant, die für die korrekte Verteilung der Chromosomen essentiell ist. In anderen Organismen wie z.B in Hefe wurde bereits gezeigt, dass dieser Prozess von dem REC8 Phosphorylierungsstatus abhängt. Allerdings ist die Kinase, die REC8 phosphoryliert in Pflanzen nicht bekannt. Eine vorherige *in vitro* Analyse hat CDKA;1 als potenzielle Kinase identifiziert. Auf dieser Annahme basierend, habe ich die identifizierten CDKA;1 Phosphorylierungsstellen in der REC8 Proteinsequenz mutiert und ihren Einfluss auf die Meiose analysiert. Die Mutation aller sieben Phosphorylierungsstellen resultierte in einem *rec8* ähnlichen Phänotyp. Dieses verdeutlicht die generelle Relevanz der REC8 Phosphorylierung auch in Pflanzen. Darüberhinaus führte die Analyse einzelner Phosphorylierungsstellen zur Identifikation einer besonders wichtigen Stelle, da die Expression zu einer Reduktion der Fertilität, charakterisiert durch eine veränderte Meiose, geführt hat.

Interessantwerweise, zeigen *rec8* Mutanten eine komplette Infertilität auf. Dennoch sind diese Pflanzen in der Lage die Centromere teilweise bis fast

zum Ende der Meiose I zusammenzuhalten. Dieses hat zu der Frage geführt, ob ein weiterer Cohesin Komplex für diese Beobachtung verantwortlich ist. Daher habe ich die Lokalierung der α-kleisine RAD21.1, RAD21.2 oder RAD21.3 während der Meiose analysiert. Für RAD21.1 und RAD21.3 konnte lediglich eine Lokalisierung in vegetativen Zellen gefunden werden. Für RAD21.2 konnte ich in beiden Zellteilungen eine Lokalisierung an die Chromosomen feststellen. Interssanterweise steht dieses im Kontrast zu vorangegangen Studien. Darüberhinaus, konnte ich eine Anreicherung von RAD21.2 in repetitiven DNA (rDNA) Regionen beschreiben. In rDNA Regionen findet eine Rekombinationsunterdrückung in vielen Organismen statt. Allerdings, ist der zugrunde liegende Mechanismus bis heute nicht verstanden. Die Erstellung und Analyse von *RAD21.2 RNAi* knock-down Mutanten hat jedoch zu einem Rekombinationsanstieg in rDNA Regionen mit einhergehender Genomdestabilisierung geführt. Dies führt zur Hypothese, dass RAD21.2 für die Rekombinationsunterdrückung an heterochromatischen Bereichen benötigt wird. Da die reduzierte Expression von RAD21.2 auch zu einer REC8 Lokalisierung in den rDNA Regionen geführt hat, wird darüberhinaus gemutmaßt, dass beide Cohesin Komplexe bei der Verteilung von Rekombinationsstellen an den Chromosomen beteiligt sind.

1. Introduction

1.1 Meiosis

The faithful transmission of chromosomes during cell division is essential for the survival of eukaryotic organisms. In the somatic cell cycle, the genome is duplicated during S-phase via DNA replication, leading to a pair of identical sister chromatids that are tightly connected throughout G_2-phase and are finally separated by mitotic meta- to anaphase transition. The final products of the mitotic division are two identical daughter cells with the same chromosome content as the mother cell (Gutierrez et al., 2009).

In contrast, the meiotic cell division of a diploid cell, which is essential for sexual reproduction, results in four haploid gametes. After one round of DNA replication, the meiocyte undergoes two successive nuclear divisions termed as meiosis I and meiosis II. During meiotic prophase I, homologous chromosome pair and exchange their genetic material via homologous recombination. Progressing in meiosis I, the homologous chromosomes then segregate and move to opposite cell poles.

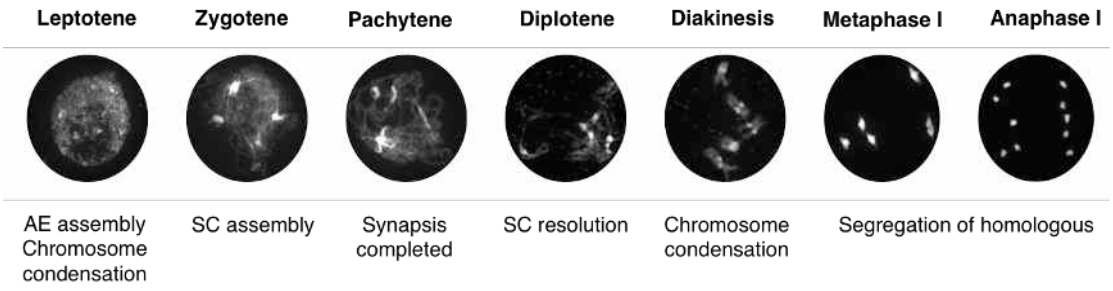

Figure 1: Schematic representation of chromosome dynamics and major events during meiosis I.

After this first reductional division (Fig. 1) during which the sister chromatids stay physically connected follows meiosis II, in which the chromatids segregate in a mitotic-like way. Subsequently, four haploid cells, containing half of the genetic material from the parental cells, are generated (Harrison et al. 2010). Failure in these meiotic segregation events eventually can lead to

imbalanced gametes and thus aneuploidy or polyploidy in the progeny of an organism (Schwarzacher et al., 2003). From previous studies, it is well known that meiosis is tightly regulated and requires many dynamic processes like homologous recombination and rearrangements of the chromatin structure (Fig. 1).

1.2 The chromosome axis

A major contribution to the rearrangements of the chromatin structure is mediated by the Synaptonemal complex (SC), a proteinaceous tripartite structure that connects homologous chromosomes along their lengths until pachytene. The SC is found in all eukaryotic cells and many proteins of the SC have been identified in various organisms. In the beginning of meiosis, sister chromatids are arranged in a loop structure that extends about 300 nm from the axial core (axial element) (Armstrong et al., 2002). From Leptotene onwards, the chromosome axis starts to be formed by ASY1 and ASY3 (Fig.2). From zygotene to pachytene, the chromosomes are synapsed by ZYP1 linking the central and axial elements. In the zipped conformation the axial element is called lateral element. The central element is composed of the transverse filamentous proteins and the central region proteins. The deconstruction of the SC takes place until diplotene and dramatic chromosome condensation occurs (Golubovskaya et al., 2010).

All in all this dynamic chromatin remodeling process is essential for the exchange of genetic material via homologous recombination and failure results in severe meiotic outcome that is represented by SC mutant. The *asy1* mutant shows an asynaptic chromosome behavior with a reduction of chiasmata. The axial element protein ASYNAPTIC1 (ASY1) is found in Arabidopsis, maize and rice (Golubovskaya et al., 1997; Carly et al., 2000; Armstrong et al., 2002 and Nonomura et al., 2004). Characteristic for ASY1 is the HORMA domain that is found in the N-terminus, typical for proteins that interact with chromatin. Recently, it was shown that the recruitment of ASY1 to the chromosome is regulated by the phosphorylation of CDKA;1 (Yang et al., 2019).

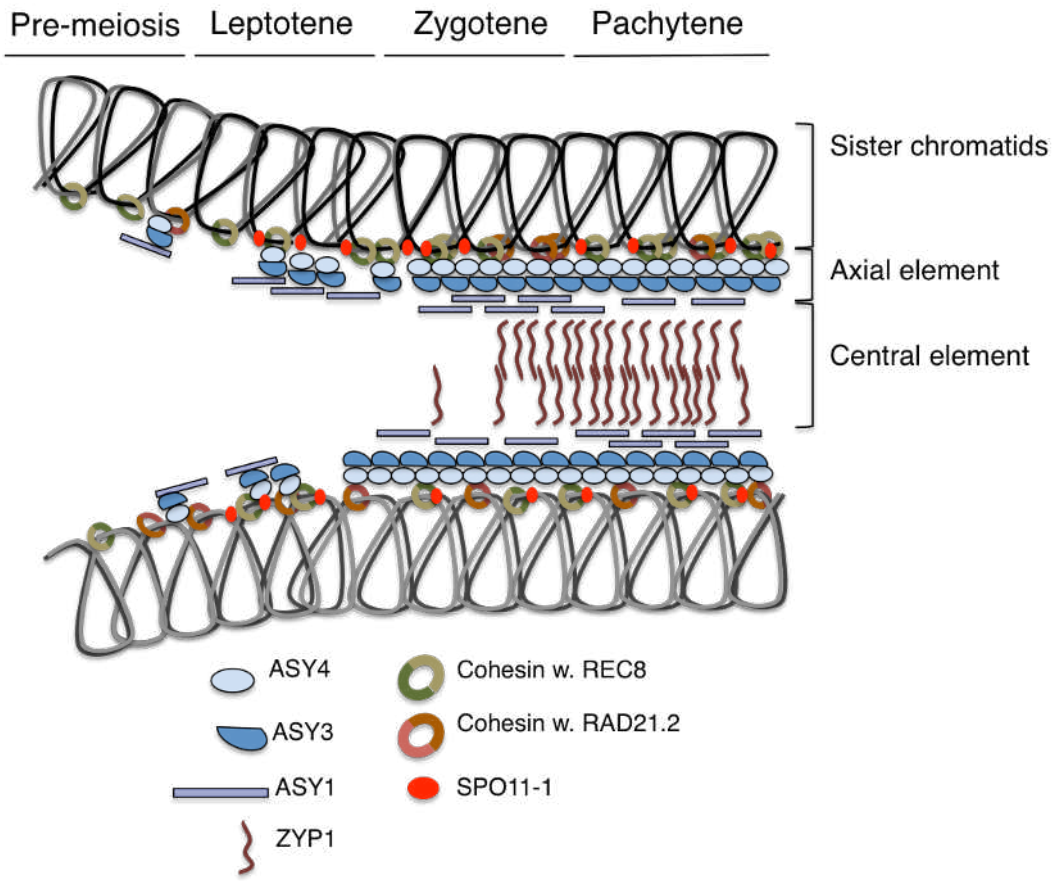

Figure 2: Schematic Representation of the dynamics of chromosome axis

Furthermore the localization of ASY1 is dependent on the other axis protein ASY3 in *Arabidopsis thaliana* (Ferdous et al., 2012; Lee et al., 2015). In yeast, it is shown that cohesins recruits ASY3/ASY1 and that all three proteins interact with each other (Sun et al., 2015; Osman et al., 2018). *Asy3* mutants fail to form chiasmata and present univalents at metaphase I revealing a function in synapsis and DSB induction. In the further process of the SC assembly, ASY1 gets released from the chromosome axis mediated by the triple AAA^+ ATPase PCH2 (Lambing et al., 2015). In the absence of PCH2, ASY1 is not removed from the chromosome axis, therefore the SC fails to assemble and chromosomes cannot synapse (Lambing et al., 2015). A similar regulation of ASY1 was described for yeast and mouse (Wojtasz et al., 2009). In contrast, mutants of the PCH2 homolog in rice CRC1 (CENTRAL REGION COMPONENT) display an asynaptic phenotype with the inability of DSB formation, indicating a different function of both proteins (Nonomura et al.,

2004; Miao et al., 2013). Another protein of the ASYNAPTIC family was identified in 2018. The short coiled-coil containing ASY4 protein shows structural similarities with the C-terminus of ASY3 and was found to be an axis-associated protein. Furthermore, it was shown that the localization of ASY1 and ASY3 requires ASY4. An interaction with ASY1 and ASY3 was confirmed *in vitro*. The *asy4* mutant shows a lack of full chromosome synapsis and univalent chromosomes appearance at diakinesis (Chambon et al., 2018).

The ZYP1 protein has been identified in Arabidopsis, rice, maize, wheat and barley (Higgins et al., 2005; Wang et al., 2010; Golubovskaya et al., 2010; Khoo et al., 2012; and Barakate et al., 2014). Arabidopsis genome encodes for the redundant acting ZYP1a and ZYP1b proteins that are part of the transverse filament. The coiled-coil ZYP1 proteins comprise globular domains at their N- and C-termini. Studies in yeast show that ZYP proteins form homodimers whereas the C-termini are oriented along the lateral elements and the N-termini of the dimers overlap in the central region of the SC. The analysis of knockout mutants revealed that ZYP1 is required for chromosome synapsis. The spatial and temporal localization analysis of ZYP1 uncovers that the protein becomes detectable at early leptotene as foci. Progressing in prophase I lead to a more continuous ZYP1 signal. At the end of pachytene the ZYP1 signal is found along the whole chromosome axis. *RNAi* knock down of *ZYP1* in Arabidopsis leads to synapsis failure resulting in multivalents at late prophase I and metaphase I (Higgins et al., 2005). The knock down of ZYP1 in barley leads to a similar phenotype like the failure in SC formation and defects in recombination (Barakate et al., 2014).

1.3 The cohesin complex

A major contribution to ensure proper chromosome segregation is mediated by the cohesin complex. The highly conserved multi-subunit cohesin complex is responsible for sister chromatid cohesion during mitosis and meiosis (Nasmyth and Haering, 2009). A large part of the ring shaped complex is built by a heterodimer of SMC1 and SMC3, which belong to the STRUCTURAL

MAINTENANCE protein family (Fig. 3) (Schubert, 2009). SMC proteins consist of an ATP binding-head and a hinge domain that are connected by an antiparallel coiled-coil structure. During mitosis of mammals, SMC1 and SMC3 bind via their globular ATP bound head domains the *α*- kleisin RAD21 (SCC1 in yeast). In the meiotic cohesion complex RAD21 is replaced by the *α*- kleisin REC8 (Skibbens, 2019). The recruitment of the SISTER CHROMATID COHESION protein SCC3 to the *α*- kleisin has been shown to stabilize the cohesin complex (Fig. 3).

It is well accepted that the cohesin complex forms a ring shape structure (Haering et al., 2008). However, how the complex embraces the DNA is still under discussion. There are two main models: the ring model proposes that a single complex encircles both sister chromatids, whereas in the handcuff model two cohesin complexes encircle one sister chromatid each and both complexes are connected via one SCC3 molecule (Barrington et al., 2017). The second model is based on studies in yeast (Zhang et al., 2008). To get a better understanding of how the cohesins embrace the chromatid, it is recommended to perform structural analysis.

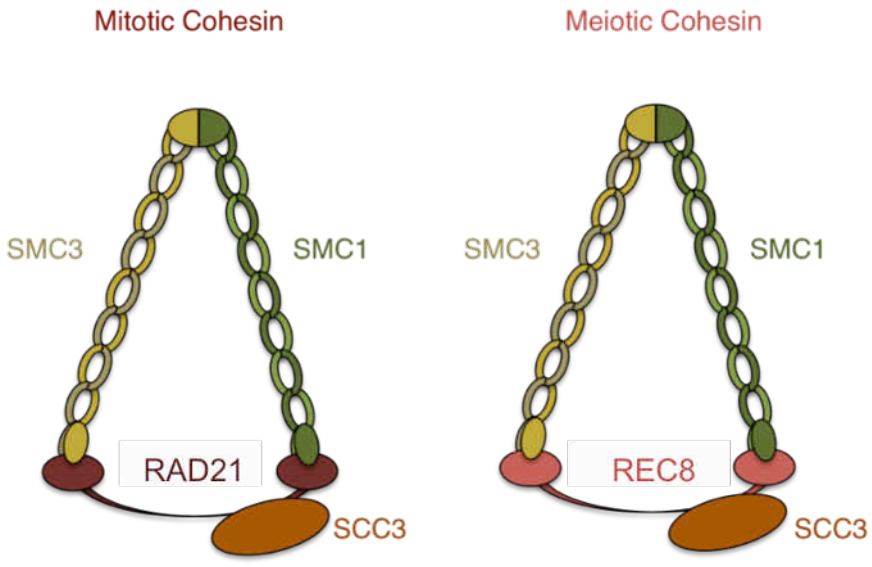

Figure 3: Schematic representation of the mitotic and meiotic cohesin complexes.

1.3.1 The structural maintenance proteins SMC1 and SMC3

The *Arabidopsis thaliana* genome contains one copy of the *SMC1* gene (AT3G54670) and one of the *SMC3* gene (AT2G27170), coding for proteins ata size of 143 kDa and 139 kDa, respectively (Liu et al., 2002; Lam et al., 2005). For SMC3 a localization in the cytoplasm and the nucleus of somatic and germ cells has been detected by using immunolocalization studies. In more detail, SMC3 binds to the chromosomes until the nuclear envelope breakdown. Furthermore, a spindle association was found from metaphase to telophase during mitosis and meiosis (Lam et al., 2005). This seems to be a plant specific feature since spindle localization was never observed in other organisms. However, a further function of SMC3 in addition to sister chromatid cohesion, which seems conserved between species, is the formation of the synaptonemal complex (SC) as it was shown for yeast, mammals and *Arabidopsis thaliana* (Jones and Sgouros, 2001; Eijpe et al., 2000; Liu et al., 2002). Less is known about Arabidopsis SMC1 since localization studies of SMC1 have not yet been published. However, SMC1 shows a SMC3-like localization pattern in tomato (*Solanum lycopersicum*) meiocytes (Lhuissier et al., 2007).

Arabidopsis thalaiana plants harboring a knockout mutation of *SMC1* (ttn8-1 and ttn8-2) or *SMC3* (ttn7-1 and ttn7-2) are defective in embryo and endosperm development. The resulting phenotype is called titan (ttn) due to the giant endosperm nuclei and arrested embryos plants exhibit. The embryonic lethal phenotype confirms the essential function of both proteins during mitosis (Liu et al., 2002). However, a meiotic phenotype description remains missing.

1.3.2 The sister chromatid cohesion protein SCC3

The sister chromatid cohesion protein SCC3 has been shown to be a part of the cohesin complex in a range of organisms like yeast and humans. In the genome of *Arabidopsis thaliana* one copy of *SCC3* is annotated. The expression of this gene is essential for normal plant growth and fertility since null mutants are embryonic lethal and a weak SCC3 allele leads to dwarf and

sterile plants. The SCC3 protein is a hook-shaped protein that is composed of repetitive HEAT domains and is expressed in all plant organs like roots and flower buds (Chelysheva et al., 2005, Roig et al., 2014). Meiosis specific immunolocalization of SCC3 revealed that the protein is loaded onto the chromosome arms starting at meiotic interphase up to metaphase I supporting a role in sister chromatid cohesion. Aside from its role in sister chromatid cohesion, SCC3 is important for the monopolar orientation of the kinetochores during meiosis I and the maintenance of centromeric cohesion at anaphase I (Chelysheva et al., 2005). However, a proof for a REC8/SCC3 interaction is still missing in *Arabidopsis thaliana*. However, an interaction of SCC3 with the mitotic and meiotic *α*-kleisins has been shown in yeast and humans (Haering et al., 2002).

1.3.3 The α-kleisins

More mechanistic studies have been conducted regarding the α-kleisin subunits due to their central role in the life cycle of cohesion in mitosis and meiosis (Brar et al., 2006). *Arabidopsis thaliana* has four different homologs of *α*-kleisins*,* which are called REC8 (SYN1/DIF1), *RAD21.1* (*SYN2*), *RAD21.2* (*SYN3*) and *RAD21.3* (*SYN4*) (Schubert et al., 2009). RAD21.1 and RAD21.3 are expressed in mitotic tissues. In addition to a likely role in mitotic chromosome cohesion, deduced from sequence homology and protein localization, an additional function of RAD21.1 and RAD21.3 in somatic double strand break (DSB) repair has been reported (da Costa-Nunes et al., 2006). Surprisingly, single and double mutants of both *α*-kleisins do not show defects in plant growth and embryo development unlike what has been shown for other mitotic cohesin proteins in different organisms (Mishra et al., 2010; Wang et al., 2018).

The *RAD21.2* gene has been reported to be important for female and male gametogenesis development. However, an essential role in female gametogenesis has been declared since the backcross of heterozygous *rad21.2* plants used as female with wild-type plants as male revealed no heterozygous offspring. In contrast, the backcross of heterozygous *rad21.2*

plants used as male with wild-type as female lead to 36% heterozygous offspring indicating that the *rad21.2* mutations were transmitted in a lower level through the pollen (Jiang et al., 2007). A reduction of the *RAD21.2* expression by *RNAi* approach results in plants that are defective in homologous synapsis and synaptonemal complex formation indicating a role of RAD21.2 in meiosis (Yuan et al., 2012 and 2014). Surprisingly, immunolocalization studies revealed an enrichment of RAD21.2 in the nucleolus of mitotic and meiotic cells although the mutant phenotype is typical for cohesin mutants e.g *smc1* and *smc3* mutants (Jiang et al., 2007). However, as suggested by the localization studies, a role in controlling the rDNA structure, its transcription or processing was assumed.

While there is an apparent paucity of information on the assumed mitotic *α*-kleisins in Arabidopsis, the meiosis specific REC8 is studied more intensively. The *REC8* gene is strongly expressed from meiotic interphase to metaphase I (Bai et al., 1999). In immunolocalization studies, the Arabidopsis REC8 protein was found to bind to chromosome until metaphase I. However, a localization of REC8 to the centromeres after metaphase I, as reported for other organisms, could not be detected by this technique (Chelysheva et al., 2005). But when the dynamic localization of a REC8-GFP fusion protein was followed in male meiocytes using a live cell imaging approach, a centromeric signal of REC8-GFP after metaphase I could be observed (Prusicki et al., 2019). Additionally, a REC8 ChIP-seq experiment revealed that REC8 is enriched at centromeric heterochromatin and binds to chromosome areas that anti-correlate with double strand breaks (DSB) and crossovers. This indicates that REC8 is not randomly distributed along the chromosomes although the mechanisms are not well understood yet (Lambing et al., 2020).

From the analysis of the *rec8* mutant plants, which display normal vegetative growth but are male and female sterile, functions beyond sister chromatid cohesion were suggested. For example, *rec8* mutants show an alteration of the chromosome axis and synapsis observed by the abnormal distribution of ASY1 and ZYP1 (Tiang, 2011). Also for maize meiocytes, it has been reported that REC8 is necessary for the formation of a proper chromosome

axis, homologous chromosome pairing and the normal distribution of RAD51 (Golubovskaya et al., 2006). Finally, rice *rec8* mutants display a similar overall phenotype characterized by additional condensation problems (Zhang et al., 2006; Shao et al., 2011).

1.4 The cohesin life cycle

1.4.1 Cohesin recruitment and loading

Recent studies identify a growing number of auxiliary proteins, which tightly regulate the cohesin life cycle.

In G_1-phase, the cohesin complex is recruited to the chromosomes by the heterodimeric complex SCC2/SCC4. The underlying mechanism is still not well understood. However, in yeast, it is shown that the fully assembled cohesin complex is loaded onto actively transcribed chromatin regions (Lopez-Serra et al., 2014) by SCC2/SCC4. In *Arabidopsis thaliana* there is only one homolog of SCC2 found. Its absence leads to an embryo lethal phenotype and knockdown mutants display sterility caused by meiotic defects similar to the defects that are observed in *rec8* mutants (Schubert et al., 2009). Recently, an SCC4 homolog was characterized in *Arabidopsis thaliana*. An interaction of SCC4 with SCC2 was proven and it was shown that both are indispensable for the cell fate determination during early stages of embryo development (Minina et al., 2017). In maize, DEK15 (DEFECTIVE KERNEL 15) has been identified as an SCC4 homolog (He et al., 2019). Mutant *dek15* maize plants display embryonic lethality due to impaired chromosome segregation in mitosis. Thus although the main players involved in the recruitment of the cohesin complex have been identified in plants, it remains unclear how they move to specific chromatin regions and determine the positioning of cohesins along chromosomes.

After cohesins are loaded onto the chromosomes they are not tightly associated with chromatin because of the activity of the “anti-establishment” or “Releasin” complex formed by the WINGS APART-LIKE (WAPL) and PRECOCIOUS DISSOCIATION OF SISTERS 5 (PDS5) proteins (Gligoris et

al., 2016). In Arabidopsis, two *WAPL* genes act redundantly since the single mutant plants do not show problems in vegetative growth, development or fertility, while the double homozygous mutant displays a reduction in seed set and several meiotic defects like impaired homologous pairing, spindle deformation, prolonged cohesion and alterations of the heterochromatin structure (De et al., 2014). For *PDS5*, five genes were identified within the genome of Arabidopsis. Depletion of *PDS5* leads to smaller plants with a reduced seed set. However, only minor meiotic defects like chromosome bridges in anaphase I were observed. Since the localization of REC8 and SMC3 is not affected in *pds5* mutants, only a minor role of PDS5 in meiosis was assumed. Therefore, separate meiotic functions were suggested for the *Arabidopsis thaliana* WAPL and PDS5 homologs (Pradillo et al., 2015).

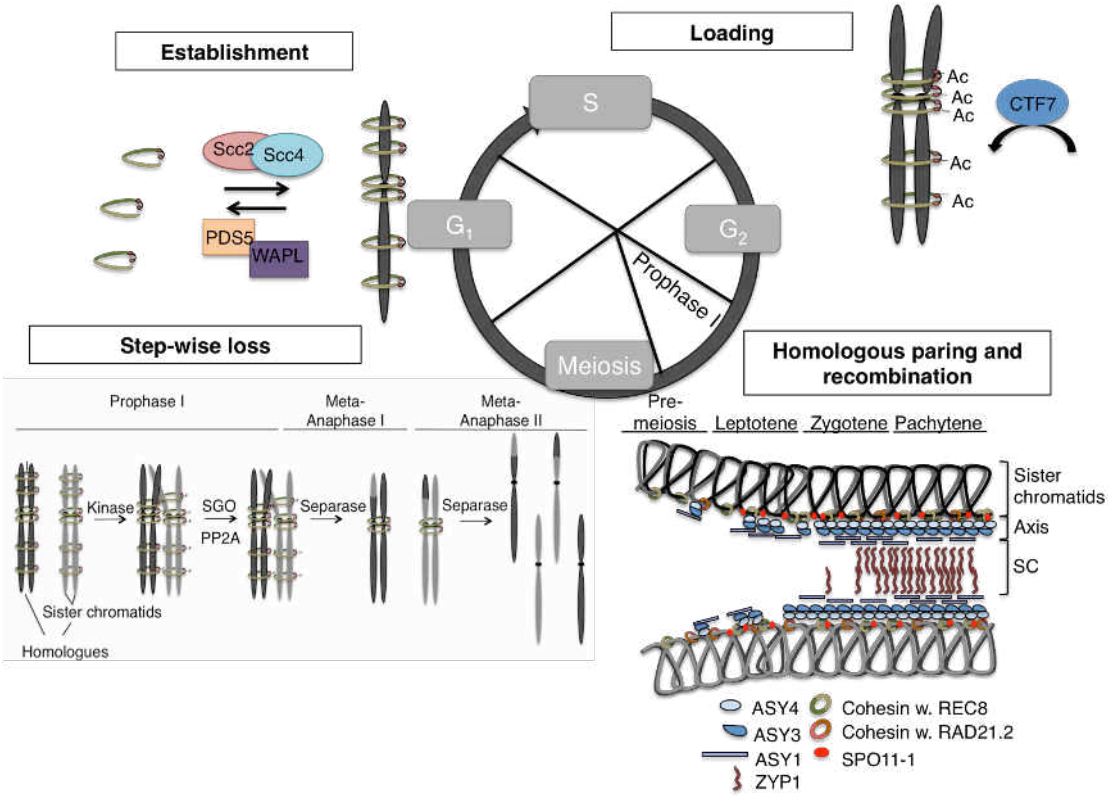

Figure 4: Schematic representation of the cohesin life cycle to highlight specific events that are important for a proper chromosome segregation during meiosis in plants (modified from Zamariola et al., 2014).

1.4.2 Establishment of cohesion and its removal during prophase I

The second step of the cohesin life cycle is the establishment that takes place during S-phase in a replication dependent manner and ensures the tight association of the cohesins with the chromatin. In yeast, a protein called ECO1/CTF7 acetylates two conserved lysine residues of SMC3 counteracting the action of the WAPL-PDS5 complex. An acetyltransferase activity was proven for the CHROMOSOME TRANSMISSION FIDELITY (CTF7) protein of Arabidopsis in vitro (Jiang et al., 2010). An overexpression of CTF7 results in female gametophytic lethality, while heterozygous mutation of *ctf7* leads to minor female gametophyte developmental abnormalities. Although most *ctf7* homozygous mutants are embryonic lethal, *ctf7* plants can be detected at a very minor frequency with a dwarf phenotype and strong defects in chromosome pairing and segregation in male and female meiosis (Bolaños-Villegas et al., 2013; De et al., 2016). The impact from CTF7 on meiosis was further revealed by the analysis of CTF7 knock down plants applying the *RNAi* approach since plants exhibit chromosome fragmentation and loss of sister chromatid cohesion during meiosis (Singh et al., 2013).

In vertebrates, another cohesin associated protein, called Sororin, is found to be crucial for stabilizing the complex. The binding of the Sororin protein to PDS5 prevents an interaction of PDS5 with WAPL (Zhang et al., 2012). Since no obvious sequence homolog to Sororin has been found in plants so far, it was unclear if a similar mechanism exists in plants to prevent a premature loss of cohesion. However, since WAPL is already expressed from the onset of meiosis there is an anticipated regulation mechanism to counteract WAPL at early stages was anticipated. Recently, it was shown that SWITCH1 (SWI1) or also known as DYAD antagonizes the action of WAPL during meiosis of *Arabidopsis thaliana* (Yang et al., 2019). Rice and maize *swi1* mutants show severe defects in meiosis: impaired chromosome cohesion, lacking of homologous pairing and defective synapsis. (Pawlowski et al., 2009; Che et al., 2011). In Arabidopsis, different mutant alleles with diverse defects in fertility have been intensively studied. For example, the *swi1-2* allele leads to 20 chromosomes (univalents) in metaphase I and to pollen containing

unequal chromosome numbers at end of meiosis (Mercier et al., 2003). As a consequence of defective cohesion, plants are impaired in chromosome pairing, synapsis and recombination. Recently, it was shown that SWI1 interacts with PDS5 in a competing manner to WAPL for antagonizing WAPLs anti-cohesin-establishment action in *Arabidopsis thaliana* (Fig. 5). Furthermore, it was proven that the antagonizing mechanism is diminished at late prophase I by the phosphorylation of SWI1 by CDKA;1. The phosphorylation of SWI1 is a mark for its degradation via the 26S proteasome (Yang et al., 2019). Interestingly, a similar mechanism is reported for Sororin, which is phosphorylated by CDK in vertebrates (Dreier et al., 2011). After SWI1 is depleted from the chromosomes, WAPL removes most of the arm cohesion until late prophase I. This conserved mechanism is known as the WAPL-dependent prophase pathway and disconnects the *α*-kleisin from SMC3 and thus opens the ring (Chan et al., 2013).

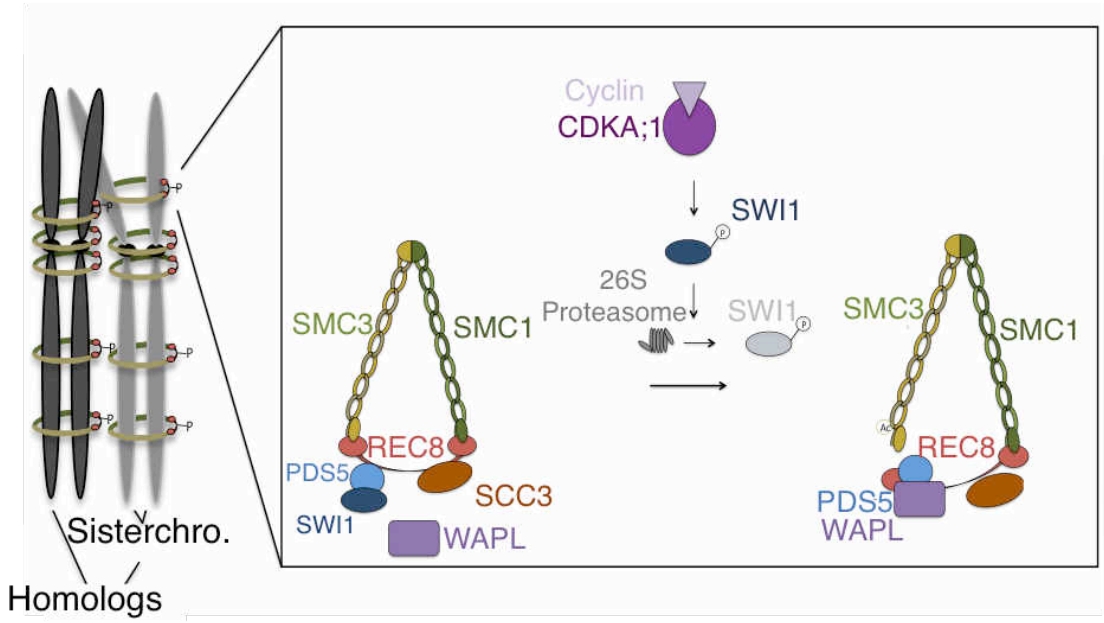

Figure 5: Prophase pathway mediates the removal of cohesion located at chromosome arms.

1.4.3 Separase mediated removal of cohesion

Another mechanism that contributes to the stepwise loss of cohesion in meiosis is based on the activity of a cysteine protease called SEPARASE

(ESP) and is largely conserved among different species (Luo et al., 2018). In Arabidopsis, mutations of the *separase* result in embryo lethality and a reduction of the ESP transcript leads to compromised fertility and defects in meiotic chromosome segregation caused by persisting cohesin on chromosomes in meiosis I and meiosis II (Liu et al., 2006). However, the separase activity is inhibited by securin until the onset of anaphase I (Fig. 6). The binding of securing to separase prevents that the protease can bind its substrate REC8. At the transition from metaphase I to anaphase I ubiquitylation of securin via the APC/C results in its degradation and thus to the activation of the separase. Subsequently, the separase recognizes and cleaves the α-kleisin REC8. It is important to mention that only phosphorylated REC8 is a cleavable target. Recently, distant securin homologs were discovered in *Arabidopsis thaliana*, i.e. PATRONOUS 1 and PATRONOUS 2 (PANS) (Cromer et al., 2019) and their thorough analysis lead to the well-founded hypothesis that PANS is the securin homolog in plants.

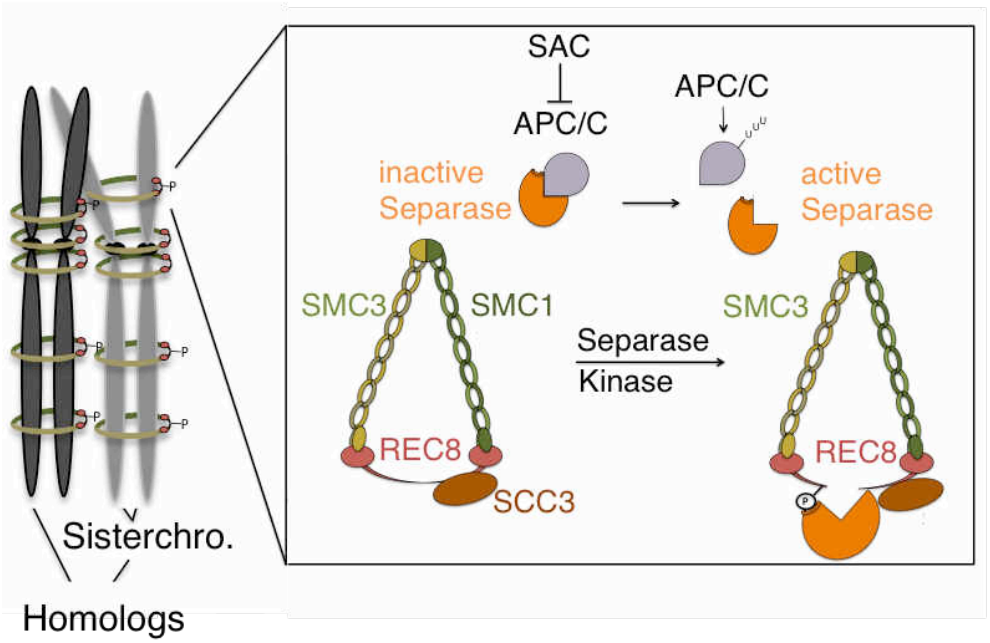

Figure 6: Chromosome arm Cohesion is cleaved by the separase at Meta-Anaphase I.

Pans1 mutants display defective chromosome segregation since sister chromatid cohesion is lost prior to metaphase II resulting in aneuploid

gametes, while *pans2* mutants show no defects. However, the double mutant is lethal indicating a redundant function (Cromer et al., 2013) which corroborated by the finding that PANS1 and PANS2 both directly interact with the separase and the APC/C. Furthermore, plants harboring a modified PANS1 protein that mediates a resistence to the regulation by the APC/C show loss of cohesion and chromosome miss-segregation (Cromer et al., 2019).

During meiosis I, the separase-dependent REC8 cleavage affects only arm cohesion (Nakajima et al., 2007) since centromeric cohesion needs to be maintained until the onset of anaphase II to prevent a premature segregation of sister chromatids. This is assured by the SHUGOSHIN (SGO) proteins which shield centromeric cohesins at anaphase I from being removed (Watanabe, 2005). The mechanism is more intensively studied in organisms like humans and yeast and it was revealed that SGO recruits the phosphatase PP2A to the pericentromeric heterochromatin. This enzyme constantly dephosphorylates REC8 and thus prevents its cleavage.

PP2A is heterotrimeric serine/ threonine phosphatase that is built by an A-subunit, a regulatory or targeting B subunit and a catalytic C-subunit. In general, PP2A phosphatases are involved in many different processes like cell division, hormone signaling and development. The genome of *Arabidopsis thaliana* encodes three genes for the A-subunit of PP2A, 17 genes for the B-subunit and five genes for the C-subunit. Proteins of the specificity mediating B-subunit family are further divided into four groups, B to B′′′, each with several members (Farkas et al., 2007). A role in reproduction was assumed for the PP2AB´α and PP2AB´β subunits, since the double mutant is almost sterile (Jonassen et al., 2011). Detailed mutant analysis revealed that both proteins are redundantly required for the cohesin protection during meiosis (Yuan et al., 2018; Zhang et al. 2019). The double mutant shows normal chromosome behavior with no defects in REC8 loading until prophase I, but then defects are observed starting from the beginning of anaphase I. The premature loss of cohesion results in 10 univalents instead of five bivalents in metaphase I. However, evidence that REC8 is phosphorylated and which

kinase might be responsible for such a phosphorylation, mediating the separase-dependent cleavage in plants is still missing. In yeast, three kinases have been identified to mediate the phosphorylation of REC8, a polo-like kinase, the Casein kinase CK1δ/ε and DBF4-dependent CDC7 kinase (Attner, et al. 2013; Katis et al., 2010). The identification of functional homologs in Arabidopsis or other plant species could lead to a better understanding of the regulatory mechanism for a major meiotic event, the stepwise-loss of cohesion.

During the second meiotic division, the protection of centromeric cohesion by SGO and PP2A is not maintained, centromeric REC8 is phosphorylated and cohesion is removed to allow the separation of sister chromatids (Clift and Marston, 2011).

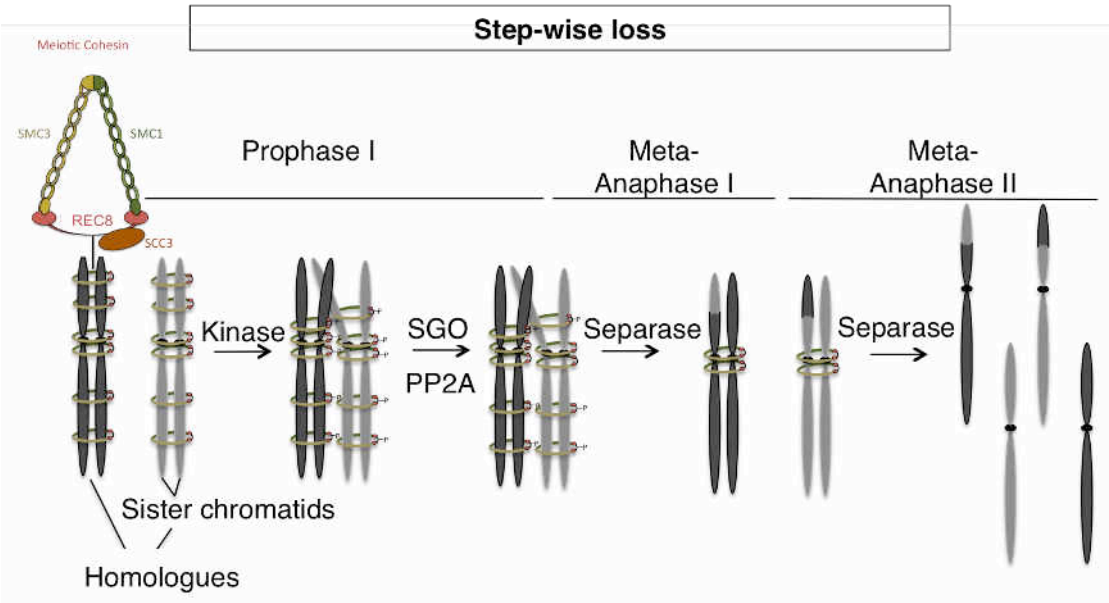

Figure 7: Schematic representation of the stepwise loss of cohesion during meiosis.

An analogous model of action is described for different plant species like maize, rice and *Arabidopsis thaliana* (Fig. 7). Arabidopsis contains 2 *SGO* homologs that play a role as centromere protectors in meiosis. Loss of *sgo1* causes premature segregation of sister chromatids in anaphase I whereas *sgo2* mutants do not show any meiotic defects. However, since the *sgo1 sgo2* double mutant displays a slightly stronger, almost sterile phenotype, a

redundant function of both proteins in meiosis is assumed (Zamariola et al., 2014). In *sgo1* maize mutants the chromosome structure is not impaired and meiotic defects could not be detected until metaphase I. However, a premature loss of sister chromatids during telophase I gave rise to defective chromosome segregation during meiosis II. In maize and in contrast to other organisms, the centromeric localization of SGO1 is dependent on REC8 (Hamant et al., 2005). SGO2 is analyzed neither in maize nor in rice. To this end, it remains unknown how the dissociation of cohesins from the chromosomes is regulated during the second meiotic division.

1.5 Cohesion and recombination

Aside from proper chromosome segregation, the exchange of genetic material via homologous recombination (HR) is a major aim of meiosis, ensuring genetic variety. Meiotic recombination is initiated by the formation of DNA double strand breaks by SPO11 mediated catalytic cleavage. In *Arabidopsis thaliana*, two *SPO11* genes and several additional DSB inducing factors have been identified (Stacey et al., 2006), while it is still unknown which mechanism DSB distributes along the chromosomes in plants. For yeast and plants, it was shown that the distribution is not random and DSB hot- and coldspots can be identified (Smagulova et al., 2011; Choi and Henderson, 2015). In many organisms, hot spots are found in chromatin regions marked by low nucleosome density and enriched histone3 Lys-4 trimethylation (H3K4me3), that is typical for an open chromatin formation since it is often mapped to active promoters (Pan et al., 2007; Yelina et al., 2015; Wijnker et al., 2013; Choi et al., 2018). Besides the chromatin state, it was shown that chromosome axis proteins are involved in DSB distribution in yeast (Panizza et al., 2011). Here, DSB sites are found within chromatin loops that are tethered to the chromosome axis where DSB accessory proteins are bound as well. Such a chromatin tethering process is not reported for plants so far, but chromatin axis mutants like *asy1* show a reduced DSB level in *Arabidopsis thaliana* (Lambing et al., 2020), supporting a role of the axis in DSB formation.

DSB can be repaired in different ways resulting either in crossover (CO) or non-crossovers (NCO). Interestingly, Arabidopsis has 15 times more DSB than CO (Varas et al., 2015). However, also CO are distributed in a characteristic way along meiotic chromosomes (Choi et al., 2013). The highest CO frequency was found in chromosome arms, decreasing towards the telomeric and centromeric regions. Interestingly, the CO frequency varies between male and female meiocytes with female meiosis displaying the slightly higher recombination frequency (Giraut et al., 2011). An interesting phenomenon called CO homeostasis has been found in different species, describing that no changes in CO are observed when the DSB number is increased (Cole et al., 2012; Varas et al., 2015).

In general, two types of CO are formed by different mechanisms including specific proteins (Mercier et al., 2005). For both, the DSB ends are processed to single stranded 3´ends by a complex formed by MRE11, RAD50 and NBS1 (Osman et al., 2011). The action of the recombinases RAD51 and DMC1 propagates the DSB repair by single strand DNA invasion giving rise to a D loop intermediate (Mercier et al., 2015). After this step, a double Holiday junction (dHJ) is formed and the joined DNA molecules are resolved by different pathways determining if class I or class II COs or NCOs are formed.

A direct role of cohesins in recombination has not been reported for any organism. However, it was shown that REC8 binding sites correlate with CO hot spots in mammals (Paranov et al., 2017). In contrast, REC8 was found to localize to DSB cold spots in yeast (Ito et al., 2014). Furthermore, an involvement of cohesins in suppression of recombination at ribosomal DNA regions (rDNA) has been postulated (Huang et al., 2006). Ribosomal DNA regions are composed of repetitive sequences that are characterized by a heterochromatic environment (Riddle and Richards, 2005). In *Arabidopsis thaliana*, the 45S rRNA genes are tandemly arranged close to the telomeres of chromosome 2 and 4 and as in other species are referred to nucleolus organizer regions (NOR), since they play a predominant role in nucleolus architecture (Rabanal et al., 2017). However, these highly repetitive regions

need to be protected from recombination events since to avoid the loss of genetic information and genome instability.

Taken together, the analysis of cohesin mutants has shown that the cohesin complex is conserved among various organisms and share their main function in sister chromatid cohesion. However, intensive studies further revealed differences and led to new unsolved questions regarding further functions and their underlying mechanisms. Especially, the mechanism of the stepwise loss of cohesion that ensures a proper chromosome segregation is rarely analyzed in plants. In contrast to yeast and animals, it is not yet shown that the separase cleaves only phosphorylated REC8. Therefore, this thesis will provide data targeting the identification of a kinase that phosphorylates REC8, and further focuses on the identification of phosphorylation sites within REC8, indicating the importance of REC8 phosphorylation in plants. In addition, I generated a genomic GFP reporter for the cohesin component SMC1 and described the dynamics in Arabidopsis for the first time. Finally, this thesis focuses on the localization analysis of the three RAD21 α-kleisins of *A. thalinana*. In contrast to previous studies, we found a localization of RAD21.2 to mitotic and meiotic chromosomes. Furthermore, we determined an enrichment of RAD21.2 at heterochromatic regions and provide data suggesting a role of RAD21.2 in the suppression of non-homologous recombination. This is an important finding since a positive role in recombination has only been reported for REC8 in yeast so far (Kugou et al., 2009). However, a function as a recombination suppressor is not known for any cohesin complexes in other organisms.

Chapter I

Dissecting the molecular function of α-kleisin proteins during meiosis in *Arabidopsis thaliana*

The major part of this chapter has been summarized in the Manuscript: "**The cohesion subunit RAD21.2 functions as a recombination silencer of ribosomal DNA arrays"**

Authors: Viola Kuttig[1], Jason Sims[2], Yuki Hamamura[1], Shinichiro Komaki[3], Maren Köhler[1], Sara Christina Stolze[4], Hirofumi Nakagami[4], Peter Schlögelhofer[2], and Arp Schnittger[1,*]

2.1 Scientific background

Analysis of cohesin mutant phenotypes suggests that RAD21 proteins may play a redundant role since double *rad21.1* and *rad21.3* mutant plants do not show an aberrant phenotype in Arabidopsis (Schubert et al., 2009). In contrast, the observation that *rec8* mutants maintain sister chromatid cohesion until anaphase I in *A. thaliana*, *C. elegans* and *M. musculus* raises the hypothesis that (Severson and Meyer, 2014) α-kleisin subunits mediate different functions during meiosis (Ishiguro, 2019). In vertebrates, the RAD21L cohesion protein has been identified besides the typical meiotic specific REC8-type cohesion and was shown to be required for synapsis and recombination (Herrán et al., 2011). Furthermore, differences have been found for their dynamics and their localization patterns. In *C. elegans*, COH-3 and COH-4 were found to be present in addition to REC8 during meiosis (Severson et al., 2009). Also *D. melanogaster* possesses the additional α-kleisins, i.e. C(2)M and SOLO which have specific functions in meiosis (Heidmann et al., 2004; Yan et al., 2010). In this chapter, I describe an analysis of three non-REC8 α-kleisins of *A. thalinana* with a focus on their potential role in meiosis. In contrast to previous studies, I can show that RAD21.2 localizes to mitotic and meiotic chromosomes. Furthermore, I see an enrichment of RAD21.2 at heterochromatic regions and provide data suggesting a role of RAD21.2 in the suppression of recombination in the rDNA regions.

2.2 Results

2.2.1 RAD21 protein sequence analysis in plants

The four α-kleisin homologs of Arabidopsis thaliana, RAD21.1, RAD21.2, RAD21.3 and REC8 are most conserved at their N- and C-terminus that is visualized by the CLUSTALW alignment of the protein sequences by using the webtool T-Coffee (Fig. 8). Also for α-kleisin proteins from yeast, humans and flies it is described that at the N- and C-terminus the pfam domains (pfam04825 and pfam04824) are located (Zhang et al., 2004). Comparing the

protein sequence of all RAD21/REC8 proteins determined an overall similiarty of 18 percent.

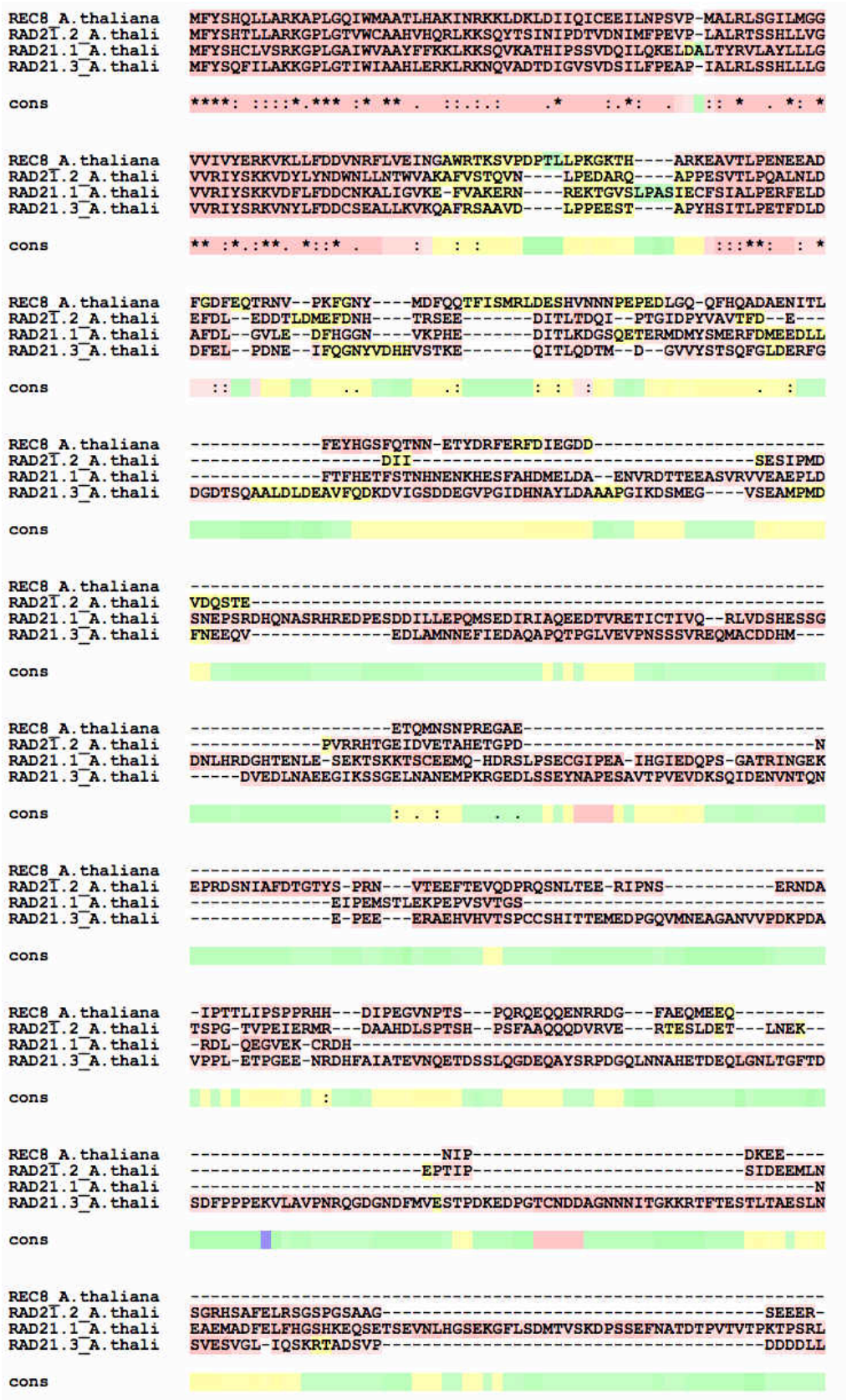

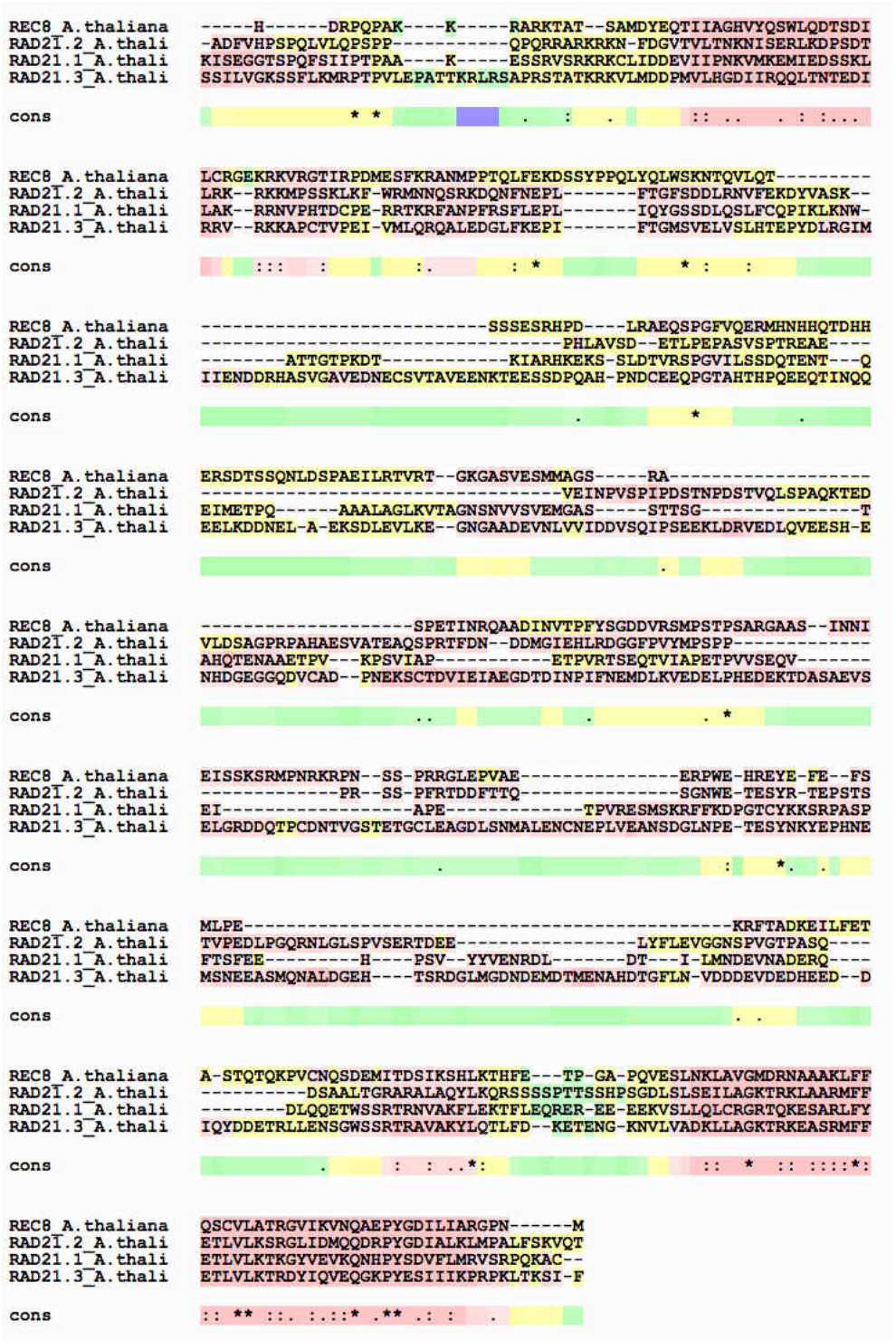

Figure 8: CLUSTAL W alignment of RAD21 proteins from Arabidopsis thaliana.

This tree revealed that three subfamilies are formed. In table 1 protein sequences that were used are listed.

Table 1: List of sequence identifiers of α-kleisin used for phylogentic tree construction. The phylogenetic tree was generated with the webtool "One Click" Mode from Phylogeny.fr.

Name	Species	Gene identifier
RAD21.1	*A. thaliana*	AAL62058.1
RAD21.2	*A. thaliana*	AAL62059.1
RAD21.3	*A. thaliana*	AAL62060.1
REC8	*A. thaliana*	AAF08981.1
RAD21-1	*B. napus*	XP_022556831.1
RAD21-2	*B. napus*	XP_022570817.1
RAD21-3	*B. napus*	CDY55566.1
REC8	*B. napus*	XP_022549394.1
RAD21-1	*O. sativa*	BAS75717.1
RAD21-2	*O. sativa*	BAS89814.1
RAD21-3	*O. sativa*	BAT04628.1
REC8	*O. sativa*	BAF18340.1
RAD21-1	*Z. mays*	ACN33882.1
RAD21-2	*Z. mays*	PWZ43924.1
RAD21-3	*Z. mays*	ACN33677.1
REC8	*Z. mays*	NP_001105829.1

The first one is built by RAD21-3 of dicots with RAD21-1 proteins of monocots. The second consists of the meiotic specific REC8 proteins while the third one is formed by the RAD21-1 of dicots with the RAD21-2 of monocots. The RAD21-2 proteins of dicots does not cluster with the RAD21-3 of monocots, that are closer related to the meiotic REC8 proteins, indicating that RAD21.2 of dicots represent a special form of α-kleisins (Fig.9).

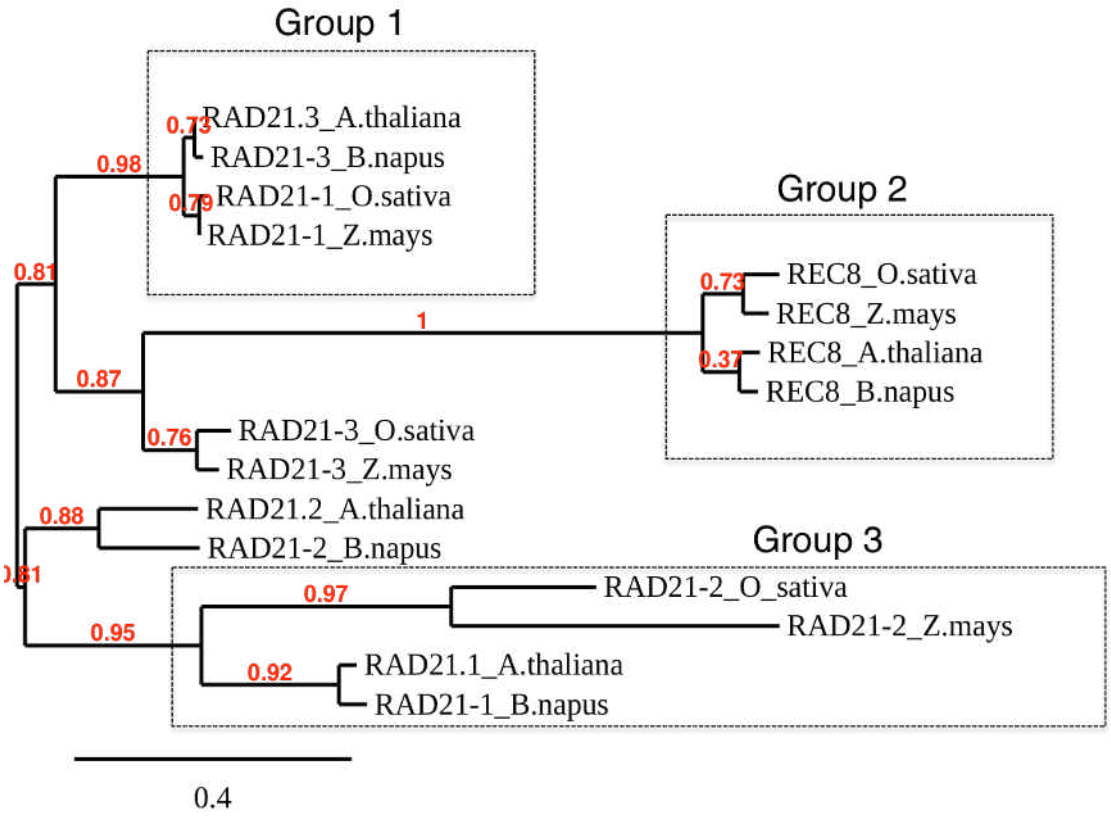

Figure 9: Phylogentic tree of α-kleisin proteins of different species generated with "One Click" Mode from Phylogeny.fr.

2.2.2 Localization of RAD21 proteins in mitosis

To determine the expression and localization pattern of RAD21 proteins in *Arabidopsis thaliana*, genomic reporter constructs of RAD21.1, RAD21.2 and RAD21.3 were generated. For the constructs, GFP was inserted at the C-terminus of the respective gene. Since single and double mutants of *RAD21.1* and *RAD21.3* do not show any obvious phenotype, it was not possible to perform rescue experiments with the corresponding reporter constructs. However, the localization analysis of these reporters revealed that both proteins are expressed in somatic tissues like in root cells (Fig. 10). A fluorescence signal of both proteins was found to be equally distributed in the nucleus of interphase root cells. Furthermore, for $Pro_{RAD21.1}$*:RAD21.1:GFP* and $Pro_{RAD21.3}$*:RAD21.3:GFP* a fluorescence signal was found in between the two halves of a spindle, which could be visualized by using the tubulin reporter construct Pro_{RPS5}*:RFP:TUA5* (Fig. 10, aII and bII). This observation matches

with reports about localization patterns of cohesin complex proteins from other organisms (Stanvitch and Moore, 2008).

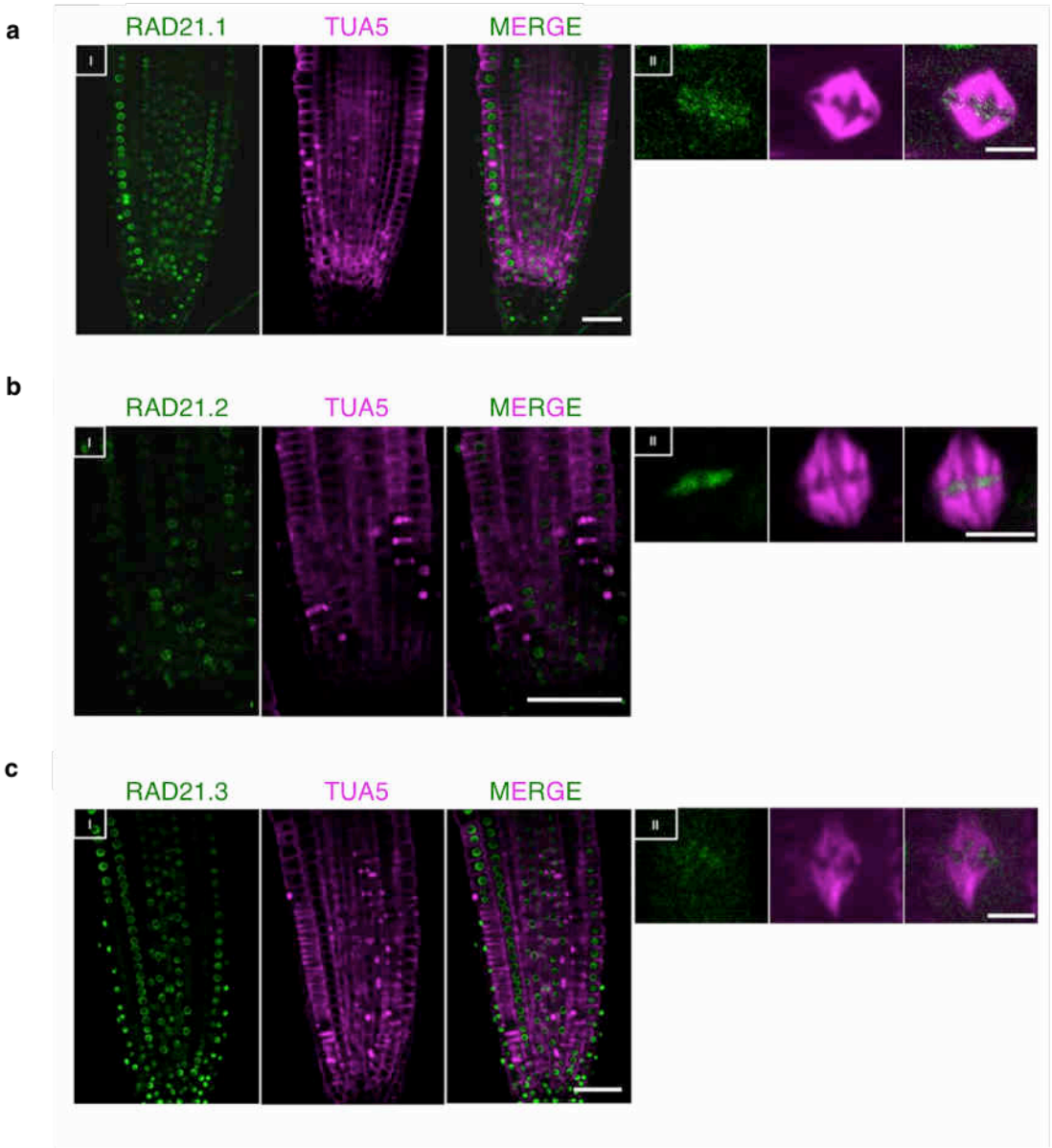

Figure 10: Confocal laser scanning micrographs of Arabidopsis root tips expressing *Pro$_{RPS5}$:RFP:TUA5* (magenta) together with *Pro$_{RAD21.1}$:RAD21.1:GFP* (a), *Pro$_{RAD21.2}$:GFP:RAD21.2* (b) and *Pro$_{RAD21.3}$:GFP:RAD21.3* (c) (green). (I) Overview of the root tip. (II) Close up showing the localization pattern of RAD21 fusion proteins on chromosomes in the metaphase plane. Scale bar in (I): 50 μm and in (II): 5 μm.

In contrast to *rad21.1* and *rad21.3*, *rad21.2* homozygous mutants are not viable and heterozygous plants show reduced fertility, i.e a pollen abortion level of about 40% and a seed abortion level of about 50%, indicating a

requirement of RAD21.2 also in the gametophyte (Jiang et al., 2007). It was possible to generate 25 independent lines that expressed *Pro$_{RAD21.2}$:RAD21.2:GFP*. However, I could only find plants with a *rad21.2* homozygous background for a single line (#15) although several generations were checked. Chromosome spreads of PMCs revealed that line #15 was tetraploid and therefore it was not analysed further. Localization studies showed that the resulting fluorescence signal in the *Pro$_{RAD21.2}$:RAD21.2:GFP* lines was generally very weak, thus it is possible that due to higher copy number the expression of RAD21.2 reached the necessary expression level in the tetraploid allowing for rescue *rad21.2* mutant phenotype. Another reason for the non-rescue by the C-terminal GFP construct could be that the fusion protein is not fully functional. Thus, a N-terminally tagged RAD21.2 reporter construct *Pro$_{RAD21.2}$:GFP:RAD21.2* was generated. In this case for one line out of 6 a complementation of the gametophytic lethality and fertility defects in *rad21.2* mutant was observed (Fig. 11).

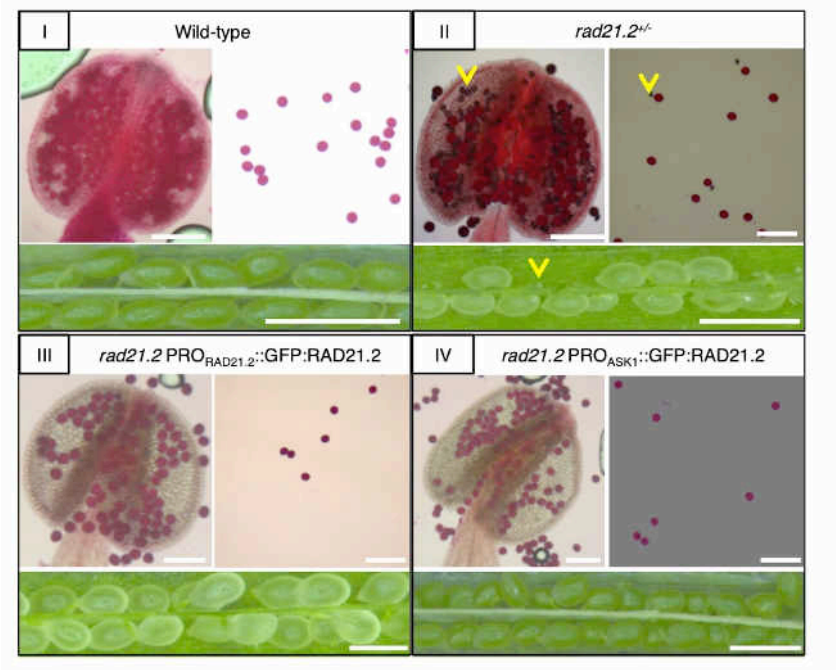

Figure 11: *RAD21.2* reporter complementation assays. Peterson staining of mature pollen. Aborted pollen are visible by blue color and shrunken appearance (arrow head). Aborted seeds are highlighted by arrowheads. Phenotype of the wild-type (I), *rad21.2* heterozygous mutants (II), and rad21.2 homozygous plants carrying the reporter construct *PRO$_{RAD21.2}$:GFP:RAD21.2* (II) and *PRO$_{ASK1}$:GFP:RAD21.2* (III). Heterozygous mutants for *RAD21.2* show a 40% pollen and 50% seed viability reduction. Scale bar for seed analysis: 1000 μm, scale bar for pollen analysis: 100 μm.

The expression analysis of plants expressing *Pro$_{RAD21.2}$:GFP:RAD21.2* in root cells exhibit a localization pattern different from what was observed for RAD21.1 and RAD21.3. In some cells, I found a weak signal of RAD21.2 that was equally distributed in the nucleus, while in cells undergoing mitosis, a strong accumulation of RAD21.2 at the metaphase plate was observed (Fig. 10). Since another fraction of root cells showed a dotty accumulation of RAD21.2, I wondered if in these cells RAD21.2 might be enriched at specific domains of the chromatin, such as the centromeres for example.

Therefore, a co-localization analysis with the centromeric reporter *Pro$_{CENH3}$:CENH3:RFP* was conducted. Interestingly, a partial co-localization of RAD21.2 and CENH3 was seen in cells where RAD21.2 displayed the dotty pattern, indicative of a pericentromeric localization of RAD21.2 (Fig. 12a, arrow). However, there were also regions of RAD21.2 accumulation where there was no CENH3 staining in close proximity (Fig. 12a, star).

Since not all of the analyzed root cells exhibit a dotty pattern, I suspected a cell-cycle dependent localization of RAD21.2. To more closely describe the RAD21.2 distribution with respect to cell cycle progression, I combined my RAD21.2 reporter with the S-phase marker PCNA1 (Fig. 12b) (Yokoyama et al., 2016). This reporter is evenly distributed in the nucleus in G_1 while in early S phase, a fine-grained dotty signal of PCNA1 is found which changes to larger speckles in late S phase. In G_2 an even distribution can be observed again and no PCNA signal is found during M-phase.

In my co-localization study, I found cells that showed an even distribution of PCNA1 and had either no RAD21.2 staining, an even distribution of RAD21.2 or a dotted structure. When PCNA1 showed its early S-phase distribution, i.e. fine- grained dots, the RAD21.2 signal was weakly co-localized, while I saw a distinct dotty RAD21.2 signal when PCNA1 formed larger speckles indicative of late S-phase.

Assuming that RAD21.2 behaves like a bona fide alpha-kleisin, I hypothesize that cells showing an even PCNA1 and no RAD21.2 signal are in early G_1 phase, while cells with even PCNA1 and even RAD21.2 would represent cells a little later in G_1. Since S-phase can be nicely resolved by the characteristic

PCNA1 dynamics, I can state that in early S-Phase, RAD21.2 shows diffuse dots, while they are more distinct in late S-phase.

The dotty pattern of RAD21.2 coinciding with an even PCNA1 distribution might correspond to G_2 phase and indicate a successful loading of the cohesin complex to the chromosomes. However, for a detailed analysis of the loading mechanism of RAD21.2, a co-localization analysis with a G_1 or G_2 cell phase marker or an observation of the double reporter line PCNA1 RAD21.2 line by live-cell imaging is required.

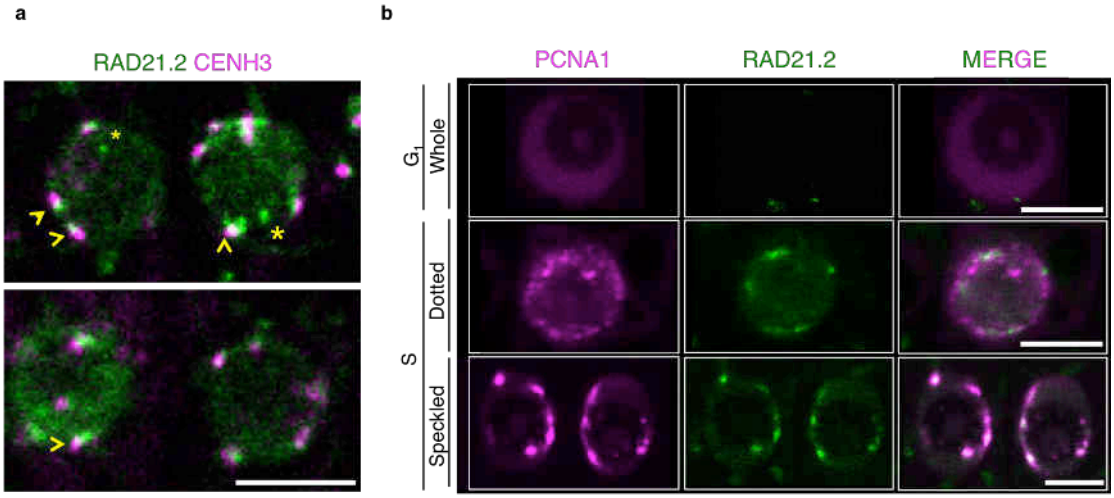

Figure 12: Confocal laser scanning micrographs of *Arabidopsis* root tip cells expressing *Pro$_{RAD21.2}$:GFP:RAD21.2* (green) together with *Pro$_{CENH3}$:CENH3:RFP* (magenta) (left panel) or *Pro$_{PCNA1}$:PCNA1:RFP* (magenta) (right panel). Left panel depicts a pericentromeric localization of RAD21.2 (arrow head). RAD21.2 dots with no co-localization of CENH3 are indicated by a star. The right panel indicates a cell-cycle dependent dynamics of RAD21.2 in root cells. Scale bar: 5 μm

The co-localization analyses with CENH3 and PCNA1 both indicate an accumulation of RAD21.2 in heterochromatic regions, since heterochromatic regions are found close to the centromeres and are replicated in late S phase. To investigate this further, the marker *Pro$_{H2A.W.6}$:H2A.W.6:RFP* was used (Yelagandula et al., 2014). The H2A.W6 protein is a histone variant that is specific for heterochromatic regions. Indeed, when I analyzed root cells of plants co-expressing *Pro$_{H2A.W.6}$:H2A.W.6:RFP* and *Pro$_{RAD21.2}$:GFP:RAD21.2* I saw that the characteristic RAD21.2 dots correspond to regions of strong H2A.W.6 signal was (Fig. 13).

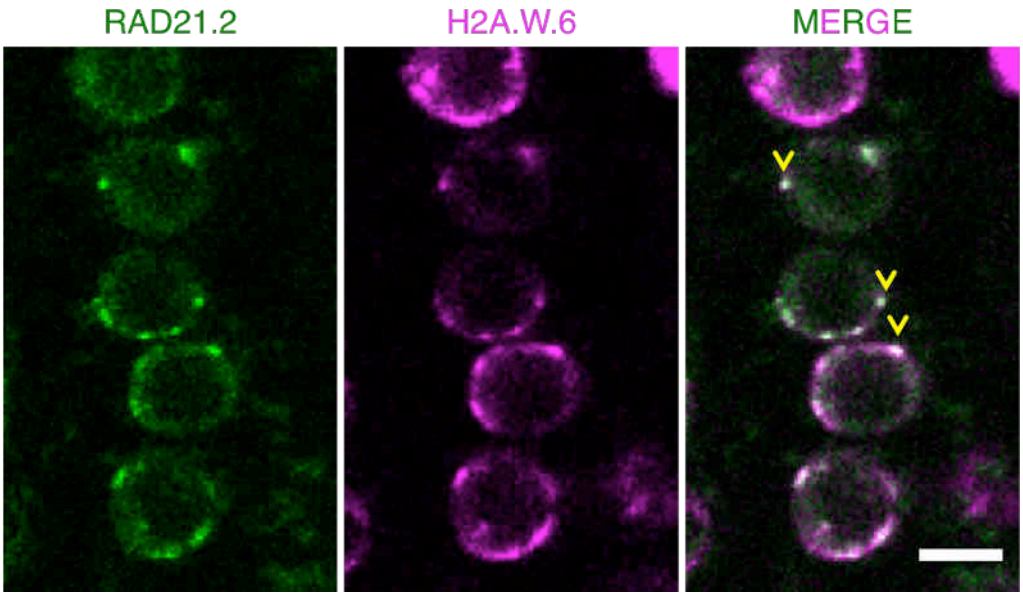

Figure 13: Confocal laser scanning micrographs of Arabidopsis root tip cells expressing *Pro$_{RAD21.2}$:GFP:RAD21.2* (green) together with *Pro$_{H2A.W.6}$:H2A.W.6:RFP* (magenta) showing a co-localization of both reporters (arrow head). Scale bar: 5 μm

Taken together, all RAD21 proteins of *Arabidopsis thaliana* are expressed in somatic tissues as exemplified here by root tip analysis. RAD21.1 and RAD21.3 exhibit a similar localization pattern that is characterized by an even distribution in the nucleus of interphase cells, while metaphase plate association is seen in mitotic cells. However, since I could not test for functionality of the respective constructs this results has to be interpreted with caution. In contrast to earlier studies that reported a localization of RAD21.2 to the nucleolus of mitotic and meiotic cells (Jiang et al., 2007), I could show here, using a functional *Pro$_{RAD21.2}$:GFP:RAD21.2* reporter, that in root cells this α-kleisins localizes to heterochromatic regions in a cell cycle dependent manner.

2.2.3 Localization of RAD21 proteins in meiosis

As a first indication, whether the RAD21 proteins also play a role in meiosis, the expression of the reporter constructs was analyzed in meiocytes. To facilitate a co-localization study with the meiotic specific α-kleisin REC8, we used the reporter construct *Pro$_{REC8}$:REC8:RFP* in combination with

Pro$_{RAD21.1}$:RAD21.1:GFP, *Pro$_{RAD21.3}$:RAD21.3:GFP* and *Pro$_{RAD21.2}$:GFP:RAD21.2,* respectively. An expression of all three *RAD21* genes was observed in the pre-meiotic cells and in the surrounding tissues (Fig. 14, upper panels). Mitotically dividing cells were identified by the absence of a REC8 signal. Meiotic cells could be identified by their REC8 accumulation. Similar to the observation in Arabidopsis root cells, RAD21.1 and RAD21.3 showed an expression in tapetum cells, while RAD21.3 exhibited a stronger expression level as RAD21.1 and RAD21.2 (Fig. 14c). A weak fluorescence signal was observed in meiocytes expressing *Pro$_{RAD21.1}$:RAD21.1:GFP* or *Pro$_{RAD21.3}$:RAD21.3:GFP*. In contrast, RAD21.2 showed a dotty signal in tapetum cells and slightly structured staining of the nucleus in pre-meiotic cells, including a distinct protruding into or over the otherwise unstained nucleolar region (Fig. 14b). An expression of RAD21.1 and RAD21.3 was never detected in prophase while RAD21.2 was found to decorate meiotic chromosomes from leptotene to metaphase-anaphase I transition.

Since the expression of *Pro$_{RAD21.2}$:GFP:RAD21.2* results in a very weak signal which was difficult to assign to subnuclear structures, I exchanged the native promoter against the ASK1 promoter, which is known to result in strong expression also in meiocytes. The *Pro$_{ASK1}$:GFP:RAD21.2* construct fully complemented the mutant phenotype of *rad21.2* (Fig. 11). Thus, these complementing lines were used for further analysis of RAD21.2 protein behavior.

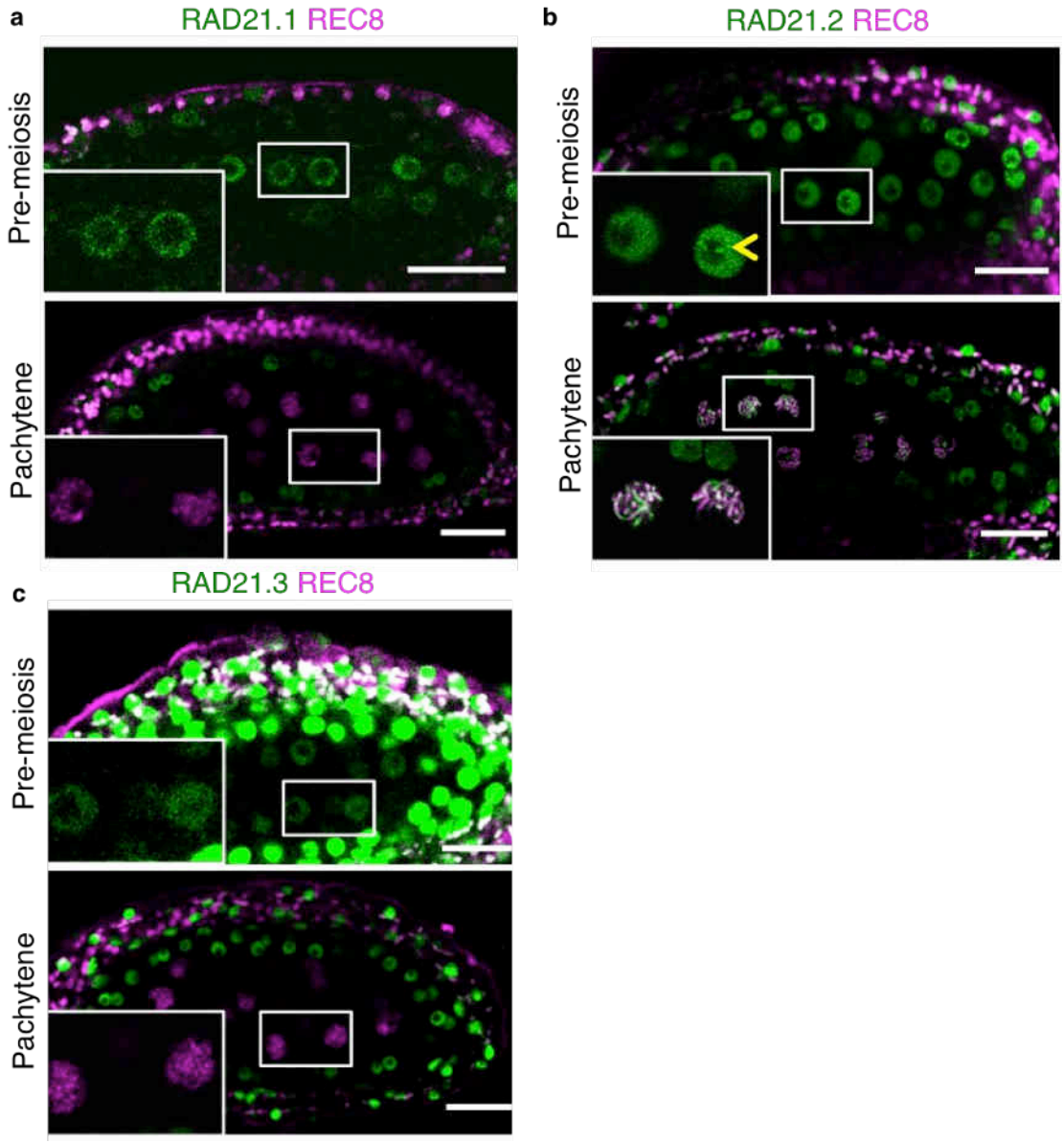

Figure 14: Confocal laser scanning micrographs of Arabidopsis anthers expressing *Pro$_{REC8}$:REC8:RFP* (magenta) together with either *Pro$_{RAD21.1}$:RAD21.1:GFP* (green), *Pro$_{ASK1}$:GFP:RAD21.2* (green) or *Pro$_{RAD21.3}$:RAD21.3:GFP* (green). Upper row, RAD21.1, RAD21.2 and RAD21.3 but not REC8 are present in all cells prior to meiosis (close-up highlighted in box). Note the thread-like structure decorated by RAD21.2 reaches into or over the nucleolar region (arrow head). Lower row, next to REC8, only RAD21.2 out of the three RAD21 proteins accumulates in meiosis (here pachytene stage) and decorates chromosomes. Scale bar: 20 μm.

A detailed co-localization analysis of plants expressing *Pro$_{ASK1}$:GFP:RAD21.2* and *Pro$_{REC8}$:REC8:RFP* reveals that both cohesion proteins show a different pattern during prophase I (Fig. 15). The even distribution of REC8 stands in contrast to a more patchy appearance of RAD21.2. Interestingly, RAD21.2 strongly accumulates on chromosomes in the vicinity of the nucleolus from

leptotene through zygotene till early pachytene. A REC8 signal was very weak or absent in these accumulation regions of RAD21.2 in direct proximity of the nucleolus (Fig. 15). In late pachytene, the chromosomal regions enriched with RAD21.2 do not cluster anymore and become more diffusely distributed in the nucleus. During metaphase I, the fluorescence intensity of *Pro$_{ASK1}$:GFP:RAD21.2* increases likely due to the condensation of chromosomes (Fig. 15). However, such a strong increase in signal was not observed for REC8. At anaphase I onset, the RAD21.2 signal has completely disappeared and a re-appearance after anaphase I was never detected during the course of meiosis.

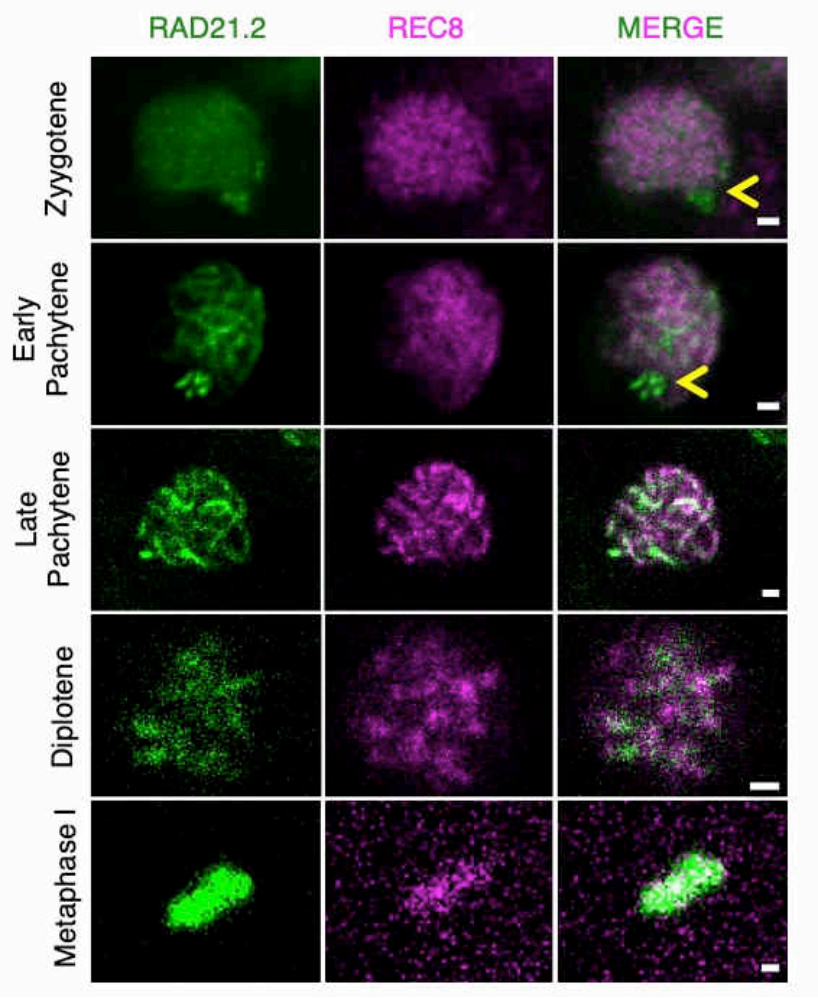

Figure 15: Confocal laser scanning micrographs of male meiocytes revealing distinct and partially overlapping localization patterns of *Pro$_{ASK1}$:GFP:RAD21.2* (green) and *Pro$_{REC8}$:REC8:RFP* (magenta). Notably, RAD21.2 is enriched at nucleolar chromatin (arrow head) in early prophase I. Scale bar: 1 μm.

Also, RAD21.2 is still not found in the post-meiotic tetrad stage (Fig. 16). However, a new RAD21.2 signal was observed from microspores stage onwards (Fig. 16). This further supports the hypothesis that RAD21.2 is loaded on chromosomes during S-phase since microspores have to undergo one round of DNA replication before entering into the first pollen mitosis.

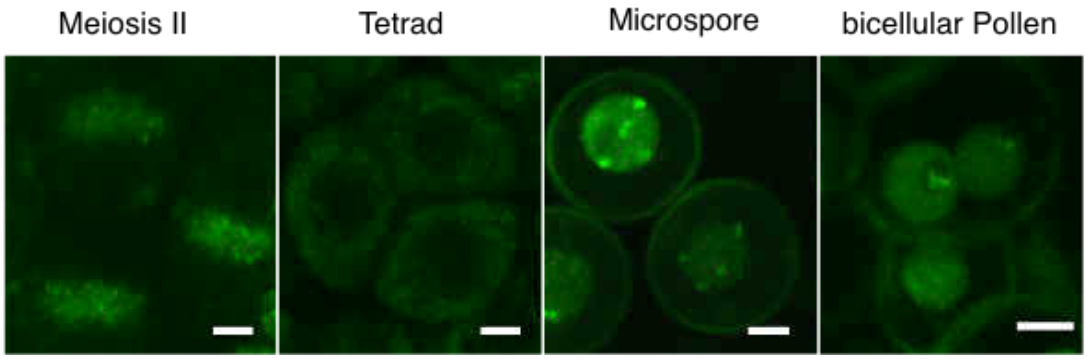

Figure 16: Confocal laser scanning micrographs of cells expressing *Pro$_{ASK1}$:GFP:RAD21.2* (green) at the end of meiosis II, here the autofluorescense of the organellar band becomes visible, tetrads do not exhibit a nuclear RAD21.2 signal, microspore and bicellular pollen stage show a strong nuclear accumulation of RAD21.2. Scale bar: 1 μm.

To address the question, if RAD21.2 also associates preferentially with heterochromatic regions in meiocytes, I combined the reporter for heterochromatin *Pro$_{H2A.W.6}$:H2A.W.6:RFP,* with the strong expressing RAD21.2 reporter *Pro$_{ASK1}$:GFP:RAD21.2* (Fig. 17a). By detailed confocal analysis, I found that when RAD21.2 is predominantly enriched close to the nucleolus at zygotene stage this region is clearly marked by the histone variant H2A.W.6 (Fig. 17a). Also at pachytene, regions with strong Rad21.2 accumulations were marked by H2AW.6. A quantification of the RAD21.2 fluorescence signal at H2A.W.6 regions compared to non- H2A.W.6 regions revealed that RAD21.2 is 2.74 times more enriched in heterochromatic as opposed to non-heterochromatic regions (Fig. 17b). In diplotene, RAD21.2 staining regions clustered and partially co-localized with H2A.W.6.

An especially interesting pattern was observed for metaphase I cells. Looking at metaphase chromosomes perpendicular to the spindle, RAD21.2 is found at an inner layer of the metaphase I plate, while H2A.W.6 seems to extend to

regions flanking this RAD21.2 positive region. From other localization analysis, it is well known that the centromeres face the spindle poles while the chromosome arms localize more centrally and are still linked by crossovers (Ravi et al., 2010). If the strong H2A.W.6 staining regions flanking the RAD21.2 signal at metaphase I indeed represent centromeres could be tested by co-localization analysis with the centromere marker CENH3.

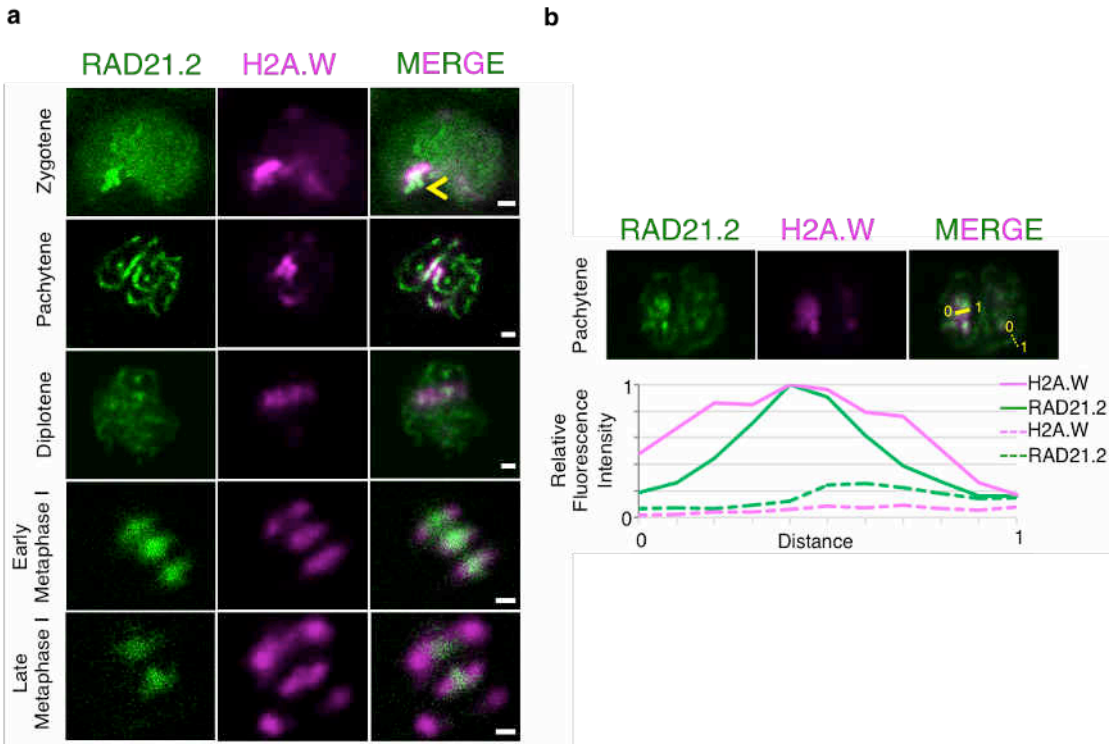

Figure 17: Confocal laser scanning micrographs of male meiocytes expressing *Pro$_{ASK1}$:GFP:RAD21.2* and *Pro$_{H2A.W.6}$:H2A.W.6:RFP*. Left panel indicates that H2A.W.6 (magenta) largely co-localizes with a sub-fraction of the RAD21.2-marked chromatin (green), for instance in the perinucleolar region (arrow head). Scale bar: 1 μm. Right panel shows the quantification of the overlap between H2A.W.6 and RAD21.2 performed by Dr. Yuki Hamamura. Upper row indicates a region in the perinuclear region (yellow line) and a region distant from the nucleolus (dashed line) used for quantification. Lower row: Profile plot of the relative fluorescence intensities of RAD21.2 (green lines) and H2A.W (magenta lines) in the nucleolar area (solid line) and outside of the nucleolus (dashed line). The fluorescence intensities were normalized to the highest fluorescent value (set to one). Scale bar: 1 μm.

A hallmark of heterochromatic regions is an elevated level of GC methylation of the DNA. Therefore the methylation marker *Pro$_{HTR5}$:MBD6:RFP* was introduced into a *Pro$_{ASK1}$:GFP:RAD21.2* expressing line. To concomitantly

visualize the nucleolus, a third marker, i.e *Pro$_{FIB2}$:FIB2:TFP* was added. Detailed observation of this triple marker line further supported the hypothesis that RAD21.2 is enriched at heterochromatin since pachytene cells showed an evaluated binding of RAD21.2 to highly methylated chromatin regions, identified by strong MBD6 staining (Fig. 18). Furthermore, I did not observe co-localisation with Fibrillarin 2 (FIB2) at late pachytene stage. Thus I conclude that RAD21.2 mainly binds to heterochromatin in the nucleoplasm and not in the nucleolus. However, in early pachytene the largest and most concentrated RAD21.2 patch is found in close proximity to the nucleolus.

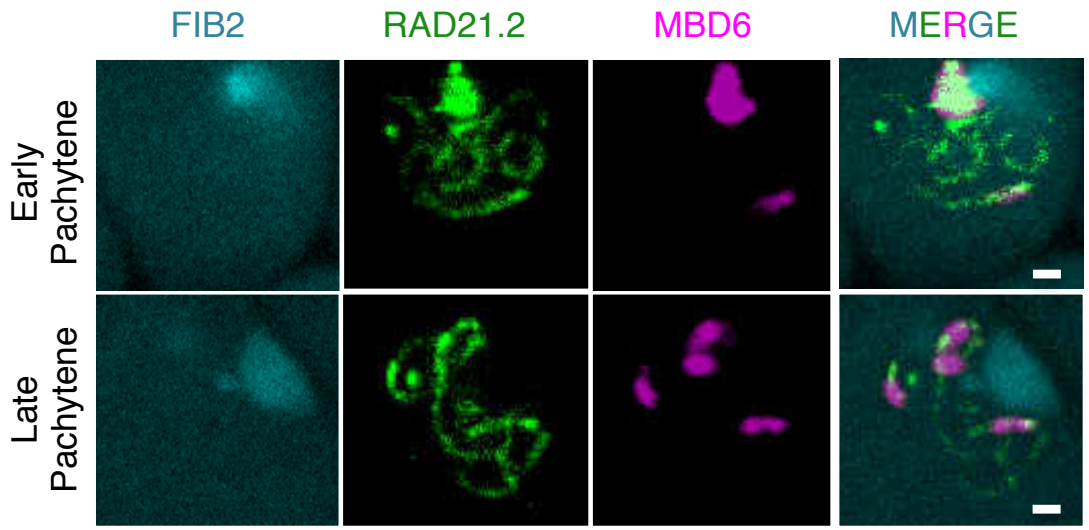

Figure 18: Confocal laser scanning micrographs of meiocytes expressing the nucleolus reporter *Pro$_{FIB2}$:FIB2:Turq* (cyan), *Pro$_{ASK1}$:GFP:RAD21.2* (green) and *Pro$_{HTR5}$:MBD6:RFP* (magenta). Representative images showing highly methylated DNA regions, which are decorated by RAD21.2, clustered in the proximity of the nucleolus at early pachytene (upper row) and a distributed pattern during the dissolution of the nucleolus in late pachytene (lower row). Scale bar: 1 μm.

Taken together, my analysis of RAD21 protein expression in meiocytes revealed that RAD21.1 and RAD21.3 do not seem to be expressed, while in contrast to previous studies RAD21.2 could be shown to localize to meiotic chromosomes until metaphase I. Interestingly, I could show that RAD21.2 is enriched at heterochromatic regions contrary to the even distribution of the other α-kleisin proteins of *Arabidopsis thaliana*. Furthermore, my data

supports the hypothesis that RAD21.2 is loaded during S-phase preceding a mitotic or meiotic division.

2.2.4 Analysis of RAD21.2 interacting proteins

Based on the above described localization data, it is likely that RAD21.2 functions as a α-kleisin, which was put in question due to an earlier publication showing RAD21.2 accumulation in the nucleolus and thus suggesting a role in rDNA transcription (Jiang et al., 2007). Another indication for α-kleisin function would be a strong co-localization with other cohesin core components. Indeed, in root cells, showing an even distribution of RAD21.2 in the nucleus, a similar localization pattern was seen for SMC1 using *Pro$_{SMC1}$:SMC1:Turq* described in chapter II in more detail (Fig. 36). However, I did not observe any root cells that showed a patchy RAD21.2 like accumulation of SMC1. Unfortunately, the expression of the *Pro$_{SMC1}$:SMC1:Turq* reporter was very weak with a high background signal in the cytoplasm (Fig. 19), so local enrichment might have been difficult to discern.

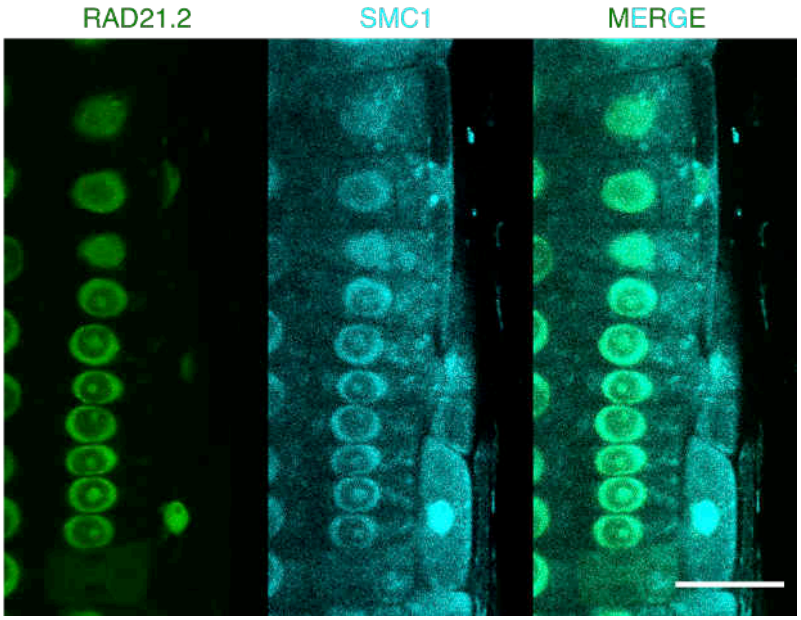

Figure 19: Confocal laser scanning micrographs of root ccells expressing the cohesin reporter *Pro$_{ASK1}$:GFP:RAD21.2* (green) and *Pro$_{SMC1}$:SMC1:mTurq* (cyan). Scale bar: 20 μm.

To directly test, if RAD21.2 is able to interact with other cohesin complex proteins, Yeast two hybrid (Y2H) assays were performed. RAD21.2 was fused to the GAL4 activation domain (AD) and was used as the prey. The bait constructs were built by the fusing the GAL4 DNA binding domain (BD) to SMC1 or SCC3. The bait and prey constructs were co-transformed into the yeast strain AH109. Double transformed yeast colonies were selected on SD media, lacking leucine and tryptophan. In case of interacting proteins, the GAL4 transcription factor is reconstituted and facilitates the synthesis of the amino acid histidine. Therefore, an interaction is visualized by yeast growth on media also lacking histidine.

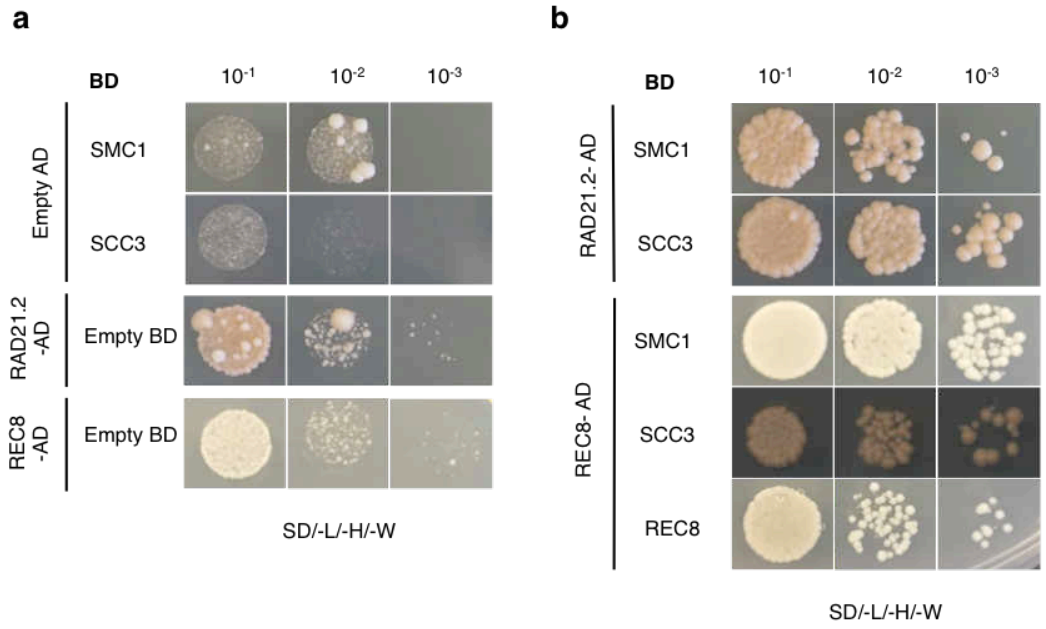

Figure 20: Yeast two-hybrid interaction assay of RAD21.2 and REC8 with the core cohesin components SMC1 and SCC3. The left panel shows the autoactivation test for the respective BD/AD constructs. The right panel shows the evaluation of the interaction. Different dilutions of yeast (10^{-1}/10^{-2}/10^{-3}) were spotted on SD plates lacking leucine, tryptophan and histidine (-L/-H/-W) to test for interaction strength.

For RAD21.2-AD and REC8-AD an interaction with SMC1-BD and SCC3-BD were discovered (Fig. 20b). Neither for SCC3 nor SMC1 an autoactivation was detected (Fig. 20a). Therefore, an interaction of RAD21.2 and REC8 with other core cohesin proteins could be confirmed. Importantly, an interaction of RAD21.2 and REC8 with SCC3 has never been shown so far. Furthermore, a

homodimerization of REC8 was observed. This couldn't be tested for RAD21.2 since the RAD21.2-BD construct displayed a strong autoactivation (tested by Dr. Chao Yang).

To confirm an interaction of RAD21.2 with the core cohesin components *in vivo* a Co-IP analysis was performed. However, the limited number of meiocytes makes biochemical analyses of meiotic proteins difficult. To overcome the limited yield of meiotic cells, *35S:AP1-GR ap1cal* mutant plants, which show synchronized flower development, were used (Wellmer et al., 2006). The ap1 cal mutant background leads to an over-proliferation of an inflorescence-like meristem in which flower development is blocked. Due to the presence of the *35S:AP1-GR ap1cal* construct, AP1 transcription factor activity can be induced by treatment with the steroid hormone dexamethasone which leads to the induction of flower formation, i.e. to a massive formation of synchronized flower buds.

First, total protein was extracted from flower buds of *35S:AP1-GR ap1cal* 8-9 dai plants that were transformed with the reporter construct *Pro$_{RAD21.2}$:GFP:RAD21.2.* To identify RAD21.2 specific interactors, I also extracted total protein from *35S:AP1-GR ap1cal* plants co-expressing REC8:GFP as a control. After total protein extraction an immunoprecipitation using anti-GFP antibody coupled to a magnetic bead column was performed. In previous studies, it was shown that using this approach an enrichment of REC8 from Arabidopsis flower buds was possible (Master thesis VK). Similarly, I tested here whether the purification and enrichment of RAD21.2 was equally feasible. Thus, aliquots of the wash and elution fraction of the anti-GFP column loaded with GFP:RAD21.2 were separated by SDS-PAGE and analyzed by Western Blot using an anti-GFP antibody as a primary antibody. In the eluted fraction (E) a band around 100 kDa could be detected (Fig. 21). This corresponds with the predicted size of RAD21.2 (about 77 kDa) plus the GFP size (27 kDa).

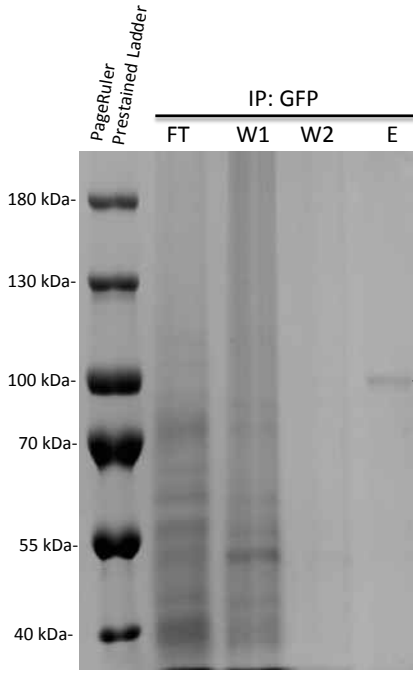

Figure 21: Western blot analysis of GFP:RAD21.2 protein purified from *35S:AP1-GR ap1cal* $Pro_{RAD21.2}$*:GFP:RAD21.2* flower buds. For total protein extraction 5 g flower buds were harvested and 15 ml extraction buffer were used. 20 µl of flow through (FT), wash fractions (W1/W2) and elution (E) were used for SDS-PAGE. A primary anti-GFP (1:100) and a secondary anti-mouse antibody were used to detect GFP:RAD21.2.

The eluted fraction of columns loaded with eiter REC8:GFP or GFP:RAD21.2, were used for MS-MALDI-TOF analysis at the Max Planck institute by the group of Dr. Hirofumi Nakagami. In a second analysis the same purification and analysis procedure was used for protein extracts from seedlings either Pro_{ASK1}*:GFP:RAD21.2* or Pro_{35S}*:GFP* as control.

In both RAD21.2:GFP setups I could detect RAD21.2 in the elution fraction, indicating a successful extraction from somatic and reproductive tissue. 31 peptides correlating to the RAD21.2 protein were identified with sequence coverage of 55% in the reproductive sample. In the somatic sample, 12 peptides could be found with sequence coverage of 33%.

Furthermore, for RAD21.2 an analysis of phosphorylated peptides was performed and led to the identification of 10 phosphorylated sites within the protein sequence of RAD21.2 (Fig. 22). In addition, I looked for potential separase cleavage sites with the consensus sequences ExxR or DxxR within the RAD21.2 sequence. Since a proximity of REC8 phosphorylation sites to

the consensus sequence was shown to be required for yeast, I found in total, six potential phosphorylation sites that might be important for a separase-dependent cleavage of RAD21.2.

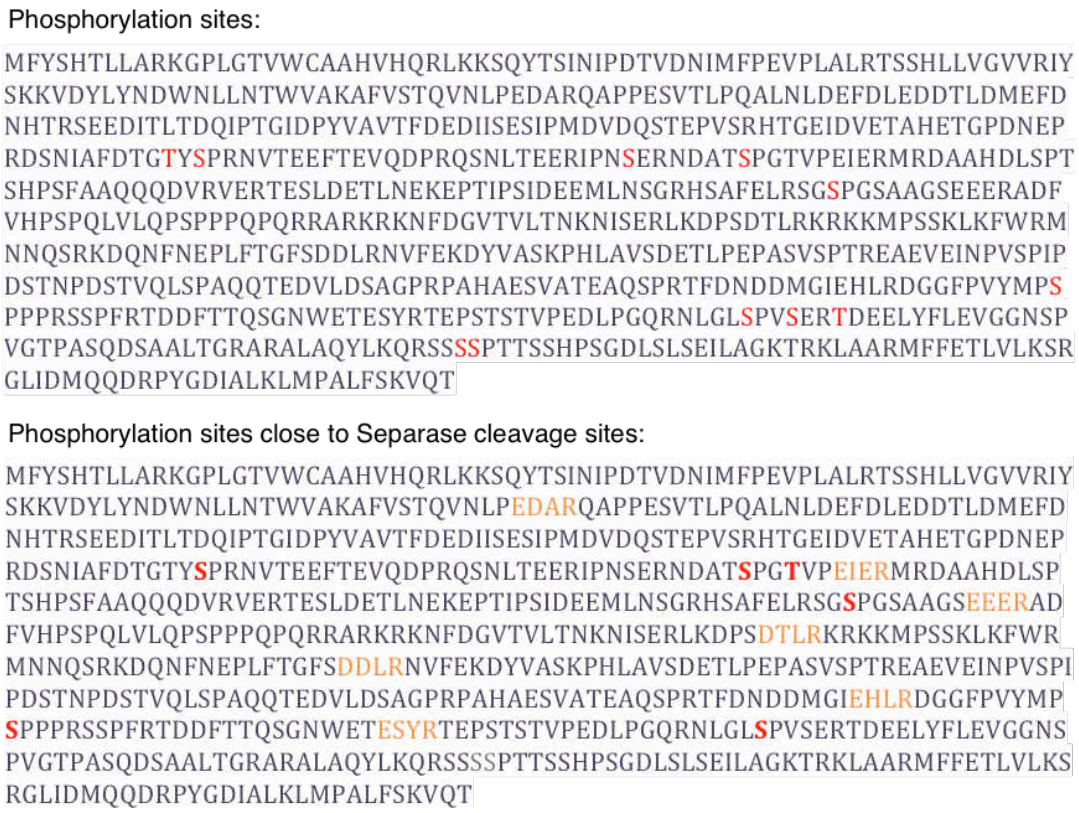

Figure 22: Phosphorylation sites within the RAD21.2 protein sequence identified by mass spectrometry. Upper panel represents all phosphorylation sites highlighted in red. Lower panel shows potentially important phosphorylation sites that are important for a cleavage by the separase. Separase cleavage sites (ExxR/DxxR) have been identified by the ExPasy web tool and are highlighted in orange.

In the RAD21.2 as well as in the REC8 purification, the other I core cohesin proteins could also be identified. For SMC1 and SMC3 around 50 peptides were identified with sequence coverage of 35% in the reproductive sample The enrichment in comparison to the control is significant and shown in the volcano plots (Fig. 23).

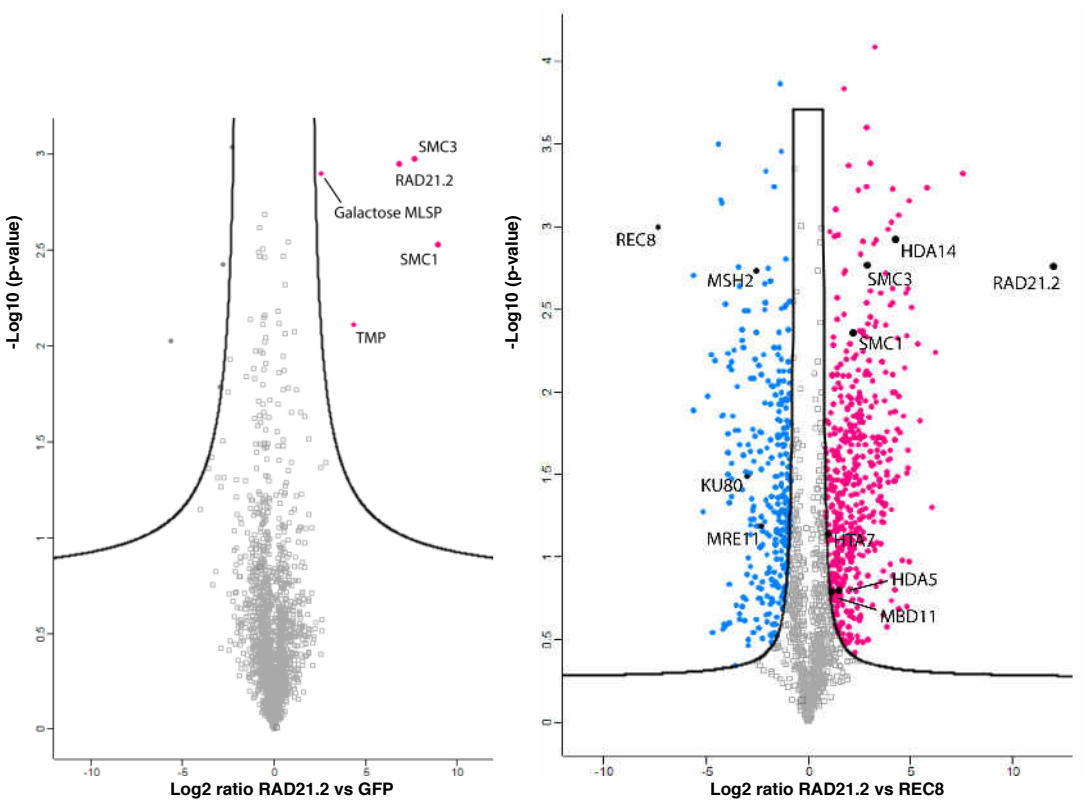

Figure 23: Volcano plot of proteins identified by mass spectrometry. The x-axis depicts the fold change value and the y-axis shows the significance by the –log 10 (p-value). Left plot: Proteins were extracted from seedlings. Interaction partners that are significantly enriched in the RAD21.2 IP sample are shown in magenta. Significantly enriched proteins of the GFP control sample are shown in blue. Other identified proteins are shown in grey. Right plot: Proteins were extracted from flower buds. Interaction partners that are specifically and significantly enriched in the RAD21.2 IP sample are shown in magenta, those specifically and significantly enriched in REC8 IP are shown in blue. Other identified proteins are shown in grey.

Among the proteins significantly enriched in the RAD21.2 purification from flower buds, I also identified several proteins functionally linked to heterochromatin (Fig. 23, highlighted in black), i.e H2A.W7 (p=0.07), encoding a heterochromatin associated histone variant H2A.W, MBD6 (p=0.16), a protein that binds methylated DNA and HDA14 (p=0.001) and HDA5 (p=0.15), two histone deacetylases. On the other hand, I found that MSH2 (p=0.002) and MRE11 (p=0.06), both involved in homologous recombination repair, were specifically enriched in the REC8 interactome.

Taken together, our IP data shows that RAD21.2 binds to the core cohesin complex proteins *in vivo*. Most interesting, the generated mass spectrometry data supports that RAD21.2 is found in a heterochromatic environment.

2.2.5 WAPL-dependent prophase I pathway

After confirmation that RAD21.2 builds a cohesin complex *in vivo*, we analyzed whether RAD21.2 is similarly regulated to REC8 in prophase I. For REC8 it was recently shown that it is already removed from the chromosomes before metaphase I (Yang et al., 2019). This process is referred as prophase pathway of cohesion removal and relies on the triple AAA+ ATPase WAPL and not on the separase that is responsible for cohesin removal at metaphase I. In Arabidopsis, two functionally redundant proteins *WAPL1* and *WAPL2* have been identified (for more information see introduction). In *wapl1 wapl2* double mutants, REC8 over-accumulates in meiosis I indicating that the prophase pathway of cohesion removal is (De et al., 2014).

To test for a similar regulation of RAD21.2, the Pro_{ASK1}*:GFP:RAD21.2* reporter was transformed in *wapl1 wapl2* mutants. In collaboration with Dr. Yuki Hamamura, I performed live cell imaging of wild-type and *wapl1 wapl2* mutant meiocytes expressing Pro_{ASK1}*:GFP:RAD21.2.* We analyzed the RAD21.2 fluorescence intensity of meiocytes over time in prophase I. In wild-type, an even distribution of the RAD21.2 fluorescence signal was found in the nucleus of leptotene meiocytes (Fig. 24). Typically, thread-like structures that loom into the nucleolus were found during leptotene which lasts around 4 hours and starts 23 hours before metaphase I which was set as time point zero (Fig. 25). In zygotene, persisting around six hours, the thread-like structure clusters around the nucleolus and is seen as a bright dotty signal. Furthermore, thin chromosome threads become visible in the rest of the nucleus. In pachytene, thicker threads are found likely representing the fully paired chromosmes. As described before some chromosome regions show an enhanced RAD21.2 signal. From diplotene to diakinesis the chromosomes de-condensate resulting in a weaker signal of RAD21.2. At metaphase, RAD21.2 is found on the chromosomes at metaphase I plane.

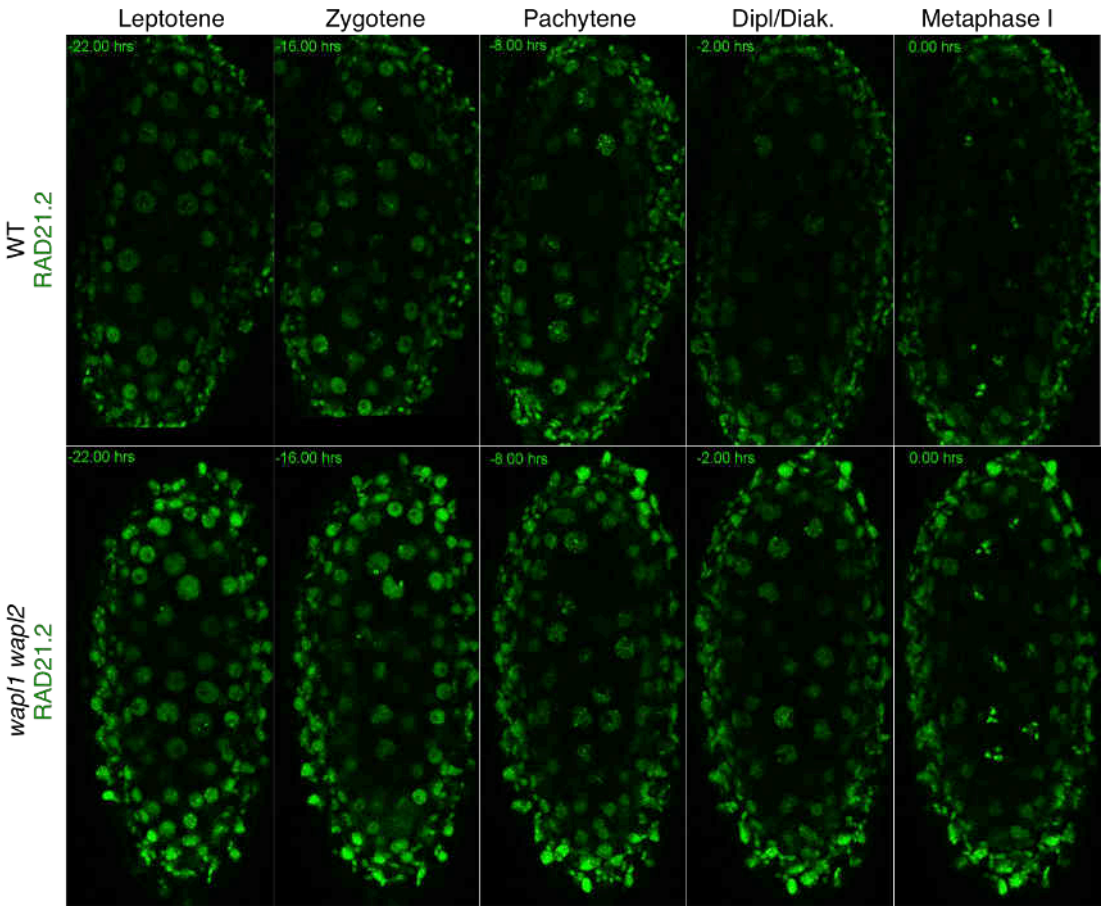

Figure 24: Confocal laser scanning micrographs of wild-type (upper panel) and *wapl1 wapl2* (lower panel) male meiocytes expressing *Pro$_{ASK1}$:GFP:RAD21.2* (green). Representing the dynamics of RAD21.2 during prophase I. Notably, a similar dynamics and fluorescence intensity from leptotene to metaphase I was observed in wild-type and *wapl1 wapl2* mutants.

Interestingly, no obvious differences of the RAD21.2 localization pattern or dynamics were observed in *wapl1 wapl2* mutants in comparison to wild-type (Fig. 24). This was confirmed by a quantitative analysis of the fluorescence signal intensity, in which we used three abthers for each genotype. RAD21.2 signal intensity over time was analyzed for at least 9 meiocytes per anther and the highest intensity was set to 100%. In both analyses, the highest fluorescence intensity of RAD21.2 was observed at the end of zygotene (Fig. 25).

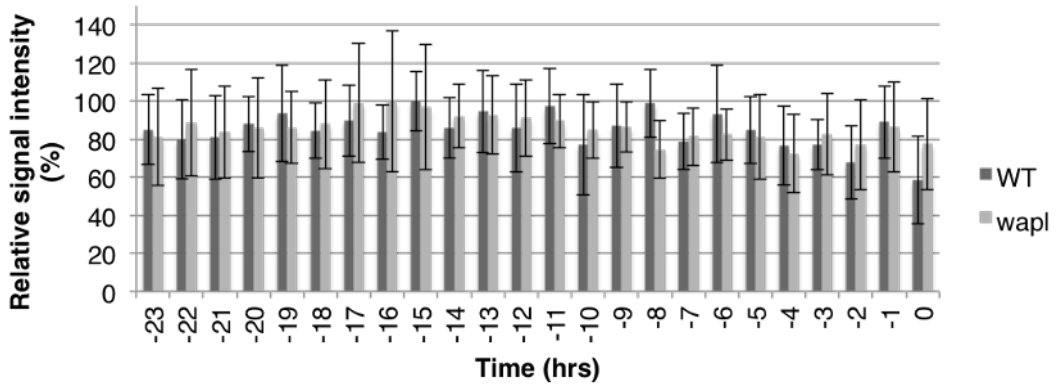

Figure 25: Representative quantification of the relative *Pro$_{ASK1}$:GFP:RAD21.2* fluorescence intensity levels in wild-type (dark grey) versus *wapl1 wapl2* (light grey) meiocytes over time. At least 9 meiocytes were analyzed per genotype; error bars depict the standard error.

Taken together, we did not see any alteration of the *Pro$_{ASK1}$:GFP:RAD21.2* signal intensity and distribution in *wapl1 wapl2* mutant compared to the wild-type, indicating that RAD21.2 is not subject to the prophase cohesin removal pathway. Furthermore, this result indicates that the two meiotic α-kleisins RAD21.2 and REC8 proteins have different properties and might not be able to substitute for each other.

To further support this hypothesis, we analyzed whether constitutive strong expression of RAD21.2 by the use of the *Pro$_{ASK1}$:GFP:RAD21.2* construct could fully or partially rescue the *rec8* mutant phenotype. However, *rec8* plants expressing *Pro$_{ASK1}$:GFP:RAD21.2* are fully sterile, i.e. not even a partial rescue could be observed (Fig. 26). Furthermore, as judged by a qualitative analysis of confocal images, the intensity and distribution of RAD21.2 was apparently not different in *rec8* mutants compared to wild-type (Fig. 26).

Taken together, our data indicates that RAD21.2 functions as a α-kleisin subunit of a meiotic cohesin complex. However, it is differently regulated than REC8 and plays a distinct role during meiosis.

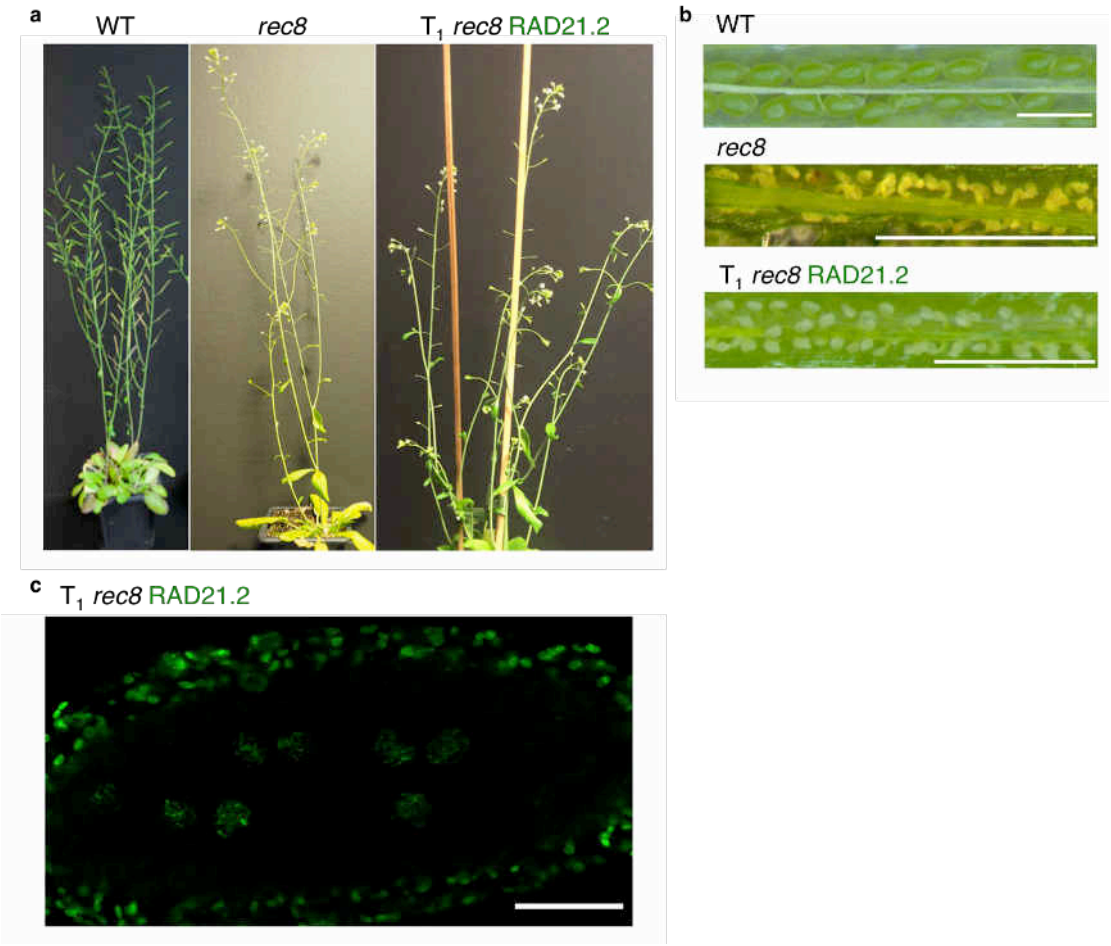

Figure 26: Expression of *Pro$_{ASK1}$:GFP:RAD21.2* does not complement the sterility of *rec8* mutants as seen by the short (a) and empty (b) siliques. Scale bar: 1000 μm. c, Confocal laser scanning micrograph of an anther expressing *Pro$_{ASK1}$:GFP:RAD21.2* in *rec8* shows the typical chromosomal localization pattern of GFP:RAD21.2 at pachytene; see figure 30 for comparison.

2.2.6 Functional analysis of RAD21.2

The functional analysis of RAD21.2 in meiosis is difficult because homozygous *rad21.2* mutant plants are gametophytic lethal (Jiang et al., 2007). Therefore we used the *RNAi* approach to reduce the expression of RAD21.2 in wild-type plants, hoping for a milder phenotype. For the generation of *RAD21.2 RNAi* lines we transformed wild-type plants with an artificial *RNAi* construct that targets 400 bp of RAD21.2 under the control of the *cauliflower mosaic virus* (*CaMV*) *35S* promoter. I recovered two transgenic lines expressing the *RNAi* construct. These plants exhibited no obvious vegetative growth defects (Fig. 26a) but showed a reduction in silique length (Fig. 27b).

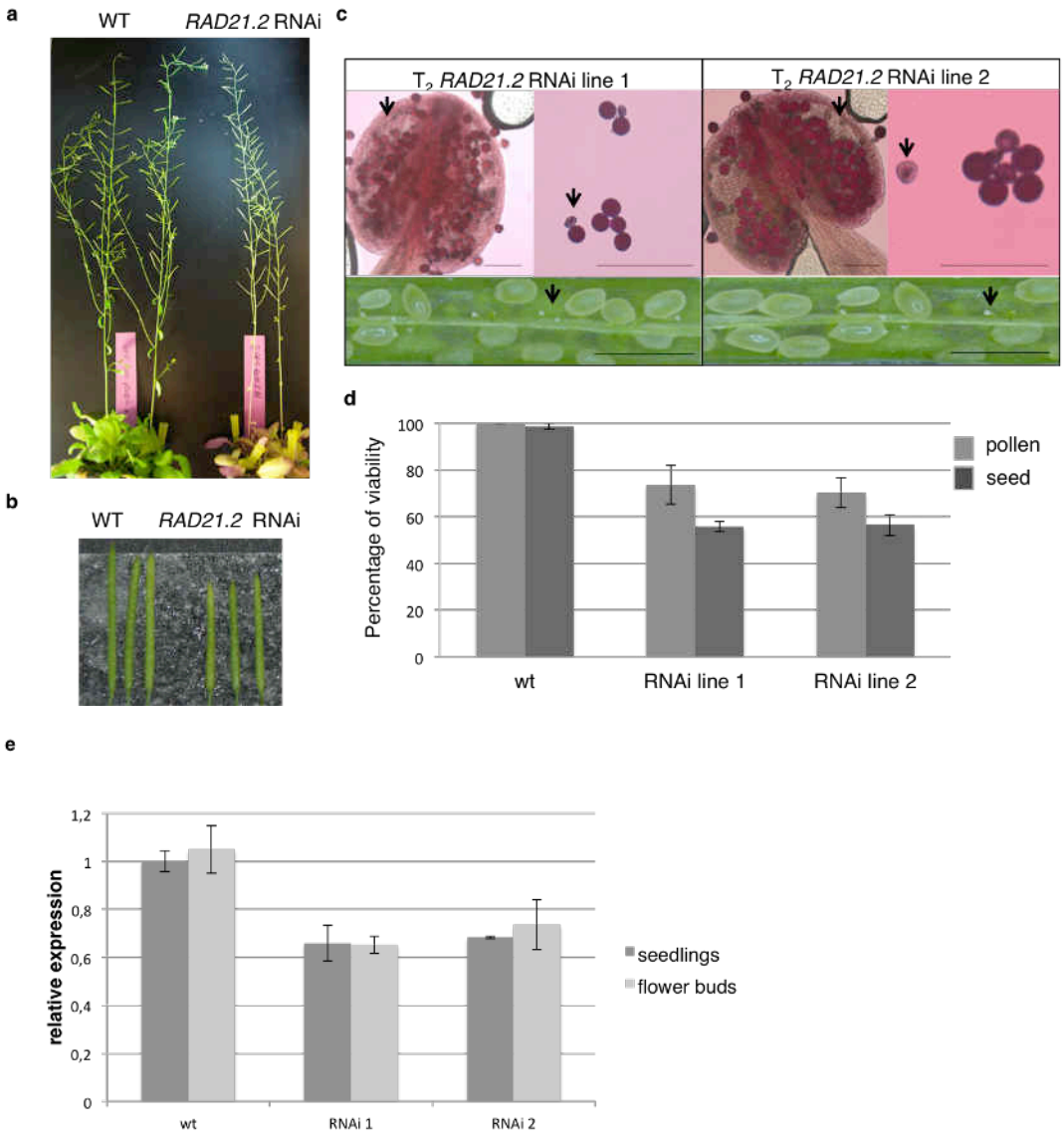

Figure 27: Phenotype of *RAD21.2* knock-down plants. a, Inflorescences of wild-type and *RAD21.2 RNAi* plants (line #1). b, *RAD21.2 RNAi* plants (line #1) have shorter siliques than the wild-type. c, *RAD21.2 RNAi* plants (line #1, left, and line #2, right) have dead pollen (one example is marked by an arrow head) and aborted and unfertilized ovules (one example is marked by an arrow head). Scale bar for silique analysis: 1000 μm, scale bar for pollen analysis: 100 μm. d, Quantification the fertility defects in *RAD21.2 RNAi* plants. e, Relative expression levels of *RAD21.2* in seedlings (dark grey) and in flower buds (light grey) in the *RAD21.2 RNAi* lines #1 and #2 compared to the wild-type (set to 1).

In detail, the RAD21.2 knock-down lines revealed an about 30% reduction in pollen viability and a seed abortion level of 45% (Fig. 27c, d). To confirm a reduction of the RAD21.2 expression *in planta*, we performed qRT-PCR that revealed a reduction in expression level of 25-35 percent compared to the wild-type (Fig. 27e).

To more closely investigate the sterility phenotype of *RAD21.2 RNAi* plants, which exhibit a reduction in fertility of around 45% (Fig. 27d), chromosome spreads of PMCs were performed. No obvious defects were observed in early meiosis (Fig. 28a) and the chromosmes of *RAD21.2 RNAi* plants are fully synapsed at pachytene. Therefore, high levels of RAD21.2 do not seem to be needed for a proper chromosome pairing and synapsis. However, it is important to mention that pairing problems still might occur if the RAD21.2 level is further reduced. During diplotene, similar to wild-type *RAD21.2 RNAi* chromosomes de-synapsed and began to re-condense at diakinesis.

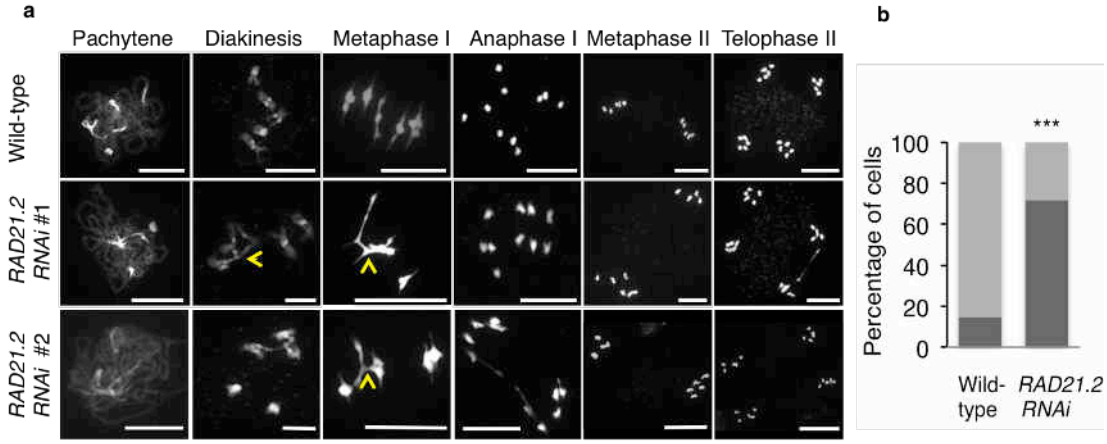

Figure 28: Chromosome spread analysis of pollen mother cells. a, Representative pictures for wild-type (upper row) spreads in comparison to *RAD21.2 RNAi* #1 and #2 plants (middle and lower row). Chromosome entanglements seen in diakinesis and metaphase I (arrow head) of *RAD21.2 RNAi* #1 and #2 PMCs. Scale bar: 10 μm. b, Graph depicting the percentage of cells with (dark grey) and without (light grey) chromosomes entanglements in metaphase I of wild-type (15% n=130) and *RAD21.2 RNAi* (72% n=130; p-value= 8.23E-27, Student's t-test).

Interestingly, meiotic defects in *RAD21.2 RNAi* plants were observed from diakinesis onwards (Fig. 28a, arrow head). In wild-type spreads, 5 bivalents separated from each other are visible at diakinesis. In contrast, five separated chromosome pools were never detected in *RAD21.2 RNAi* plants (n=63). Chromosomes appeared to be entangled and connected with each other. At metaphase I of wild-type, five distinct bivalents were detected in most of the cases, while additional chromosomes were seen in only 15% of the spreads (n=130). In contrast, 72% of the spreads of *RAD21.2 RNAi* plants showed at

least two connected chromosome pairs that showed a stretched chromosome morphology (n=130) (Fig. 28b).

Since I rarely found defects in the second meiotic division in *RAD21.2 RNAi* plants, e.g. metaphase II only 7% of the cells (n=28) showed unbalanced chromosome segregation (Fig. 28a), I conclude that meiosis I is most sensitive to a reduction in RAD21.2.

To further address the nature of the chromosomal abnormalities that became visible at metaphase I, we performed Fluorescence *In Situ* Hybridization (FISH) in collaboration with Dr. Jason Sims (Schlögelhofer Lab, Vienna). We used a centromeric probe (green) in combination with probes hybridizing to 45S rDNA (cyan) and 5S rDNA (magenta) regions allowing distinguishing the different chromosomes as exemplified by FISH analysis of wild-type PMCs (Fig. 29).

Chromosome I is marked only by the centromere probes, while chromosome II is labeled in addition with the 45S probe (Fig. 29). A centromeric, a 45S and a 5S region characterize chromosome IV. Chromosome III and V are both bound by the centromeric and 5S probe (located close to the centromeres). The difference between both chromosomes is the intensity of the 5S signal, because chromosome V harbors more 5S rDNA repeats.

In both *RAD21.2 RNAi* lines, we observed connections between non-homologous chromosomes, which were not observed in wild-type cells (Fig. 29). For instance, we found cells exhibiting connections between chromosome III, IV and V (Fig. 29a I) and between chromosome III and IV (Fig. 29b I and II). Furthermore, we identified PMCs showing genome rearrangements with the 45S rDNA region, being translocated from chromosome IV to chromosome III (Fig. 29a II). Furthermore, we found cells with a 45S fragment at prophase II. In addition to events that involve aberrant chromosome connections at the 45S region, cells with connections within the centromeres of chromosome II and III were also observed (Fig. 29c II).

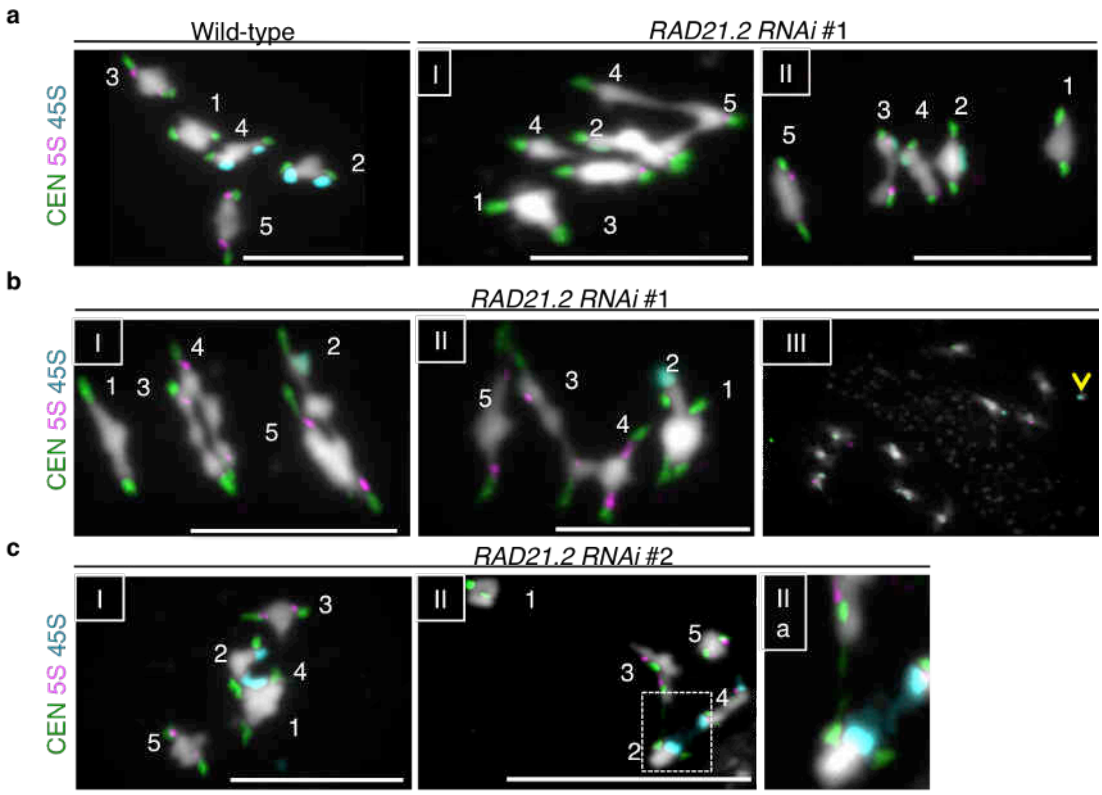

Figure 29: FISH analysis of metaphase I cells of pollen mother cells from wild-type and *RAD21.2 RNAi*. Probes against 45S rDNA (cyan), 5SrDNA (red) and CEN (green) loci were used to identify chromosomes; DNA was visualized by DAPI (grey). Different abnormalities were observed, for more information see text. Scale bar: 10 μm. (generated by Dr. Jason Sims)

These results suggested a general increase in recombination involving repetitive DNA regions that might lead to genome instability. To investigate whether recombination is enhanced in *RAD21.2 RNAi* plants, we examined the localization of the recombinase RAD51 in the 45S rDNA region at leptotene/zygotene stages by immuno-FISH. To concomitantly visualize the chromosome axis an ASY1 antibody (Fig. 30a, cyan) was used in addition to the RAD51 antibody (Fig. 30a, magenta). RAD51 foci were quantified for whole chromosomes as well as for the 45S rDNA region only. The quantification of the total number of RAD51 foci in wild-type (123±27, n=23) and in *RAD21.2 RNAi* plants (114±18, n=22) revealed a similar foci number (Fig. 30c). However, the number of RAD51 foci at the 45S rDNA region increased from 1.4±1 foci in wild-type to 2.7±1.5 ($p \leq 0.0049$) foci in the *RAD21.2 RNAi* meiocytes (Fig. 30d). This result supports the hypothesis that

RAD21.2 might be involved in the suppression of meiotic recombination at rDNA regions.

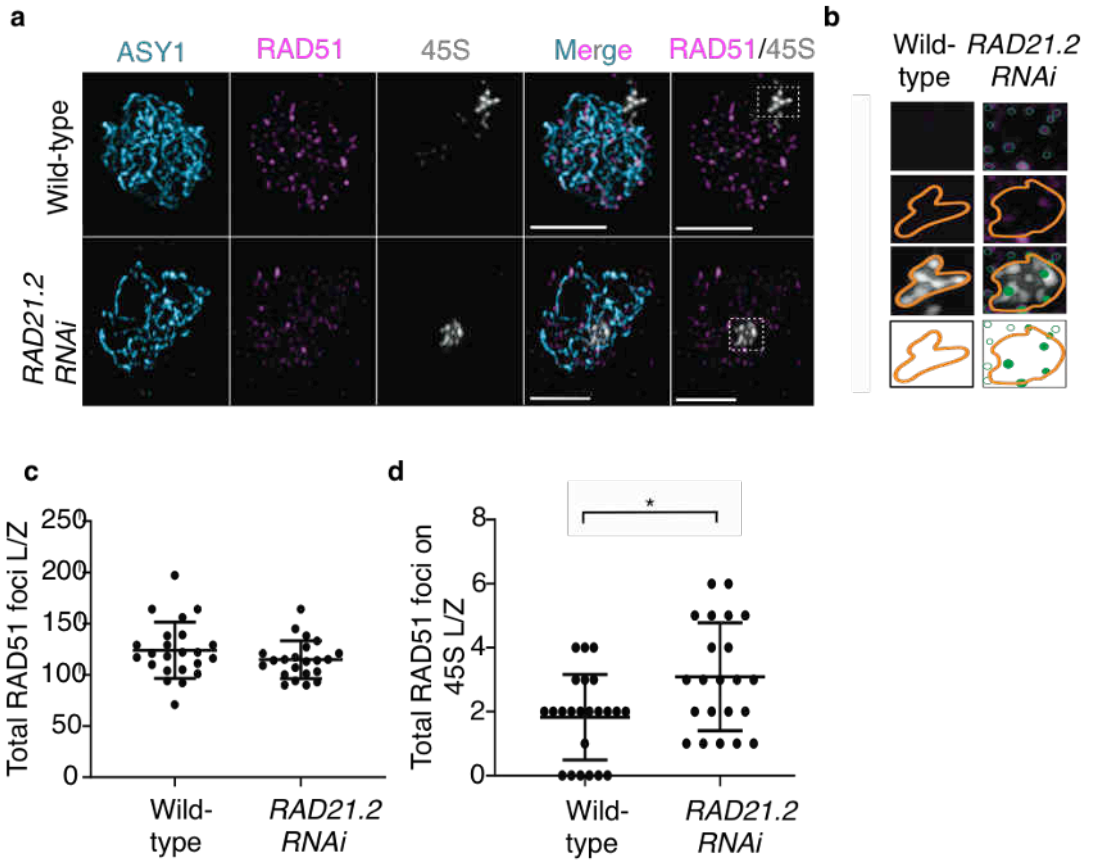

Figure 30: Immuno-FISH analysis of wild-type and *RAD21.2 RNAi* #1 pollen mother cells at leptotene/ zygotene. The axis has been stained with anti-ASY1 (cyan) for staging and the DNA repair sites are highlighted by anti-RAD51 (magenta). The 45S rDNA has been visualized with a specific FISH probe (white). Scale bar: 5 μm. e, Related to d, RAD51 foci were counted at the NOR, marked by the orange line. f, The total number of RAD51 foci at leptotene/zygotene stage in wild-type versus *RAD21.2 RNAi* plants is not significantly different. g, The number of RAD51 foci counted on the 45S region at leptotene/zygotene is significantly larger in *RAD21.2 RNAi* plants than in the wild-type. (generated by Dr. Jason Sims)

Seeing the enhanced number of RAD51 foci, I wanted to confirm if a knockdown of RAD21.2 leads to an increase in recombination in the rDNA region. An increase in recombination in these highly repetitive regions should affect the number of 45S rDNA repeats by the occurrence of deletions and insertions. Since the 45S loci on chromosome 2 and 4 are built by tandem repeats of 18S rRNA, 5.8S and 25S genes, we quantified the amount of 18S

rRNA genes as a measure for what is happening in the 45S region. Using real time PCR we quantified 18S rDNA loci in the progeny of three wild-type plants WT-1 (n=23), WT-2 (n=48) and WT-3 (n=16) in comparison to the progeny of an *RAD21.2 RNAi* plant (n=78) (Fig. 31). The qPCR using 18S rDNA specific primers was performed on DNA extracted from 4-week-old leaves. Two genes with fixed copy number, i.e HXK1 and UEV1C were used for normalization.

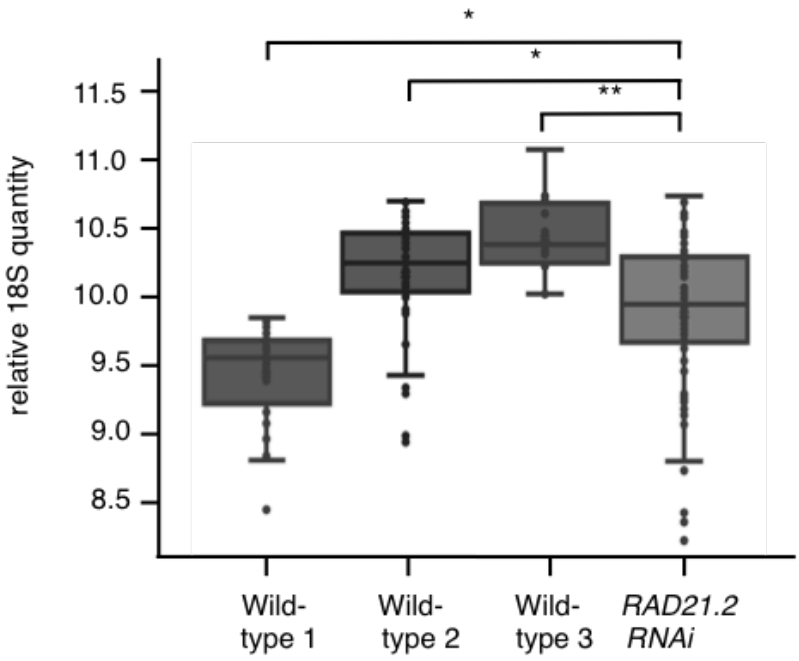

Figure 31: 18S quantification. Box plot depicting the number of 18S genes in offspring of 3 wild-type plants (WT-1 n=23, WT n=48, WT n=16) compared to the offspring of a *RAD21.2 RNAi* plant (n=78), which has a significant higher variance of the number of 18S genes than the wild-type.

As described before the number of 18S rDNA copies varies between different plant lines (Rabanal et al., 2017). However, the recombination in repetitive regions in wild-type plants is restricted which results in limited variation in the number of 18S rDNA copies in the progeny. The number of 18S rDNA copies varied significantly more in the offspring of the *RAD21.2 RNAi* plant compared to the progeny of three different wild-type plants (Fishers F test, WT-1/*RNAi* p=0,018, WT-2/*RNAi* p= 0,049 and WT-3/*RNAi* p=0,0045). This observation is

in accordance with the hypothesis that RAD21.2 is needed for a suppression of recombination at the 45S rDNA region.

To better resolve the localization of REC8 in the 45S rDNA region, Dr. Jason Sims performed immuno-FISH experiments using fixed meiocytes at pachytene stage. The NOR was stained by the 45S probe (Fig. 32a white) and REC8 was visualized by an anti-REC8 antibody (Fig. 32a magenta).

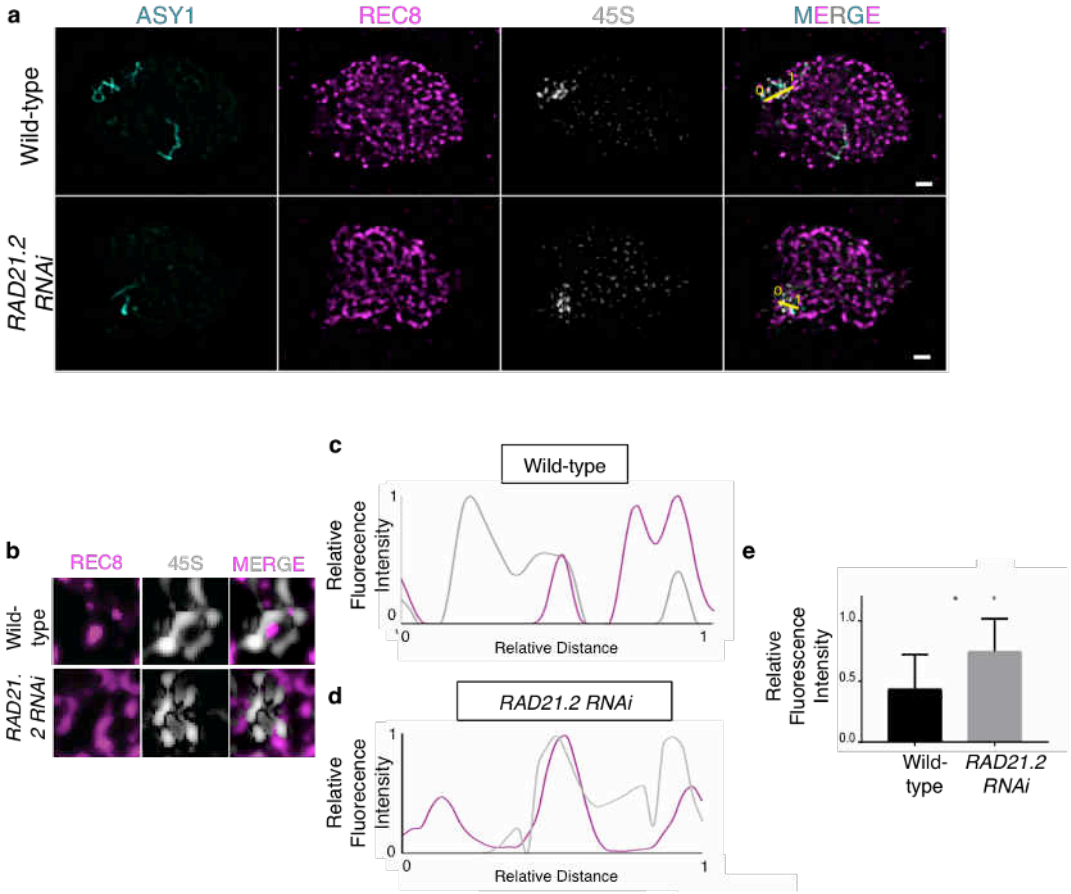

Figure 32: REC8 localization analysis in wild-type and *RAD21.2 RNAi* plants. a, Immuno-FISH analysis of wild-type and *RAD21.2 RNAi* pollen mother cells at pachytene. The axis has been labelled with anti-ASY1 antibody (cyan) and the meiosis specific cohesin subunit with anti-REC8 antibody (magenta). The 45S rDNA has been visualized with a specific FISH probe (white). The yellow line defines the region used to quantify the fluorescence intensities. Scale bar: 1 μm. b, magnification of the 45S rDNA region for wild-type and *RAD21.2 RNAi* meiocytes indicating an increased REC8 localization to the 45S rDNA in *RAD21.2 RNAi.* c and d, Profile plots of the fluorescence intensities of REC8 (magenta) and 45S rDNA (light grey) for wild-type (c) and *RAD21.2 RNAi* plants (d). The fluorescence intensity was normalized to the highest fluorescent value. e, The average relative fluorescence intensity of the REC8 signal taken at the maxima of the 45S rDNA is significantly higher in *RAD21.2 RNAi* plants (n=11) than in the wild-type (n=10) p-value = 0.032. (data generated by Dr. Jason Sims)

For staging reasons an anti-ASY1 antibody was used since ASY1 shows a characteristic pattern at pachytene (Fig. 32a cyan). Comparing the relative fluorescence intensity profile plots of REC8 at the 45S loci revealed a significant increase in abundance of the REC8 signal at the 45S region in the *RAD21.2 RNAi* plants (n=11, p=0.032) compared to the wild-type (n=10) (Fig. 32c-e). This leads to the hypothesis that in the wild-type situation invasion of REC8 into the NOR region is prevented by the presence of RAD21.2.

2.2.7 Analysis of RAD21.2 interaction with recombination proteins

Since a knockdown of RAD21.2 leads to a REC8 de-localization into and enhances the recombination level at the 45S rDNA region, it is tempting to speculate that REC8 itself might promote recombination. Based on this hypothesis, we tested if REC8 is able to interact with the topoisomerase SPO11 that induces DNA double strand breaks (DSB) during early prophase I as a prerequisite for recombination. In yeast, it was already shown that REC8 shapes the distribution of SPO11 and is needed for DSB formation (Kugou et al., 2009). In Arabidopsis, the SPO11 complex is built by the subunits SPO11-1, SPO11-2 and MTOPIVB (Stacey et al., 2006; Tang et al., 2017) and I tested whether REC8 or RAD21.2 are able to directly interact with these subunits by performing a Y2H assay (Fig. 33).

An interaction assay of AD-REC8 and AD-RAD21.2 with the SPO11 subunit MTOPIV was not possible due to a strong autoactivation of the MTOPIV-BD construct. However, the SPO11-1 and SPO11-2-BD could be tested but neither one of them interacted with AD-REC8 or AD-RAD21.2 in the Y2H system (Fig. 33).

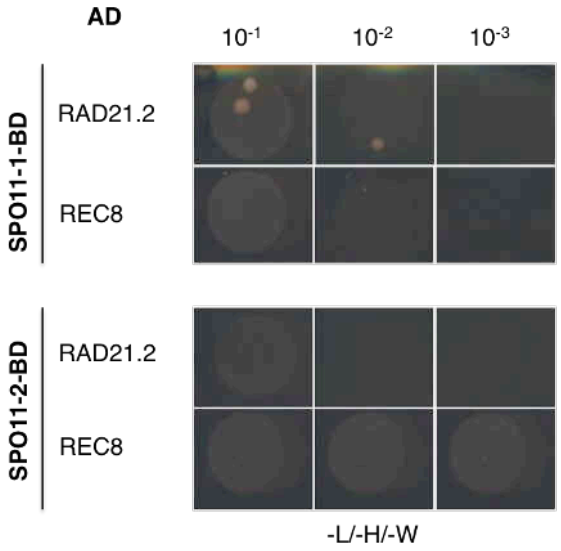

Figure 33: Yeast two-hybrid interaction assay of RAD21.2 and REC8 with the SPO11 subunits SPO11-1 (upper panel) and SPO11-2 (lower panel). An interaction was not observed in any case. Different dilutions of yeast (10^{-1}/10^{-2}/10^{-3}) were spotted on SD plates lacking leucine, tryptophan andhistidin (-L/-H/-W) to test for interaction strength.

Since it was recently shown that also chromosome axis proteins are important for recombination (Lambing et al., 2020), we used our Y2H system to test if either REC8 or RAD21.2 can interact with the axis proteins ASY1, ASY3 and ASY4. For ASY1, the full length cDNA and cDNA coding for protein parts (aa1-300 and aa1-570) were used. For ASY4 we used the full-length cDNA construct only. ASY3 could only be tested as AD-fusion since the BD-construct exhibited strong autoactivation. Therefore, it was not possible to investigate an interaction with RAD21.2 since RAD21.2-BD shows an autoactivation as well. As positive controls for the α-kleisins, we used the SMC1 and SCC3-BD constructs in combination with REC8 (Fig. 20) and RAD21.2 (Fig. 34c). An interaction of ASY3 with ASY1 and ASY4 has been described before (Chambon et al., 2018) and could be used as positive control for the respective constructs.

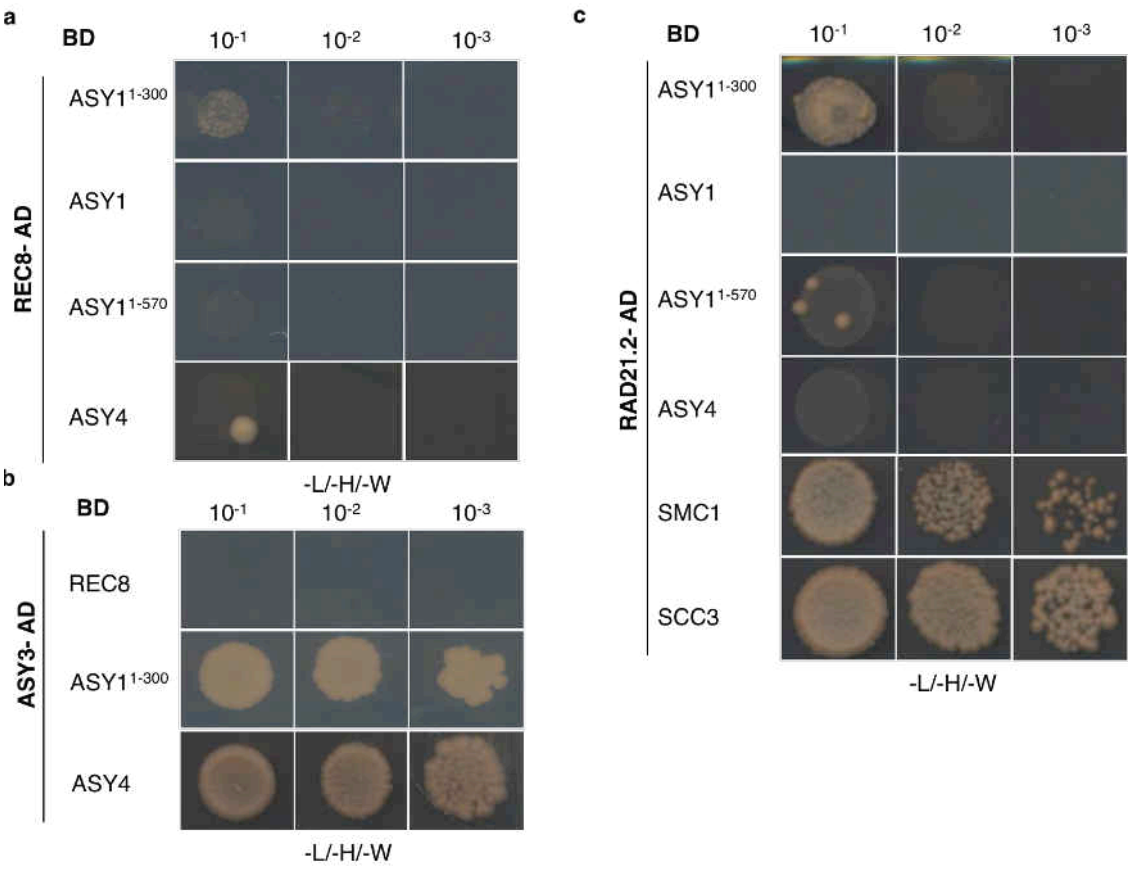

Figure 34: Yeast two-hybrid interaction assay of REC8 with the axis protein ASY1, ASY4 (see a) and ASY3 (see b). Y2H interaction assay of RAD21.2 with ASY1 and ASY4 (see c). An interaction of the α-kleisins with the axis proteins was not observed *in vitro*. Different dilutions of yeast (10^{-1}/10^{-2}/10^{-3}) were spotted on SD plates lacking leucine, tryptophan and histidine (-L/-H/-W) to test for interaction strength.

A direct interaction of the α-kleisins with the axis proteins was not observed for any axis element tested in our Y2H assay (Fig. 34). This data suggests that the observed enhanced recombination level in the 45S rDNA region of RAD21.2 *RNAi* plants is not due to specific interactions of the α-kleisins with the DSB inducing enzyme SPO11 or the axis proteins ASY1, ASY3 or ASY4.

2.3 Discussion

2.3.1 Comparative analysis of RAD21 proteins during mitosis

In contrast to other organisms like yeast and mammals for which a single mitotic α-kleisin protein termed as SCC1/RAD21 has been found, the plant and worm genome encodes for several RAD21 proteins that are expressed during mitosis. It is important to analyze the biological function of the additional RAD21 proteins to understand why higher plants exhibit three RAD21 proteins. However, studies regarding the function of Zea mays and Brassica napus are missing. Therefore I can only compare the results of RAD21 proteins from rice to Arabidopsis in the following to identify possible similarities.

The genome of *Oryza sativa* encodes for *RAD21-1*, *RAD21-2* and *RAD21-3* that are expressed in vegetative tissues. RAD21-1 was postulated to be the ortholog of SCC1 from yeast based on the sequence similarity and expression profile of RAD21-1 and SCC1 (Zhang et al., 2004). Data regarding functionality are missing so far. The phylogenetic tree showed that RAD21-1 is most closely related to RAD21.3 of *Arabidopsis thaliana*. RAD21.3 shows the highest steady state expression of the RAD21 proteins in dividing tissues (da Costa-Nunes et al., 2006). Similar observations were made in this thesis by using the reporter construct $Pro_{RAD21.3}$*:RAD21.3:GFP* that was highly expressed in vegetative tissues leading to a fluorescence signal with an equal distribution in the nucleus (Fig. 10). Since the analysis of *rad21.3* plants revealed a decrease in sister chromatid cohesion up to 55% a role in genome stability was proposed (Schubert et al., 2009). Further, RAD21.3 seems to be required for centromeric cohesion in 4C nuclei cells and shows anaphase bridges that could lead to cell lethality (Schubert et al., 2009). However, the described phenotype of *rad21.3* mutants does not lead to any obvious growth defects (Schubert et al., 2009; da Costa-Nunes et al., 2014). This stands in contrast to the observation of *rad21* mutants from yeast, which are lethal (Strunnikov et al., 1993; Birkenbihl and Subramani, 1995).

It was argued that the wild-type phenotype of *rad21.3* single mutant could be explained by the redundancy of RAD21.3 and RAD21.1 (Schubert et al., 2009;

da Costa-Nunes et al., 2006). However, it was shown that the double mutants have no obvious phenotype under normal conditions. This is a strong argument against their function as the SCC1/RAD21 homolog in plants because I expect that the depletion of the Cohesin components lead to early lethality as reported for *smc1*, *smc3* and *scc3* mutants (Schubert et al., 2009).
On the other hand a role of RAD21.1 and RAD21.3 during DNA DSB repair has been proposed (da Costa-Nunes et al., 2014) which is a typically seen for RAD21 proteins of other organisms like yeast (Birkenbihl and Subramani, 1995). In more detail, RAD21.1 is required for the recovery from DNA damage during seed imbibition and RAD21.3 is needed for DNA DSB repair (da Costa-Nunes et al., 2006 and 2014). So far only a weak steady state expression of RAD21.1 was reported. This finding is contradictory to the observations that were made with our reporter construct $Pro_{RAD21.1}$*:RAD21.1:GFP.* We found a weaker expression of RAD21.1 in comparison to RAD21.3 but the expression was not that weak compared to $Pro_{RAD21.2}$*:GFP:RAD21.2.* A similar localization pattern to RAD21.3 was observed for RAD21.1. The analysis of *rad21.1* mutant revealed impaired cohesion but no defects in centromeric cohesion (Schubert et al., 2009). RAD21.1 is most close to RAD21-2 of rice, which shows an expression in actively dividing tissues with the highest expression in pre-meiotic cells (Gong et al., 2011). The ectopic expression of RAD21-2 in yeast results in cell growth delay and abnormal morphological changes. Based on this observation, a role in cell division and growth was postulated.
So far, it was not possible to find a homolog of the yeast protein SCC1/RAD21 in Arabidopsis. Therefore I can only speculate that RAD21.1 and RAD21.3 at least reassemble the function of SCC1/RAD21 in DNA repair. Although I could show that RAD21.1 and RAD21.3 localizes to the metaphase plate during mitosis, which is typical for cohesin proteins, their function in sister chromatid cohesion under non-stress conditions need to be further analyzed. This will be complicated since mutants show no obvious phenotype.
In contrast, for RAD21.2, which is essential for plant viability, a role in vegetative growth has been postulated. Thus the localization of RAD21.1 and

RAD21.3 to the metaphase plane is in accordance with cohesion function, they apparently cannot compensate for a loss in RAD21.2. If this is due to functional differences on protein level needs further analysis.

In previous studies, a weak expression was detected in somatic tissue (da Costa-Nunes et al., 2006), matching my results of the localization analysis by using the *Pro$_{RAD21.2}$:GFP:RAD21.2* reporter construct (Fig. 10). In contrast, a reported localization of RAD21.2 to the nucleolus (Jiang et al., 2007) with no chromosome association during mitosis was not confirmed in my studies. In my opinion, the observed nucleolar localization of Jiang et al. might be due to an unspecific RAD21.2 Antibody since it is know that nonspecific antibodies give rise to a nucleolar accumulation as mentioned by themselves. In addition to a RAD21.2 specific antibody, C-terminal tagged (YFP and Myc) RAD21.2 proteins were used for the immunolocalization study. Since the C-terminal tagged RAD21.2:GFP did not fully rescue the rad21.2 phenotype in my experiments it might explain why there is a discrepancy in the localization analysis. Interestingly, I showed for the first time that RAD21.2 localizes to the nucleus and is associated with chromosomes. To further evaluate its role in sister chromatid cohesion during mitosis I would perform chromosome spreads of *RAD21.2 RNAi* knockdown plants to analyze the appearance of cohesion failures during mitosis. Furthermore, it makes sense to test if the *RAD21.2 RNAi* knockdown plants show sensitivity to DNA damage to investigate the role of RAD21.2 in DNA repair.

Taken together, it is difficult to identify the ortholog of SCC1/RAD21 from yeast in Arabidopsis. Based on previous results and my localization analysis, I speculate that it is likely that RAD21.1 and RAD21.3 are required for DNA repair, which is especially required during stress conditions. To this end, the role of RAD21.2 during mitosis remains unclear. However, the essential for plant viability and the fact that *smc1*, *smc3* and *scc3* leading to embryonic lethality give rise to the speculation that RAD21.2 might be the major α-kleisin in mitosis of Arabidopsis.

2.3.2 Comparative analysis of RAD21 proteins during meiosis

2.3.2.1 RAD21 localization during meiosis

During meiosis, the mitotic α-kleisin protein SCC1/RAD21 is replaced by REC8 in yeast. For all species undergoing sexual reproduction this replacement is observed. However, for *C. elegans*, *D. melanogaster* and mammals it was shown that additional meiotic α-kleisins exist. In the following I will summarize the described dynamics and functions of the α-kleisins from different organisms and finally compare and discuss my findings of RAD21.2 as an additional meiotic α-kleisins in Arabidopsis.

For *C. elegans* the highly identical and redundantly functioning proteins COH-3 and COH-4 have been identified (Severson et al., 2009). While REC8 is loaded on chromosomes in a replication dependent manner during pre-meiotic S-phase, COH3/4 is loaded in a DSB-dependent manner in early prophase I (Severson and Meyer, 2014). In pachytene, both α-kleisins are bound along the chromosomes. Chromosomal regions that show an overlapping signal of both kleisins were found in addition to regions that are either labeled by REC8 or COH3/4. However, data regarding the characteristics of the different chromosomal regions are missing. Progressing to pro-metaphase I, COH3/4 becomes restricted to the short arm and REC8 is only found on the long chromosome arm of *C. elegans*. COH3/4 is not found after metaphase I while REC8 is expressed until metaphase II. It has been reported that COH3/4 is not able to co-orient sister chromatids mediating a mitotic-like separation in the absence of REC8, indicating that the α-kleisin protein can not compensate for each other and might have specific functions (Severson et al., 2009). However, overlapping functions of REC8 and COH-3/-4 in axis assembly and maintenance of the synaptonemal complex stability has been reported (Severson et al., 2009, Castellano-Pozo et al., 2020). Further it is speculated that the artificial induced removal α-kleisin are either directly or indirectly

involved in recombination since a removal of these proteins led to an increase of DSB. Interestingly, removing REC8 leads to increased RAD51 foci (Lambing et al., 2020) similar to the observation that I made with my *RAD21.2 RNAi* line at rDNA regions. On the other hand it was recently published that *rec8* mutants exhibit decreased DSB numbers and RAD51 foci in Arabidopsis (Lambing et al., 2020). The involvement of RAD21.2 and REC8 in recombination will be further discussed in 2.3.3.

In mammals, the α-kleisin RAD21L was identified in in addition to REC8 and for both the similar function in AE formation has been revealed (Gutiérrez-Caballero et al., 2011; Ishiguro et al., 2011, Llano et al., 2012). Interestingly, in mice meiosis an association of the mitotic RAD21 kleisin to meiotic chromosomes is found (Rankin, 2015). Similar to REC8, RAD21L is loaded in pre-meiotic S-phase onto chromosomes (Ejipe et al., 2003; Lee and Hirano, 2011). A high-resolution analysis revealed that REC8 and RAD21L localize to the axial element and are evenly distributed along the chromosome from early zygotene to late pachytene. However, the detailed analysis revealed that sub-chromosomal domains contain either REC8 or RAD21L (Lee and Hirano, 2011). Although both proteins are important for SPO11- mediated DSB (Llano et al., 2012), RAD21L overlap with recombination sites (stained by RAD51 foci) to a greater extent than REC8 (Rong et al., 2016). In contrast to REC8, which is essential for centromeric cohesion in metaphase, RAD21L disappears already from mid-pachytene onwards.

In *D. melanogaster*, two meiotic α-kleisins, termed as C(2)M and SOLO have been identified (Manheim and McKim, 2003; Yan et al., 2010). C(2)M is loaded onto chromosomes in a short period during prophase I, indicating a replication independent loading. In contrast SOLO, is a centromeric cohesin that is loaded to chromosomes prior to meiosis (Gyuricza et al., 2016) and removal is observed in anaphase II (Yan et al., 2010). C(2)M is important for synaptonemal complex assembly and crossover formation, but not important for cohesion in meiosis. While the other cohesin containing SOLO mediates

centromeric cohesion and the chromosome orientation at the meiotic spindle (Yan et al., 2010). Therefore, the overlapping functions of both proteins have not been identified yet.

In plants it has been previously shown that RAD21.2 is needed in addition to REC8 for early meiotic events (Jiang et al., 2007). However, localization to meiotic chromosomes was never observed by performing immunolocalization analysis. Instead, a localization to the nucleolus was reported for RAD21.2 in vegetative and reproductive cells and a function of RAD21.2 independent from the other core cohesin components has been hypothesized. In this thesis, I showed that RAD21.2 is a bona fide cohesin component since an interaction with SMC1 and SMC3 was determined similar to REC8 by performing a Y2H assay. And was further confirmed by the performed Co-IPs since the cohesin Complex proteins SMC1 and SMC3 were significantly pulled down and identified by mass-spectrometry analysis.
Strikingly, we showed that RAD21.2 is expressed in pre-meiosis indicating a replication dependent cohesin loading that has been also observed for REC8 by Yuki Hamamura (personal communication). Furthermore, I showed for the first time that RAD21.2 binds to chromosomes from pre-meiosis until ana-metaphase I with a distinct pattern that differs to REC8. Furthermore, a role of RAD21.1 and RAD21.3 during meiosis is unlikely since using the here developed reporter constructs an expression was not observed in meiocytes.
The analysis of meiotic kleisins in different organisms revealed that multiple cohesion complexes fulfill various functions beyond sister chromatid cohesion like axis formation and recombination. Similar to other organisms also Arabidopsis has an additional kleisin protein that differs in their localization from REC8. However, it is not possible to name which of the Notably, an additional meiotic kleisin protein has been not described in rice or maize. Therefore it remains unclear whether other higher plant species have multiple kleisins functioning in meiosis.

2.3.2.2 RAD21.2 regulation by the WAPL-dependent prophase I pathway

Our localization analysis of RAD21.2 and REC8 during meiosis revealed not only differences regarding their chromatin association but also their dynamics Cohesins can be actively removed from chromosomes by WAPL or an enzymatic cleavage mediated by separase (see introduction). In budding yeast, *C.elegans* and Arabidopsis, WAPL is needed for the removal of Cohesins during prophase I (Challa et al., 2016; Crawley et al., 2016; De et al., 2014). For budding yeast and Arabidopsis, it was demonstrated that the REC8 containing cohesin complex is regulated by WAPL (Challa et al., 2019; Yang et al., 2019). In contrast, the WAPL-dependent removal of cohesin targets the COH3/4 containing complexes but not the ones built by REC8 in *C. elegans* (Crawley et al., 2016). For mammals, a WAPL-dependent regulation was postulated based on the localization data from REC8 and RAD21L (Ishiguro, 2019). However, data showing that the chromosomal release of RAD21L is WAPL-dependent is still missing (Brieño-Enríquez et al., 2016).

I could show now for Arabidopsis that in contrast to REC8, RAD21.2 is not subject to the WAPL-dependent prophase pathway (Fig. 24 and 25). On the one hand this is similar to *C.elegans*, since the meiotic cohesin complexes are regulated differently depending on the a-kleisin involved. However while in *C.elegans* REC8 is WAPL resistant, it's RAD21.2 in Arabidopsis.

Based on our findings, further experiments should address questions realted to how the regulatory proteins distinguish between the different cohesin complexes. On the one hand, this could be via different binding affinities for interacting proteins. However, it is also conceivable that the chromosomal localization of both complexes is important for the accessibility by WAPL. Moreover, the differential sensitivity to WAPL indicates that both cohesin complexes are not functioning redundantly, which is further supported by my observation that the *PRO$_{ASK1}$:GFP:RAD21* cannot even partially rescue the *rec8* mutant phenotype.

2.3.2.3 Localization of RAD21.2 to heterochromatic regions

The localization pattern of RAD21.2 during mitosis and meiosis is particularly interesting since a patchy pattern with an accumulation at distinct sub-nuclear regions has not been reported for other kleisins so far.

My co-localization analysis of RAD21.2 with CENH3 and PCNA1 indicated an accumulation of RAD21.2 at heterochromatin (Fig. 12) which was confirmed by the co-localization analysis of RAD21.2 and the histone marker H2A.W which showed that RAD21.2 is enriched around 2.7 times at nucleolus proximal heterochromatic regions (Fig. 17) compared to euchromatin.

Therefore it raises the question why a specific cohesin complex is accumulating at heterochromatin. Is RAD21.2 required for heterochromatin assembly? Or is RAD21.2 loaded onto a heterochromatic environment?

For yeast it has been reported that heterochromatin assembly depends on the histone H3 methylation of lysine 9 (H3K9me) (Oya et al., 2019). This modification is bound by the heterochromatic marker protein (Swi6/HP1). HP1 serves as an adapter protein to recruit cohesins and other factors like histone methyltransferase (HMT) and histone deacetylases (HDA) to establish a heterochromatic environment (Nonaka et al., 2002; Fischer et al., 2009; Folco et al., 2019). For example it has been reported that *swi6* mutants exhibit a reduction in heterochromatin and cohesin binding at telomeric regions in yeast (Dheur et al., 2011). Homologues of HP1 proteins were found in *D. melanogaster* and humans (Huisingia et al., 2006) and it has been reported that heterochromatin assembly is dependent on the H3K9 methylation in plants. However, the HP1 homologue Like Heterochromatin protein (LHP1) of *Arabidopsis thaliana* is associated with histone 3 lysine 27 trimethylation (H3K27me3) (Turck et al., 2007). Therefore, it was questioned if a genuine HP1 protein binding to H3K9me exists in *A. thaliana*.

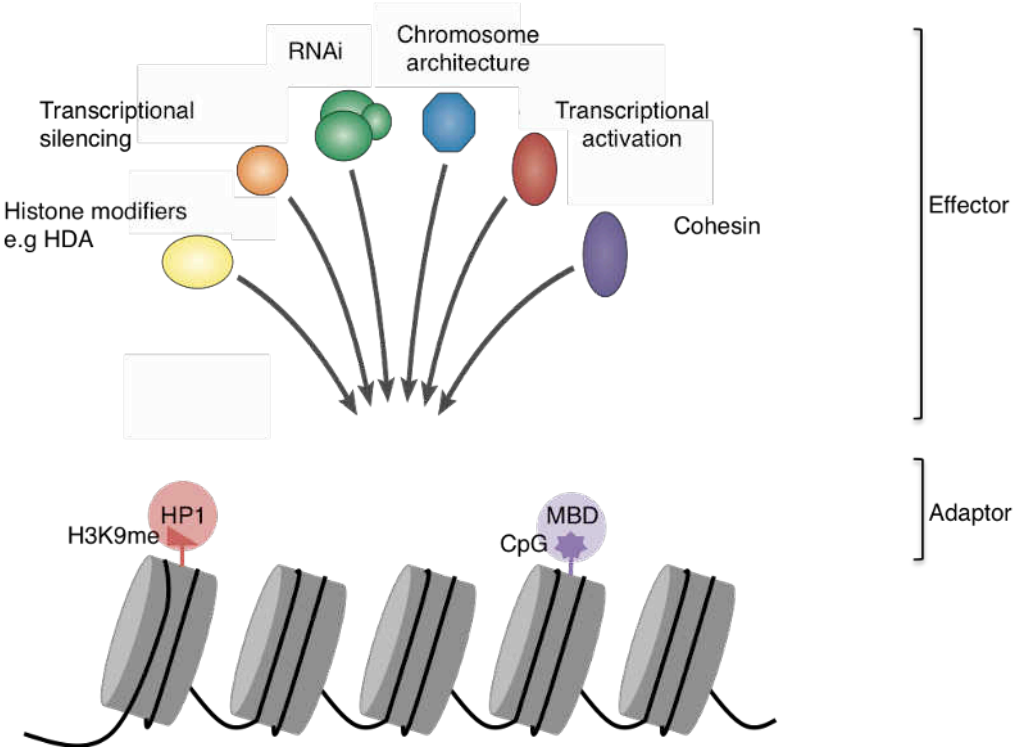

Figure 35: Heterochromatin and the major proteins that are associated with heterochromatin formation and maintenance (adapted from Grewal and Jia, 2007).

With the identification of ADCP1, a H3K9me reader protein was discovered (Zhang et al., 2018; Zhao et al., 2019). Similar to human and fly HP1, APCD1 regulates heterochromatin formation in plants. However, a recruitment of cohesin has not been reported so far. It would be interesting to analyze whether APCD1 recruits a specific, i.e. RAD21.2-containing cohesin complex to the heterochromatic regions in Arabidopsis.

Recently, using ChIP analysis an enrichment of REC8 in heterochromatic regions was reported (Lambing et al., 2020). Interestingly, this study revealed by ChIP that REC8 is also associated with other chromatin states e.g expressed genes, silent genes and silent transposons. However, the H3K9me mutant *kyp suvh5 suvh6* does not show any impaired localization of REC8, indicating that REC8 localization to the chromosomes is independent from a heterochromatic environment. This latter finding is in accordance with my REC8 and H2A.W.6 co-localization studies, which showed that in contrast to RAD21.2, there was no obvious enrichment of REC8 at heterochromatic regions. Furthermore, from the analysis of the reporter REC8:GFP, it is

obvious that REC8 is evenly distributed along meiotic chromosomes in prophase I while it is only found at centromeres at metaphase I.
Therefore, I hypothesize that REC8 might be important for the general formation of the meiotic chromosome architecture while RAD21.2 might be involved in the formation of heterochromatin or to preferentially localize to heterochromatin. To differentiate these possibilities, it would be important to analyze the localization of RAD21.2 in heterochromatic mutants as well as quantitatively analysis to which extent of *RAD21.2 RNAi* lines form heterochromatin with focusing on rDNA since the observed phenotype of RAD21.2 *RNAi* lines indicate a function in rDNA stability (see discussion below). I think it is further recommended to re-perform a ChIP experiment with GFP:RAD21.2 which unfortunately failed in the first trial. It would be interesting to repeat this experiment with another anti-GFP antibody, since the anti-GFP antibody I used did not work well in later immunolocalization studies and therefore might have also performed badly in the ChIP. The ChIP data is expected to give a more detailed description to which sequences RAD21.2 preferentially binds and if this corresponds to DNA typically found in low recombining heterochromatin. Furthermore, the comparison with the already existing REC8 ChIP data could help to see if RAD21.2 and REC8 binding is really mutually exclusive on a whole genome scale (Lambing et al., 2020).

Additionally, I found that HTA7, encoding the heterochromatic histone variant H2A.W7 (Yelagandula et al., 2014), the methylation binding domain protein MBD11 and the histone deacetylases HDA14 and HDA5 to be significantly enriched in the co-purification with RAD21.2, when compared to a purification using REC8 as bait.
Similar to the heterochromatin protein HP1 described above, MBD proteins bind to methylated DNA to interpret DNA methylation signals and recruit further proteins like HDAs (Grafi et al., 2007). In Arabidopsis, 13 genes encoding for MBD proteins were identified. While MBD5, MBD6 and 7 are known to bind methylated CpG and are mainly found at chromocenters and rDNA genes (Zemach et al, 2005), less is known about the identified MBD11

of *Arabidopsis thaliana*. MBD11 is expressed in a wide range of tissues like leaves, flowers and siliques and binding of methylCpG was hypothesized (Berg et al., 2003). HTA knock down plants exhibit various phenotypical defects like abnormal positioning of flowers, fertility problems and late flowering. Similar phenotypes were observed for mutation of genes involved in chromatin remodeling indicating a role of MBD11 in chromatin remodeling during plant development (Berg et al., 2003).

A role of histone deacetylases (HDAs) in heterochromatin regulation and transcription repression has been shown in different organisms (Berger, 2002). The 18 HDAs of Arabidopsis are grouped into three HDA families. First, the RPD3/HDA1 (Reduced Potassium Dependence 3/Histone Deacetylase 1) family, second the SIR2 (Silent Information Regulator 2) family and third the HD2 (Histone Deacetylase 2) family (Liu et al., 2015). The most studied HDAs are HDA6 and HDA19. HDA6 mutants show increased gene expression and reduced DNA methylation indicating a role in gene silencing and DNA methylation (Liu et al., 2012). A role of HDA19 in various developmental processes like flowering and seed development has been reported (Wang et al., 2013; Zhou et al., 2013). Surprisingly, for HDA14 an association with α-tubulin was found by mass-spectrometry analysis (Tran et al., 2012). Also, an organellar localization and a function in photosynthesis was reported (Hartl et al., 2017), while a function in histone modification was not found so far. Thus, co-purification of HDA14 might not necessarily be an indication for an association of RAD21.2 with heterochromatin.

However, HDA5 that belongs to the RPD3/HDA1 family like HDA6 and HDA19, seems to be involved in flowering time regulation and does interact with HDA6 to regulate gene expression (Luo et al., 2015).

Thus in total, this data set further supports the hypothesis that RAD21.2 is embedded in a heterochromatic environment where it might directly or indirectly interact with regulatory proteins like MBDs and HDAs.

It will be interesting to investigate in future, if there are functions of RAD21.2 beyond sister chromatid cohesion such as an involvement in developmental processes via regulation of heterochromatin formation.

2.3.3 Functional analysis of RAD21.2

Since *rad21.2* mutants are gametophytic lethal, it was impossible to infer any meiotic functions of RAD21.2 by reverse genetics. Therefore, we used the *RNAi* approach to knock down the RAD21.2 expression *in planta*. We found a RAD21.2 expression reduction of about 30% in flower buds of Arabidopsis. These plants did not show any growth defects. Therefore, the *RAD21.2 RNAi* plants could not be used for conclusions regarding sporophytic functions. In contrast, the observed reduction in fertility of *RAD21.2 RNAi* plants indicated that its function in reproduction was more sensitive to a change in protein level. In contrast to *rec8* mutants, we did not observe defects in homologous chromosome synapsis in pachytene in *RAD21.2 RNAi* lines. This stands in contrast to previous experiments by the Makaroff lab (Yuan et al., 2012) in which they find that targeting *RAD21.2 by RNAi* results in plants partially defective in chromosome condensation, homologous pairing and synaptonemal complex formation (SC) in male meiosis. Further female meiosis was more strongly affected since univalent and aggregates of chromosomes at metaphase I and chromosome bridges and lagging chromosomes were found. Since, plants exhibiting a RAD21.2 expression reduction of 50% were used in this study, it is possible that the observed defects in homologous pairing require a stronger reduction in expression than obtained by my *RNAi* lines. This could be investigated further by screening more *RNAi* lines or generating new lines using a promoter which is higher expressed in meiosis than the 35S promoter to drive the *RNAi* construct. Furthermore, it is recommended to analyze female meiosis of my *RNAi* lines.

Interestingly, in my *RNAi* lines I found a dramatic increase of connected chromosomes from diplotene onwards. With the help of Dr. Jason Sims, I identified connections between non-homologous chromosomes that are not observed in wild-type plants. We observed complex chromosomal rearrangements involving the 45S and 5S rDNA region and fragments of the 45S rDNA (Fig. 29). These results suggested a general increase in non-homologous recombination that might lead to genome instability involving repetitive DNA regions. While a greater number of RAD51 signals was

observed in *RAD21.2 RNAi* plants by the Makaroff lab (Yuan et al., 2012), we did not find a general increase, but we observed that the number of RAD51 foci at the 45S rDNA region is enhanced in comparison to wild-type, indicating a role of RAD21.2 in repressing RAD51 foci at this rDNA region. In future, it would be interesting to test if the number of RAD51 foci is also enhanced at the 5S rDNA region that is embedded in the pericentromeric heterochromatin. First indications are given by my results since we could identify a cell exhibiting a chromosomes entanglement of the centromeric region (Fig. 29). The pericentromeric region is known to have a low tendency to recombine (Baker et al. 2014). If RAD21.2 is found to be important for the silencing of recombination in this region, it might be a good target to modulate its activity in breeding approaches overcoming restrictions of diversity and leading to the generation of genetic variation, assuming that in crops a similar RAD21-2 based mechanism can be identified.

To generate further proof of an enhanced recombination in *RAD21.2 RNAi* plants I performed quantitative PCR (qPCR). Indeed, the number of 18S rRNA varied significantly more in the offspring of the *RAD21.2 RNAi* plants in comparison to the progeny from wild-type (Fig. 31). This observation matches phenotypes that are reported for cohesin and heterochromatic mutants e.g. *fas1* in Arabidopsis or *swi6* mutants of yeast (Kirik et al., 2006; Dheur et al., 2011), which show an increase in recombination of heterochromatic regions that rarely recombine in wild-type yeast (Nonaka et al., 2002). This leads to the interpretation that heterochromatic cohesins function in guarding genome stability (Gartenberg, 2009).

In yeast, a protein called Sir2 was shown to silence transcription at telomeres and rDNA loci and a repression of recombination at rDNA loci mediated by Sir2 was also reported (Gottlieb and Esposito, 1989; Kobayashi et al., 2004). Interestingly, Sir2 is mediating cohesins at heterochromatin via. However, the silencing of heterochromatin is independent from cohesin (Chen et al., 2016). Sir2 is a histone deacetylase (HDA) and belongs to the SIRTUIN sub-family (Michan and Sinclair, 2007). In Arabidopsis, only two SIRTUIN homologs are found: SRT1 and SRT2 (Liu et al., 2017). For SRT2 a localization to

mitochondria regulating the energy metabolism has been reported (König et al., 2014). SRT1 is a nuclear protein that is shown to be a chromatin regulator controlling stress response (Liu et al., 2017). Although no obvious phenotype was shown for *srt1* mutants it would be interesting to analyze this mutants for an increase of recombination at 45S rDNA region and to test for the localization of RAD21.2 during mitosis and meiosis (Luhua et al., 2013; Liu et al., 2017 and Zhang et al., 2018).

However, our data strongly suggests that the chromatin status could be responsible for active or inactive recombination sites. This matches observations made with the *fas1-4* mutants. FAS1 encodes for a subunit of the CHROMATIN ASSEMBLY FACTOR (CAF-1) that is required for a nucleosome assembly. Plants that are defective for FAS-1 show a severe phenotype, like less heterochromatin content and a 100-fold increased intrachromosomal recombination rate (Kirik et al., 2006). This phenotype suggests that chromatin conformation is a limiting factor for homologous recombination (Eckhardt et al., 2006). Thus, the localization of RAD21.2 and REC8 in different heterochromatic mutants like *fas-1*, *ddm1* and *hda6* should be analyzed in future. Additionally, the recombination rate of different heterochromatin mutants should be analyzed since it was shown that recombination is mainly found in chromatin structures with low DNA methylation and low nucleosome density (Yelina et al., 2015; Lambing et al., 2017). In combination with the localization data this could further help to identify whether an activator or repressor shapes recombination in Arabidopsis thaliana. Also, it is necessary to in detail analyze the chromatin status in *RAD21.2 RNAi* plants to conclude whether RAD21.2 is involved in heterochromatic or if it preferentially localizes to heterochromatin. To answer the question whether heterochromatin is needed for the binding of RAD21.2 or whether RAD21.2 is involved in the formation of heterochromatin.

Additionally, it has been reported that the chromosome axis shapes the recombination landscape of *Arabidopsis thaliana*. In particular, an involvement of the HORMA domain protein ASY1 has been reported (Lambing et al.,

2020). Also, ASY3 and ASY4 were shown to be important for the crossover formation since *asy3* as well as *asy4* mutants have a drastically reduced number of crossovers (Ferdous et al., 2012, Chambon et al., 2018). However, when I tested for an interaction of the α-kleisins with the different HORMA domain proteins ASY1, ASY3 and ASY4 in the Y2H system, no binding was found. To this end, I hypothesize due to my findings in the *RAD21.2 RNAi* plants that show an increased recombination and increased abundance of REC8 at the 45S loci that REC8 might be actively involved in meiotic recombination. This is supported by the fact that REC8 is known to be involved in meiotic recombination as part of the chromosome axis (Lambing et al., 2019, Yoon et al., 2016) and REC8 was shown to mediate the SPO11 distribution along meiotic chromosomes in yeast (Kugou et al., 2009). Therefore I tested for an interaction using the Y2H system. However, neither an interaction of REC8 nor RAD21.2 with SPO11 was observed. It was suggested that DSBs are equally distributed along the chromosomes and the repair mechanism later dictates the formation of Crossovers or DNA repair via NCO. Based on this assumption it might be a downstream factor that is regulated by REC8 as a recombination activator or by RAD21.2 as a repressor, which is responsible for the observed phenomena. Therefore, other recombination proteins like RAD51 or DMC1 could be included in the Y2H screening. Especially because also my mass-spec data further support that REC8 is found in a recombination active chromatin environment. With respect to additional functions of a-kleisin proteins, it is interesting to note that using REC8 as a bait I could significantly enrich for MSH2 and MRE11 compared to the RAD21.2 co-purifications.

MRE11 is involved in DSB repair by forming a complex with RAD50 and NBS1 in somatic and reproductive tissues (Waterworth et al., 2007). A role in recombination during meiosis was described (Šamanić et al., 2013). *Mre11* mutants show shorter root growth and sterile phenotype. Similar to *rec8* mutants, *mre11* plants show chromosome fragmentation and miss-segregation during meiosis. The observed co-precipitation of both proteins

suggests that REC8 is found in a chromatin environment that is characterized by DSB repair and recombination sites.

The Arabidopsis genome encodes for seven MSH proteins that have a wide range of functions all contributing to genome stability. A role of MSH2 in recombination repression was described for mitotic and meiotic cells in 2006 (Emmanuel et al., 2006). Similar observations were made in yeast (Chen and Jinks-Robertson, 1999). In contrast, a pro-crossover function at pericentromeric regions has been postulated for MSH2 lately (Blackwell et al., 2020). Surprisingly, *msh2* mutants show a decrease of crossover within the pericentromeric regions but an increase of crossovers at the sub-telomeric regions. Finding MSH2 to co-purify with REC8, I wonder if REC8 is involved in this crossover promoting function at centromeric regions. An enrichment of REC8 at centromeric regions has been found in different species and was explained by the step wise-loss of cohesion needed for proper chromosome segregation during meiosis. However, a reported association of REC8 with chromatin that anti-correlates with crossovers does not support my hypothesis that REC8 is involved in recombination (Lambing et al., 2020).

2.4 Summary and Future perspective

To summarize, I showed that the three RAD21 proteins of *Arabidopsis thaliana* are all expressed in somatic tissues and show a localization pattern in metaphase of mitotic cells typical for cohesin components. In contrast to previous studies, I found that RAD21.2 binds to mitotic and meiotic chromosomes. Interestingly, we observed an enrichment of RAD21.2 at particular regions that were also characterized by heterochromatic features like high methylation and the histone H2A.W.

Also, I could show that RAD21.2 is a α-kleisin that functions next to the well-described α-kleisin REC8 in Arabidopsis meiosis. Furthermore, I found that RAD21.2 cannot compensate for REC8 and is differently regulated by WAPL.

Furthermore, I found, when reducing RAD21.2 protein amount in meiocytes, we see enhanced recombination in the heterochromatic 45S rDNA region and

a slight re-localization of REC8 into this area, suggesting that REC8 and RAD21.2 distribution on the chromosomes controls the recombination pattern in *Arabidopsis thaliana*.

However, remaining questions like whether RAD21.2 is a general anti-recombination factor or whether RAD21.2 is important for heterochromatin assembly, thus leading indirectly to recombination repression needs to be targeted by future experiments.

If recombination in repetitive regions in general could be enhanced by a knock down of RAD21.2 orthologs in crops, this would be interesting for breeding purposes, since it could lead to a possible mobilization of genes located in recombination poor regions of the genome.

Chapter II

Analysis of cohesion dynamics and functional relevance of REC8 phosphorylation sites in meiosis of *Arabidopsis thaliana*

3.1 Analysis of cohesin dynamics in Arabidopsis meiocytes

In previous experiments REC8 has been used as a marker to monitor cohesion dynamics in meiocytes of Arabidopsis. As outlined in previous chapter, REC8 is not the only α-kleisin in plants we wondered if REC8 only marks a subpopulation of all cohesin complexes. Therefore, I generated a genomic GFP reporter for the cohesin component SMC1 and compared the dynamics with REC8-GFP that were previously described (Prusicki et al., 2019).

3.1.1 Results

Recently, the dynamics of the fully functional reporter *Pro$_{REC8}$:REC8:GFP* (Prusicki et al., 2019) construct was described. In brief, a REC8-GFP signal becomes visible as very thin threads at leptotene (Fig. 36). As synapsis starts, the REC8 signal becomes stronger and reaches a maximum at zygotene stage (Yang et al., 2019). At pachytene, REC8 is evenly distributed on the fully synapsed chromosome (Fig. 36). For comparison reasons, we generated the construct *Pro$_{SMC1}$:SMC1:GFP*.

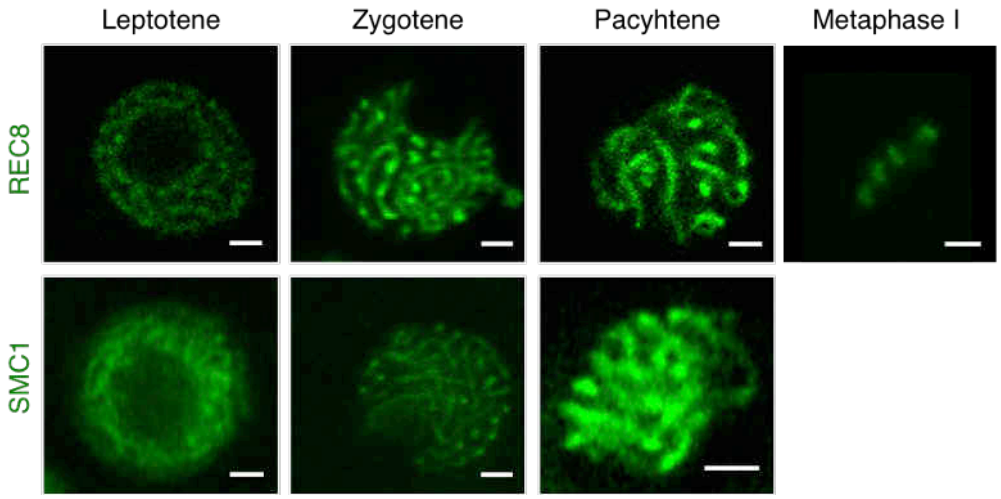

Figure 36: Confocal laser scanning microscopy of *rec8* plants expressing the construct *Pro$_{REC8}$:REC8:GFP* (upper panel) or *smc1* plants expressing the construct *Pro$_{SMC1}$:SMC1:GFP* (lower panel). A similar nuclear localization pattern was found for both cohesin complex proteins until metaphase I stage. Nuclei are cropped and therefore the cytoplasm is not shown here. Scale bar: 1 μm.

Also, comparing SMC1 to TUA5 signals in independent plant lines, a similar localization is found in pachytene, diakinesis and metaphase I, indicating a weak microtubule association (Fig. 37). To confirm this data, a line co-expressing *Pro$_{SMC1}$:SMC1:GFP* and *Pro$_{RPS5}$:RFP:TUA5* will have to be generated and analysed in future. However, consistent with the obtained results, a cytoplasmic has been reported for SMC3, the protein that forms a heterodimer with SMC1 (Lam et al., 2005).

Expression of this reporter construct in *smc1* (*ttn8*) mutants resulted in a full rescue of the embryonic lethal mutant phenotype since homozygous mutants could be generated and show no growth abnormalities. When analyzed by confocal microscopy I observed chromosome localization and expression dynamics largely similar to REC8. From early to late pachytene the signal intensity of REC8 is constantly reducing. Similar to the SMC1 signal, a clear chromosome structure is no longer visible due to the de-condensation of chromosomes in diplotene and diakinesis. In metaphase I, five small signals of REC8 become visible representing the five bivalents (Fig. 36).

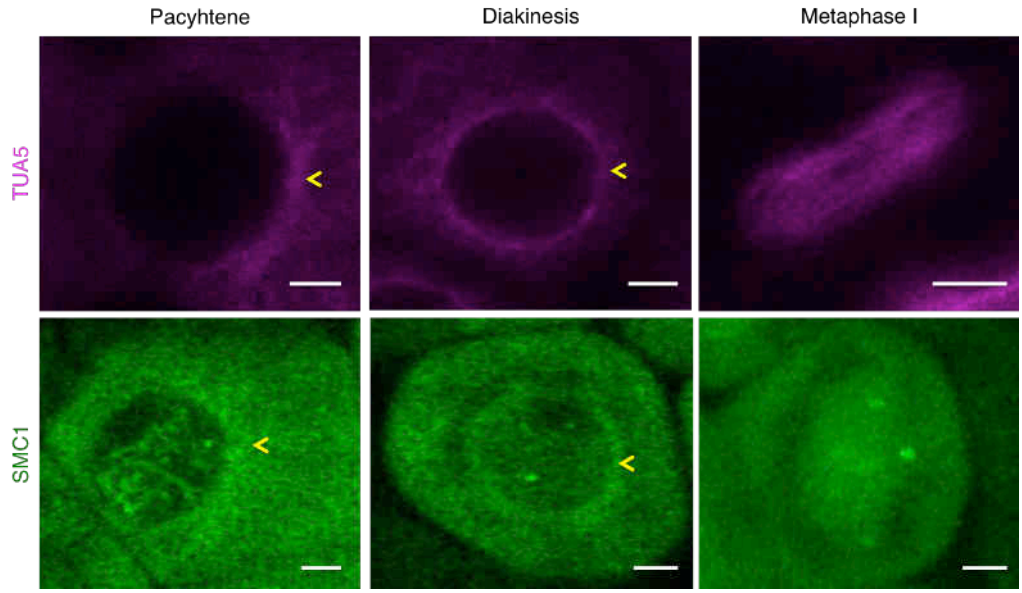

Figure 37: Confocal laser scanning microscopy of plants expressing *Pro$_{RPS5}$:RFP:TUA5* (upper panel) and *Pro$_{SMC1}$:SMC1:GFP* (lower panel). The arrows point out similar structures at pachytene diakinesis, and metaphase I of TUA5 and SMC1 close to the nuclear envelope. Scale bar: 1 μm.

Importantly, a reappearance of the REC8 signal was not observed in later stages. However, in contrast to REC8-GFP, at metaphase I we could not detect any chromosome localization for SMC1-GFP when using the live cell imaging approach. But we found a weak SMC1-GFP signal in the nucleus and the cytoplasm throughout meiosis I.

3.1.2 Summary and Future perspective

Taken together, I described the dynamics of the cohesin protein SMC1 for the first time in Arabidopsis. In contrast, to REC8-GFP I was not able to observe a signal of SMC1 at meiotic chromosomes during metaphase I. This is a surprising result since centromeric cohesion is essential for proper chromosome segregation. Further it leads to the question whether the signal is to weak to be observed or if SMC1 is not part of the centromeric cohesin complex. So far, I assume that the signal of SMC1 is too weak. Similar to the dynamics of SMC3, which has been shown to localize to meiotic chromosomes and spindles, a spindle localization has been observed for SMC1 (Lam et al., 2005). However, further experiments should confirm the interaction of SMC1 with microtubule and should then adress the function of SMC1 beyond sister chromatid cohesion. Also the identified cytoplasmic localization might indicate an additional role of SMC1 like it is already reported for animal cells (Yazdi et al., 2002; Bose et al., 2012).

3.2 Functional relevance of REC8 phosphorylation

The faithful transmission of chromosomes requires the stepwise loss of the chromatid cohesion complex during meiosis (Watanabe, 2005). First, cohesion is abolished only along the chromosome arms, allowing the segregation of homologous chromosomes in the first meiotic division. Importantly, centromeric cohesion is preserved until metaphase II. Then, the loss of centromeric cohesion leads to the accurate segregation of sister chromatids in meiosis II. In yeast, it has been shown that the separase

cleaves only phosphorylated REC8 (Brar et al., 2006). Further it has been shown that at anaphase I centromeric REC8 is constantly de-phosphorylated and thus protected against separase cleavage by the shugoshin PP2A functional unit to prevent premature loss of cohesion. Due to conservation of the proteins involved, the same mechanism is anticipated for plants. However, the kinase involved REC8 has not been described for plants. Therefore, this chapter will provide data identifying CDKA;1 as a kinase that phosphorylates REC8, and further focuses on the characterization of phosphorylation sites within REC8.

3.2.1 Results

Since CDKA;1 is a known key regulator of the mitotic and meiotic cell cycle and since a weak ckda;1 allele was shown to display an aberrant meiosis, I followed up the hypothesis that CDKA;1 might be the kinase relevant for REC8 phosphorylation (Harashima et al., 2016, Yang et al., 2020). Therefore, I screened within the REC8 protein sequence for occurrences of the short [S/T]P or the long consensus sequence [S/T]Px[R/K] which are indicative of a phosphorylation by CDKs. Using the web tool ExPASy ScanProsite, nine potential CDK sites were identified in Arabidopsis REC8 (Fig. 38).

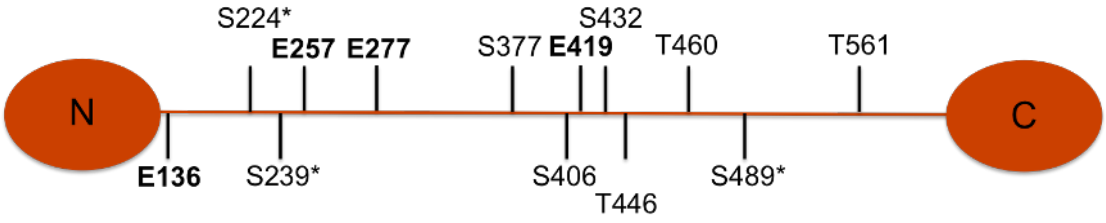

Figure 38: Schematic representation of the REC8 protein sequence. Labeled are the CDK consensus sequences by the respective S or T. Long consensus sequences are highlighted by a star. Potential separase cleavage sites are indicated by the respective E in bold.

It was shown that REC8 phosphorylation sites are located close to the separase cleavage site in yeast (Lin et al., 2016). Therefore, an additional

screening of Arabidopsis REC8 for the cleavage site motif ExxR was performed *in silico*. In total, four potential cleavage sites could be identified.

To test whether the identified phosphorylation sites are important for the cleavage of the α-kleisin by the separase, I generated a series of dephospho-mutants. Since the single mutation of S224A did not lead to any aberrant phenotype in previous studies and it was not possible to exchange the Serine 489 by an Alanine due to experimental errors, I started out by constructing a mutant REC8 version, in which seven of the nine potential CDK phosphorylation sites were mutated to alanine. The mutations were introduced in a genomic REC8 construct which was previously shown to rescue the *rec8* phenotype (Prusicki et al., 2019).

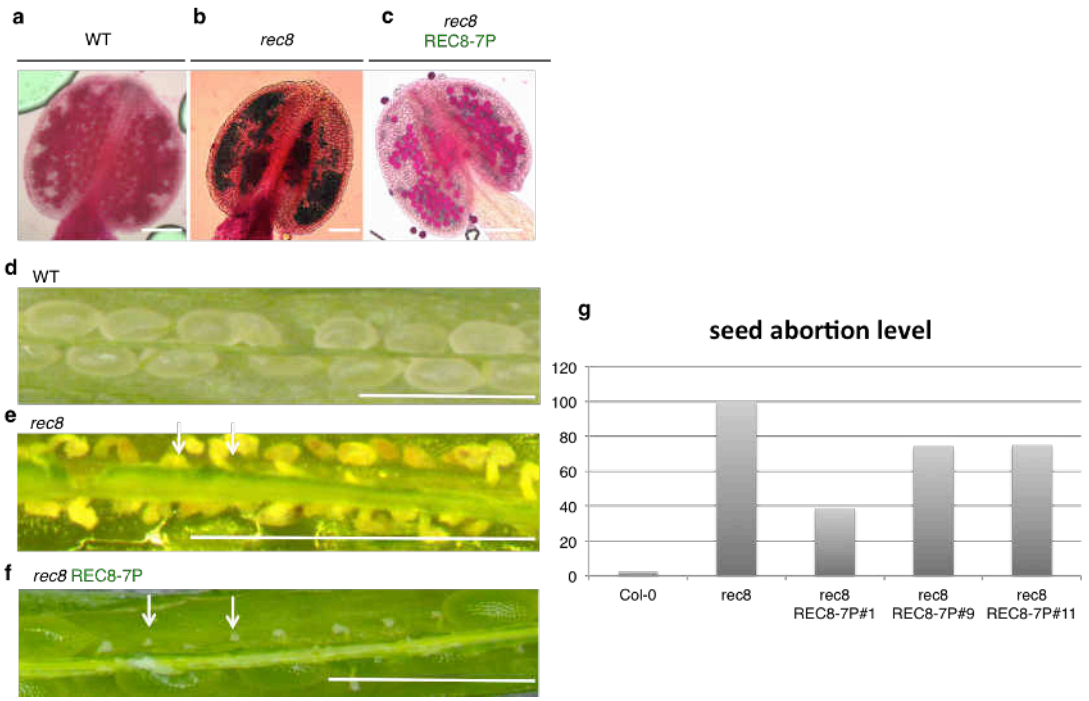

Figure 39: Phenotypical analysis of *Pro$_{REC8}$:REC8-7P:GFP rec8* plants in comparison to wild-type (WT). Panel a-c shows pollen viability analyzed by Peterson staining. A roundish shape and a pinkish color indicate viable pollen while dead pollen are characterized by a shrunken appearance and a bluish color. Wild-type plants show no pollen abortion (a). For *rec8* mutant a pollen abortion level of 100 % is found (b). The expression of *Pro$_{REC8}$:REC8-7P:GFP* leads to an intermediate pollen phenotype since a mixture of viable and dead pollen were found (c). Scale bar: 100μm. Panel d-f are pictures of opened siliques, showing the seed set. Wild-type siliques have an almost complete seed set with an abortion level of around 1%. In contrast, *rec8* mutant seeds are all aborted at an early stage, and can be recognized as small and shrunken structures (e, arrow). The expression of *Pro$_{REC8}$:REC8-7P:GFP*

results in an abortion level up to 75% (f). Graph represents the seed abortion level in the three *rec8* lines expressing *Pro$_{REC8}$:REC8-7P:GFP* in comparison to WT and *rec8* plants. Scale bar: 1000 μm.

The resulting construct, *Pro$_{REC8}$:REC8-7P:GFP,* was transformed into *rec8* heterozygous mutants, since homozygous mutants display normal vegetative growth but are male and female sterile (Fig. 39). In total, three *rec8*$^{-/-}$ plant lines expressing the *Pro$_{REC8}$:REC8-7P:GFP* construct, as verified by confocal microscopy (see below), could be recovered. These lines showed fertility problems indicated by a pollen abortion level of about 30- 50% and a seed abortion level of 38- 75% (Fig. 39). The degree of fertility was different between the lines, however I never saw a full rescue of the *rec8* mutant phenotype, indicating that the mutated amino acids are essential for the function of REC8.

To analyze meiotic defects in more detail, I performed chromosome spreads of pollen mother cells (PMC) expressing *Pro$_{REC8}$:REC8-7P:GFP*. In wild-type, chromosomes start to condense and undergo synapsis by the formation of the synaptonemal complex (SC) at zygotene stage. At pachytene, homologous chromosomes are completely synapsed and are easily recognized as thick threads (Fig. 40). Thereafter, the look of the chromosomes changes due to the dissolution of the SC and the appearance of chiasmata. In wild-type, five condensed bivalents are formed at the metaphase I plane (Fig. 40). Subsequently, homologs segregate to opposite poles by anaphase I. In the second meiotic division, aiming the segregation of sister chromatids, the two sets of five homologs align at two metaphase II plates, followed by the segregation of sister chromatids at anaphase II (Fig. 40). Based on this, four groups of chromosomes harboring five non-replicated chromosomes each can be recognized as bright distinct dots at telophase II (Fig. 40).
In contrast to wild-type, chromosome spreads of *rec8* PMC show the absence of homologous pairing (Fig. 39, arrow) and chromosome fragmentations (Fig. 40, arrowhead). In contrast, in *rec8* meiocytes expressing the construct *Pro$_{REC8}$:REC8-7P:GFP* I observed unsynapsed chromosomes at pachytene in 21 % (n=23) of the cells, indicative of defects in pairing and/or synapsis. Since

79 % of the cells were fully synapsed, a weaker phenotype for *rec8* meiocytes expressing the construct *Pro$_{REC8}$:REC8-7P:GFP* was determined when comparing to the *rec8* mutant phenotype.

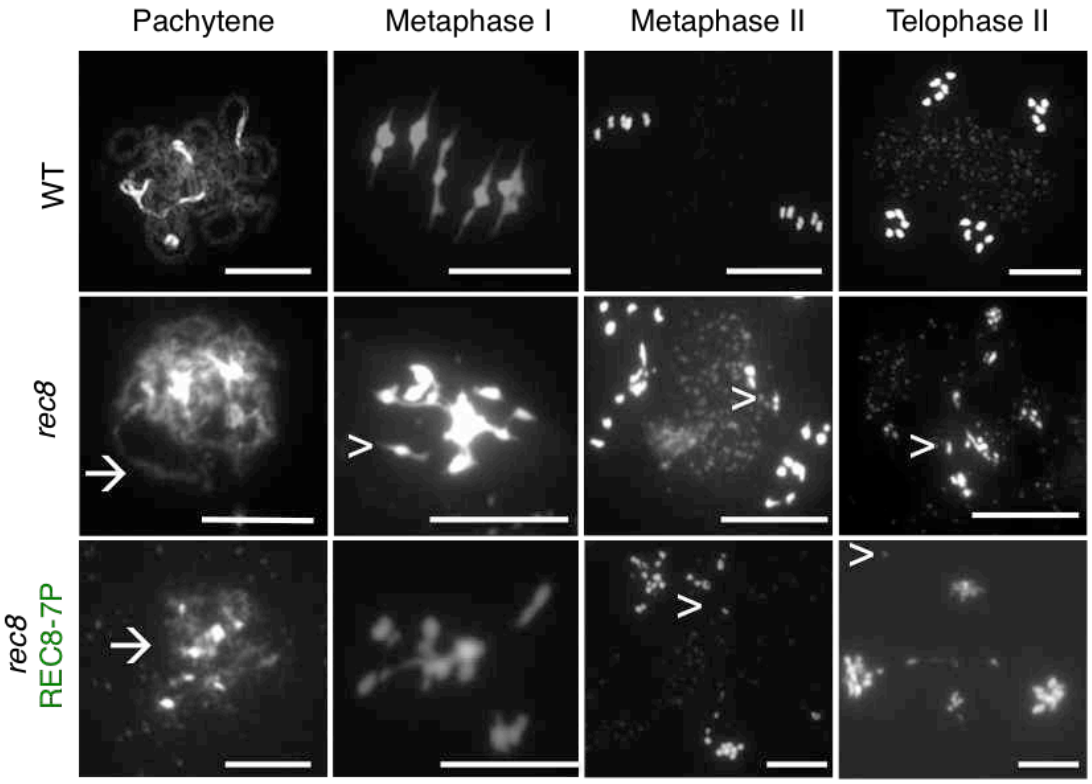

Figure 40: Chromosome spreads of PMCs from wild-type (WT), *rec8* and *rec8* plants expressing the construct *Pro$_{REC8}$:REC8-7P:GFP*. PMCs indicate pairing problems in *rec8* and *rec8* plants expressing the construct *Pro$_{REC8}$:REC8-7P:GFP* at pachytene. At metaphase I, five bivalents are formed in wild-type. In contrast, chromosomal entanglements are found in rec8 and *rec8 Pro$_{REC8}$:REC8-7P:GFP* plants. At metaphase II and telophase II similar defects e.g. chromosome fragmentation and miss-segregation are found in rec8 and *rec8 Pro$_{REC8}$:REC8-7P:GFP* plants. Scale bar: 10 μm.

In metaphase I cells, we observed chromosome entanglements in 28% (n=14) of the meiocytes and also fragmentation was found. However, comparing the metaphase I spreads to *rec8* metaphase chromosomes (Fig. 40) that always show chromosome entanglements (n=21), a milder phenotype was observed. Following meiosis in *Pro$_{REC8}$:REC8-7P:GFP rec8* plants until telophase II, chromosome fragments and miss-segregated chromosomes become obvious by unevenly distributed and lacking chromosomes (Fig. 40).

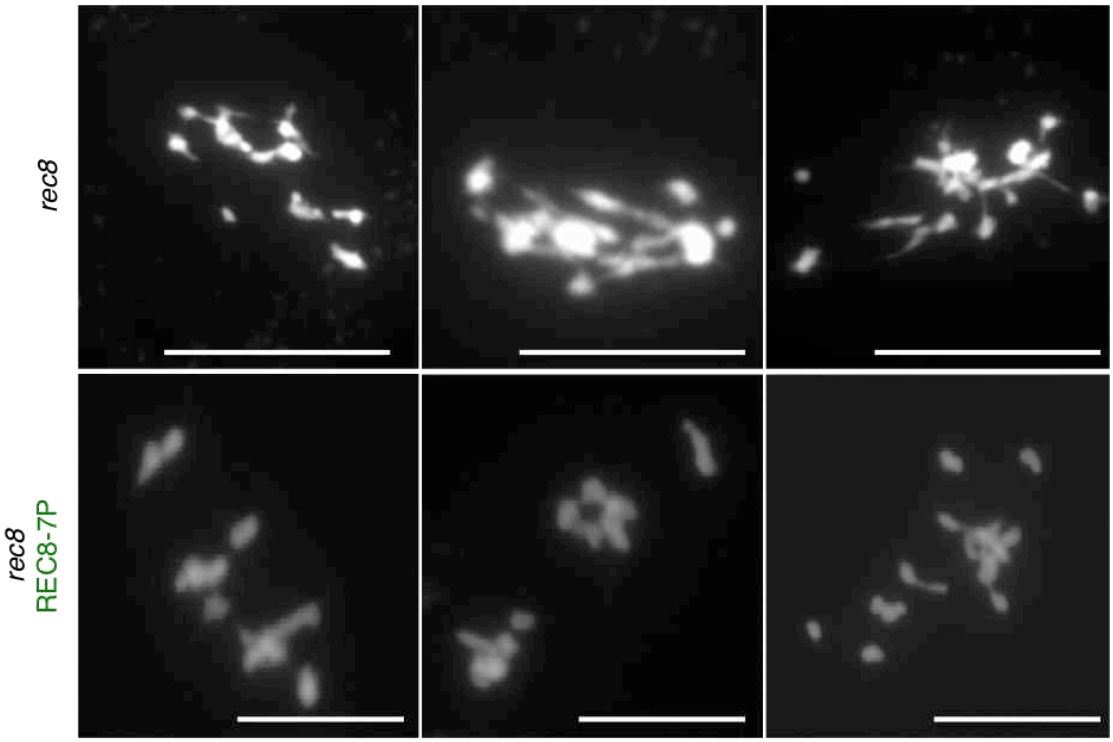

Figure 41: Comparison of metaphase I PMCs from *rec8* plants and *rec8* plants expressing the construct *Pro$_{REC8}$:REC8-7P:GFP*. Scale bar: 10 μm.

To more closely investigate the effect of mutating seven potential CDKA;1 phosphorylation sites in REC8, we asked whether the dynamics of *Pro$_{REC8}$:REC8-7P:GFP* changed in comparison to a GFP fusion of wild-type REC8. Therefore, confocal laser scanning analysis was performed. Recently, the dynamics of the fully functional reporter *Pro$_{REC8}$:REC8:GFP* has been described (Prusicki et al., 2019). In brief, a REC8-GFP signal becomes visible as very thin threads at leptotene (Fig. 36). As synapsis starts, the REC8 signal becomes stronger and reaches a maximum at zygotene stage (Yang et al., 2019). At pachytene, REC8 is evenly distributed on the fully synapsed chromosome (Fig. 36).

In meiocytes expressing *Pro$_{REC8}$:REC8-7P:GFP*, I could not detect any obvious changes of the REC8 loading or distribution along meiotic chromosomes, however when analyzing the dynamics in detail by live cell imaging, I found that REC8 persist until anaphase I on meiotic chromosomes (Fig. 42). However, the signal is lost after anaphase I and reappearance was not observed in later stages.

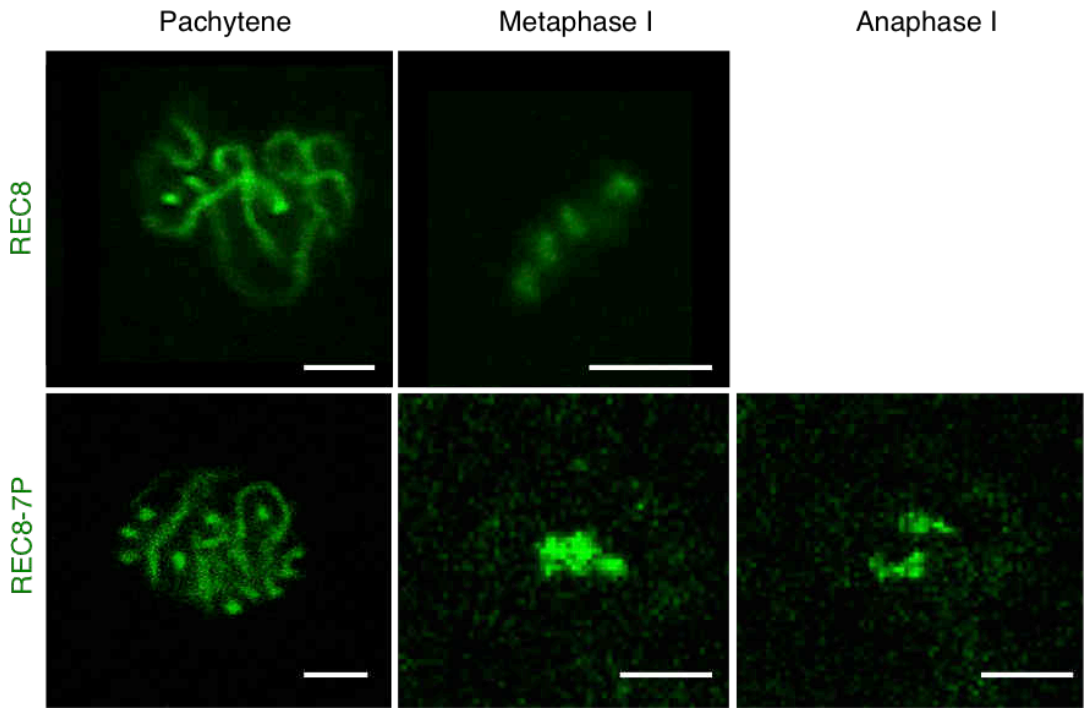

Figure 42: Confocal laser scanning analysis of meiocytes. Upper row shows the chromosomal localization of *Pro$_{REC8}$:REC8:GFP* at pachytene and metaphase I in green. A signal at later stages was never observed. Lower row represents a similar localization of *Pro$_{REC8}$:REC8-7P:GFP* to pachytene and metaphase I chromosomes. In addition a signal was observed at anaphase I. Scale bar: 1 μm.

Taken together, we found that the expression of *Pro$_{REC8}$:REC8-7P:GFP* in rec8 mutant background results in plants showing a partial rec8 phenotype as documented by chromosome spreads of PMCs. Interestingly, following the REC8-7P localization, I observed a wild-type like chromosomal distribution with a prolonged chromosomal association including anaphase I.

Next, I wanted to analyze the relevance of the individual phosphorylation sites. In previous studies, it was found that the *rec8* mutant plants expressing *Pro$_{REC8}$:REC8-S224A:GFP* lead to a full rescue of the *rec8* mutant phenotype. Therefore, to gather additional evidence which CDK phosphorylation sites might be used by CDKA;1, an *in vitro* kinase assay was performed by Dr. Hirofumi Harashima to test for a phosphorylation *in vitro* (Harashima et al., 2016). Since the CDK kinases only function in a complex with a cyclin, the meiosis specific cyclins TAM and SDS were used in the phosphorylation

assay. By this approach, it was possible to identify one CDKA;1-TAM and five CDKA;1-SDS phosphorylation sites (table 2).

Table 2: Identification of CDKA;1 phosphorylation sites of REC8. Left column indicates the first amino acid of the potential CDKA;1 consensus sequence. The amino acid that was phosphorylated by CDKA;1-TAM is highlighted by a circle in the second column. In vitro phosphorylated amino acids by CDKA;1-SDS are labeled by a circle in the third column. In the right column, phenotypes that are found for *rec8* plants expressing the respective single dephospho-mimic construct.

REC8 AA	CDKA;1-TAM	CDKA;1-SDS	Phenotype (S/T→A)
Ser224			wild-type
Ser239	○	○	*rec8* like with REC8:GFP signal in meiosis II
Ser377		○	no transformant
Ser406			wild-type
Ser432			
Thr446		○	REC8 signal in meiosis II
Thr460		○	*rec8* like
Ser489			
Thr561		○	wild-type

Based on this result, I generated single dephospho mutants taking the genomic REC8-GFP fusion as basis and converting the respective serine or threonine residue into alanine. The mutant constructs were then transformed into *rec8*$^{+-}$ mutant background and in the progeny *rec8*$^{--}$ plants carrying the transgene were analyzed for rescue. In the context of my master thesis, I analyzed the mutation of S239A. In this case, I was able to recover two *rec8* mutant plant lines expressing the construct *Pro$_{REC8}$:REC8-S239A:GFP* and both lines showed a *rec8* phenotype. As for the REC8-7P-GFP line, I found a normal chromosome localization of REC8 on prophase I chromosomes. However, in contrast to wildtype, I observed a REC8 signal also in interkinesis I. A localization of *Pro$_{REC8}$:REC8-S239A:GFP* to anaphase I has not been analyzed. Therefore a detailed analysis of the dynamics of *Pro$_{REC8}$:REC8-S239A:GFP* should be analyzed by live cell imaging. In addition to see if the

S239A mutation leads to an over-cohesion phenotype or if REC8 cohesion function is abolished, chromosome spreads of PMCs need to be performed and compared to wildtype and *rec8* mutants.

In this study, single dephospho-mimic mutants were generated for the following amino acids: S406A, S377A, T446A, T460A and T561A. Unfortunately, it was not possible to recover plants expressing *Pro$_{REC8}$:REC8-S377A:GFP*. For *rec8* mutant plants expressing *Pro$_{REC8}$:REC8-S406A:GFP* and *Pro$_{REC8}$:REC8-T561A:GFP* a resulting wild-type like phenotype, indicated by a full seed set, was observed (Fig. 43b). In addition, three independent *rec8* plant lines expressing the construct *Pro$_{REC8}$:REC8-T446A:GFP* could be recovered. In comparison to wild-type, we found a 49% reduction of viable seeds in a *rec8* heterozygous background line #1 and a reduction of maximum 72% in two *rec8* homozygous mutant background line #2 and #4 (Fig. 43b). For plants that were transformed with the *Pro$_{REC8}$:REC8-T460A:GFP*, two independent plant lines with a *rec8* background could be recovered. While line#1 showed a wild-type phenotype, a seed reduction level of 65% was observed in line #2 exhibited (Fig. 43b).

For a detailed analysis of meiotic defects, chromosome spreads of PMC were conducted. As control, chromosome spreads of *rec8* meiocytes were performed.

In *Pro$_{REC8}$:REC8-T446A:GFP rec8$^{-/-}$* plants, I observed a milder meiotic phenotype as for *rec8* mutants. In most of the pachytene cells a thread-like structures was found, showing that synapsis is possible in these lines. However, in 33% of the pachytene cells (n=36) of line #2 and 50% of the observed pachytene cells (n=22) of line #4, unsynapsed regions were found, indicating problems in pairing and/or synapsis. Furthermore, while the majority of metaphase I cells showed five bivalents, an aberrant chromosome behavior was found in 13% (n=23) of line #2 PMCs and in 12% (n=39) of PMCs of line #4 cells.

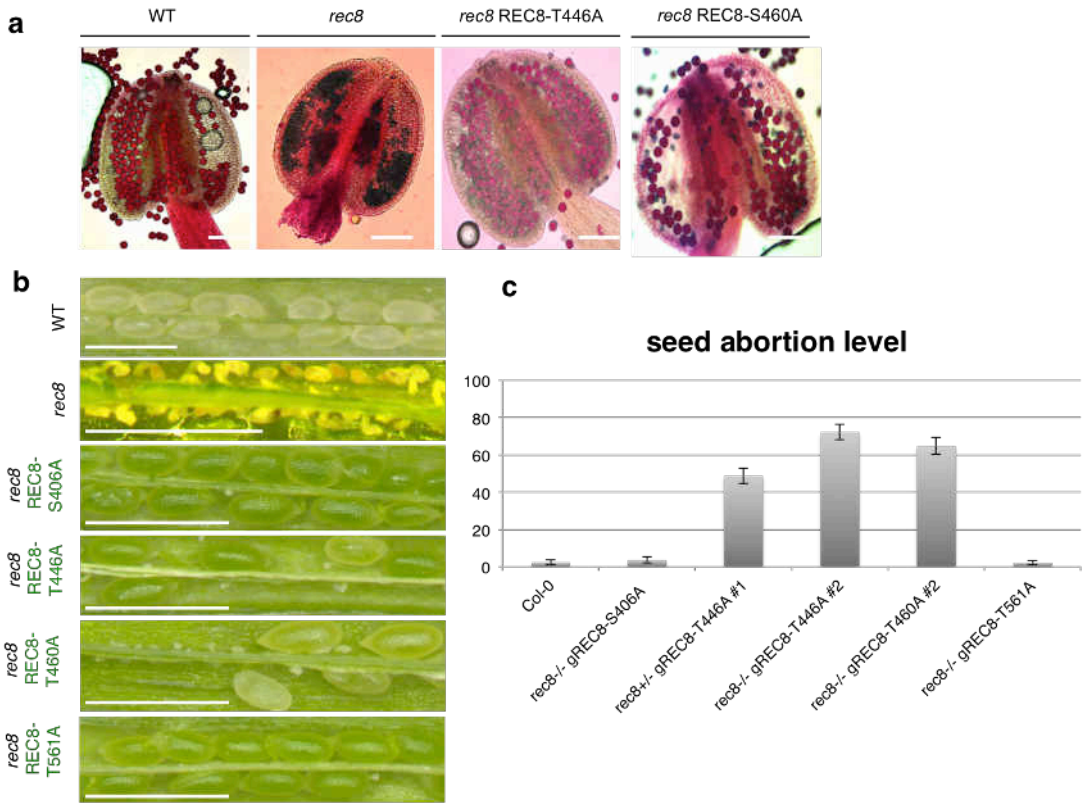

Figure 43: Phenotypic analysis of siliques of *rec8* mutants expressing the respective single dephosphomimic constructs in comparison to wild-type (WT) and *rec8* mutant. a, pollen viability has been analyzed by Peterson staining. b, a wild-type seed set was observed for the dephosphomic mutants S406A and T561A. The exchange of T446A and T460A #2 results in a mixture of viable and aborted seed, further represented in the Graph (**c**). Scale bar: 1000 μm.

Only seven cells at anaphase I were identified, six had a wild-type like anaphase I and only a single cell showed miss-segregating chromosomes (Fig. 44). Fragmentations were not found in this analysis. However, due to the low number of anaphase I cells it is not possible to draw final conclusions. For the second meiotic division, I found miss-segregating chromosomes e.g. in 54% (n=15) of anaphase II cells of line #2. Furthermore, miss-segregated chromosomes as well as chromosome bridges were found in telophase II cells of line #2 (n=10) (Fig. 44). Importantly, chromosome fragments typical for *rec8* mutants were found in both lines expressing the construct *Pro$_{REC8}$:REC8-T446A:GFP*.

The expression of the construct *Pro$_{REC8}$:REC8-T460A:GFP #2* results in a *rec8* mutant background as seen by chromosome spreads of PMC (Fig. 44). Pairing problems in these plants were found in all observed pachytene cells (n=15). Furthermore, all of the observed metaphase I cells showed a *rec8* like structure. In addition to chromosome fragmentation, miss-segregation and chromosome bridges were found for all anaphase II (n=15) and all telophase II (n=16) cells of line #2.

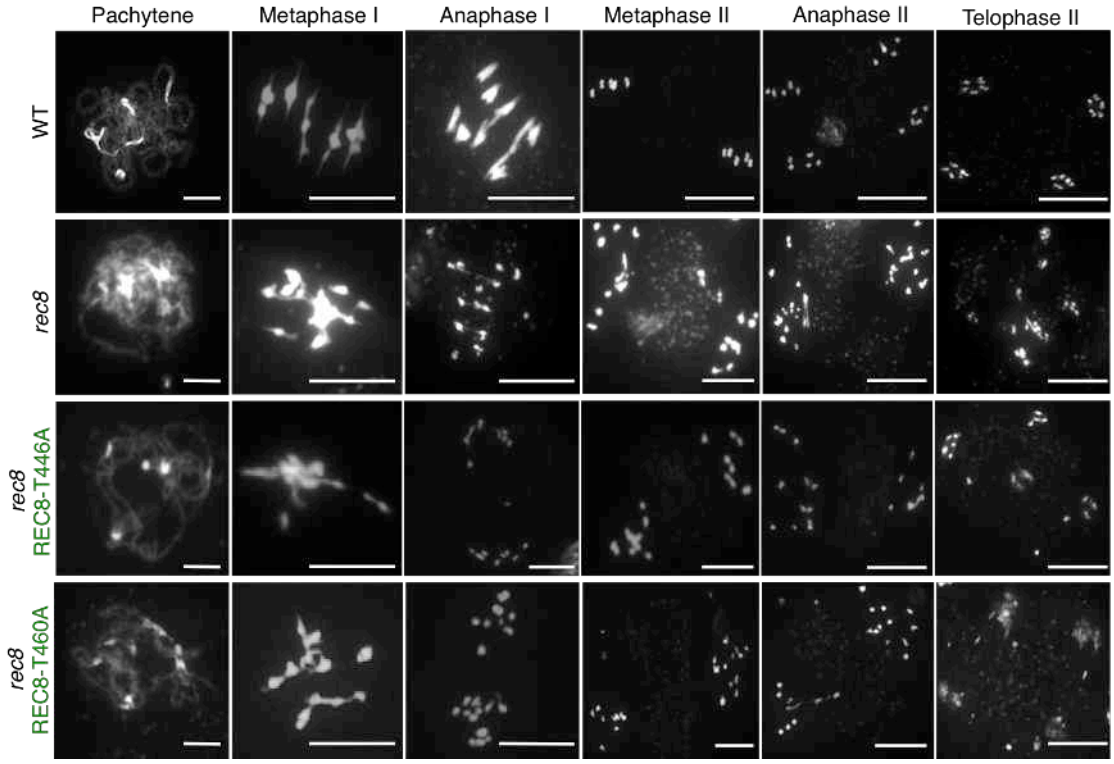

Figure 44: Chromosme spreads of PMCs from wild-type (WT), *rec8* and *rec8* plants expressing *Pro$_{REC8}$:REC8-T446A:GFP line #4* or *Pro$_{REC8}$:REC8-T460A:GFP line #2*. In pachytene, pairing problems were observed for *rec8* plants expressing the constructs *Pro$_{REC8}$:REC8-T446A:GFP* and *Pro$_{REC8}$:REC8-T460A:GFP* indicated by unsynapsed regions. In metaphase I, both constructs partially lead to a chromosome behavior similar to rec8 metaphase I chromosomes. PMCs expressing *Pro$_{REC8}$:REC8-T446A:GFP* show miss-segregated chromosomes in the 2nd meiotic division leading to lacking chromosomes at telophase II. For the expression of *Pro$_{REC8}$:REC8-T460A:GFP*, a *rec8*-like phenotype was found since chromosome fragmentation, miss-segregation and chromosome bridges were found in meiosis II. Scale bar: 10 μm.

To analyze the dynamics of *Pro$_{REC8}$:REC8-T446A:GFP* line #2, 4 and 10 and *Pro$_{REC8}$:REC8-T460A:GFP* line #2 in dividing meiocytes, confocal laser scanning microscopy was performed. For both constructs a wild-type like

localization and distribution along meiotic chromosomes was observed in prophase I.

Surprisingly, for line #10 expressing *Pro$_{REC8}$:REC8-T446A:GFP* a nuclear localization during the second meiotic division and tetrad stage was observed (Fig. 45). However, I never saw a signal in mature pollen. To this end, the localization analysis of *Pro$_{REC8}$:REC8-T446A:GFP* line #2 and #4 are missing to this end. To see if the prolonged nuclear localization in this line causes additional defects, it will be necessary to perform live cell imaging and chromosome spreads of PMCs from line #10.

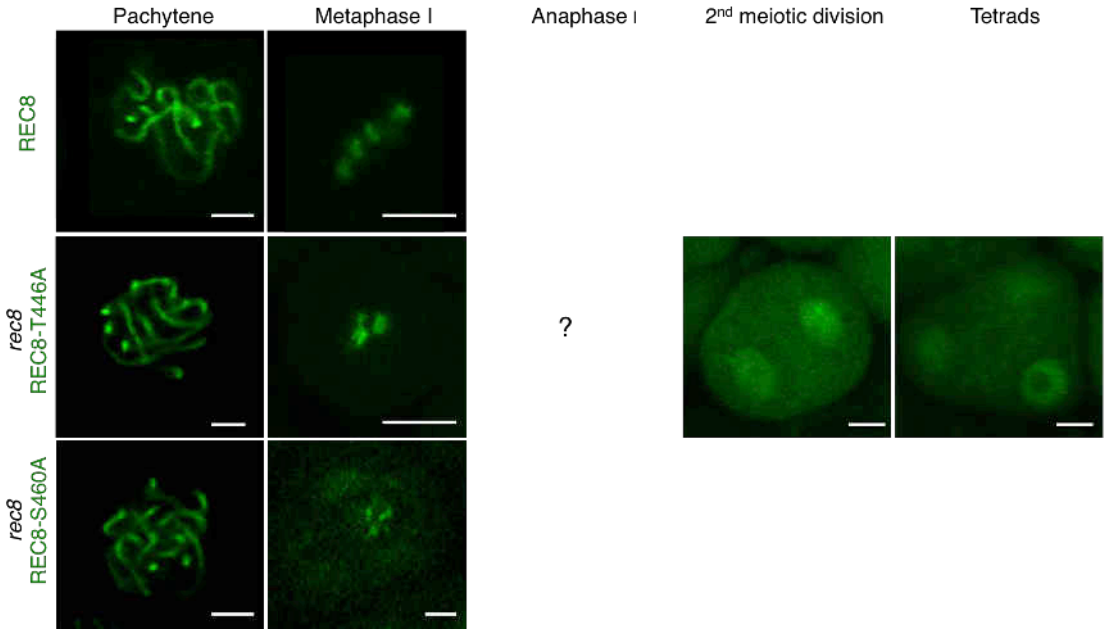

Figure 45: Confocal Laser scanning microscope analysis of *rec8* mutants expressing *Pro$_{REC8}$:REC8:GFP*, *Pro$_{REC8}$:REC8-T446A:GFP line#10* and *Pro$_{REC8}$:REC8-T460A:GFP line #2*. All constructs show a similar REC8 localization and distribution along prophase I chromosomes (green). A prolonged REC8 localization at anaphase I as seen for *Pro$_{REC8}$:REC8-7p:GFP* was not observed *Pro$_{REC8}$:REC8-T460A:GFP*. Data for T446A line #10 are missing although a signal was found in the second meiotic division and in tetrads. Scale bar: 1 μm

Taken together, I generated a multiple dephospho mutant of REC8 leading to an aberrant meiosis. Furthermore, I characterized a single dephospho (T446A) that is essential for a proper function of REC8.

3.2.2 Discussion and Future perspective

The meiotic cell division requires the stepwise loss of cohesion, which is in part mediated through the cleavage of the alpha-kleisin by separase. Since it has been shown for yeast that only phosphorylated REC8 is recognized by the separase, a kinase mediating REC8 phosphorylation is required (Katis et al., 2010; Ishiguro et al., 2010). In yeast, it was shown that the Polo-like kinase CDC5 is responsible for the phosphorylation of meiotic proteins (Lee and Amon, 2003; Clyne et al., 2003) and that one of its targets is REC8 (Attner et al., 2013). Furthermore, it was postulated that more kinases act beside CDC5 to fully ensure the stepwise loss of REC8 since the kinases Dbf4-dependent Cdc7 kinase (DDK) and casein kinase 1 (CK1) are also able to phosphorylate REC8 *in vivo* and that multiple phosphorylation sites within REC8 are required for the separase-mediated cleavage (Katis et al. 2010). Homologs of Shugoshin and PP2A proteins which are needed for the protection of REC8 at centromeres are found in mammals and plants, indicating a role of phosphorylation in these organisms as well. However, the kinases involved in this process have not been identified yet (Gutiérrez-Caballero et al., 2012). Furthermore, a sequence homolog of CDC5 is not found in *Arabidopsis thaliana*, making the search for the relevant kinase more difficult.

A complete sterile phenotype of a weak *cdka;1* alleles indicated a central role of the major mitotic cell cycle regulator CDKA;1 also in meiosis (Dissmeyer et al., 2009). Since this initial finding several functions of CDKA;1 have been identified, e.g. the control of crossover distribution and the assembly of the chromosome axis (Wijnker et al., 2019; Yang et al., 2019). To investigate a possible role in the control of cohesin, we tested whether the CDKA;1 is able to phosphorylate REC8 by generating dephospho mutants. The exchange from serine or threonine to an alanine leads to a non-phosphorylatable REC8 version, which should be resistant to a separase-mediated cleavage. I expected that the mutation of phosphorylation sites that are responsible for protection of centromeric cohesion during meiosis, would lead to a prolonged persistence of cohesion along the chromosomes through meiosis that could

be confirmed by live cell imaging of the corresponding GFP reporter construct. In addition, I expect that an over-cohesive phenotype (chromosome mass in metaphase I) should be seen in chromosome spreads of PMCs. Further, I speculated that no defects e.g. impaired pairing or fragmentation should be visible in early prophase if the mutated phosphorylation sites are only needed for the centromeric cohesion protection. Defects in chromosome segregation might be visible from metaphase I onwards since I assume that the segregation of homologous and of sister chromatids could not take place.

In general, a separase resistant REC8 should exhibit a similar phenotype that was observed in *separase* knockdown mutants. In Arabidopsis, *separase* mutants show chromosome segregation problems starting from late metaphase I onwards leading to a reduction of fertility (Liu and Makaroff, 2006). Chromosome spreads of pollen mother cells (PMC) revealed chromosome fragmentation and bridges in *separase* plants. I speculate that the spindle might still attach to meiotic kinetochores and tries to pull homologous apart during meiosis I subsequently leading to chromosome fragmentation. Furthermore, intact bivalents were observed in anaphase I because of persistent sister chromatid cohesion.

Interestingly, *rec8* plants expressing a REC8 variant in which 7 out of 9 consensus CDKA;1 phosphorylation sites were mutated to alanine (*Pro$_{REC8}$:REC8-7P:GFP*) exhibit fertility defects with a partial *rec8* like phenotype on the chromosomal level since not all of the analyzed meiocytes exhibit defects. I observed a longer persistence of *REC8-7P:GFP* on meiotic chromosomes matching to the expected consequences of mutating phosphorylation sites that are required for a separase-mediated cleavage.

Unexpectedly and in contrast to the observation in *separase* mutants, I further identified that the expression of *Pro$_{REC8}$:REC8-7P:GFP* leads to chromosome pairing and/ or synapsis problems at early meiosis I. This finding indicates that the phosphorylation sites might be essential for other functions of REC8.

In contrast to the over-cohesive phenotype that was found in *separase* mutants at metaphase I, the mutation of seven phosphorylation sites leads to chromosome fragmentation and entangled chromosomes typically found in

rec8 mutants (Yang et al., 2011). However, it could be possible that major cohesin is removed from chromosomes arms by a separase independent pathway. It was shown that besides the separase-dependent cleavage of cohesins, the WAPL-dependent prophase I pathway removes cohesins. For example, it was recently described for yeast that 50% of cohesins are removed along the chromosome arms by WAPL (Challa et al., 2019) already before anaphase I and corresponding observations have also been made in plants (De et al., 2014; Yang et al., 2019). It is possible that in meiocytes expressing *REC8-7P:GFP*, the major amount of cohesin is removed by WAPL which does not require a phosphorylated REC8. This could be tested by combining *rec8* Pro_{REC8}*:REC8-7P:GFP* with *wapl* mutants which should result in a stronger over-cohesion phenotype as seen for *wapl* alone if Pro_{REC8}*:REC8-7P:GFP* indeed represents a separase resistant version of REC8.

From our results, it can be concluded that the mutated phosphorylation sites are important for the function of REC8 in general, since the rescue of the rec8 mutant phenotype is not 100% However, aside from the function of sister chromatid cohesion REC8 was shown to be involved in homologous pairing and recombination. Therefore *rec8* mutants exhibit a complex phenotype that makes it complicated to decipher if the observed defects in plants expressing *REC8-7P:GFP* at least in part result from a problem in REC8 cleavage by separase. However, the longer persistence of REC8-7P:GFP on meiotic chromosomes already indicates a problem in cleavage by separase at anaphase onset (Fig. 42). Therefore, a detailed analysis of the meta-to-anaphase transition is required. Interestingly, A longer metaphase I duration was observed in yeast cells that were mutated in 24 REC8 phosphorylation sites, which leads to defects in the stepwise loss of cohesion (Katis et al., 2010), which could be checked by live cell imaging of the Pro_{REC8}*:REC8-7P:GFP* expressing lines.

Furthermore, I was able to analyze four single REC8 Phosphomutants (S406A, T446A, T460A and T651A). Since, it was not possible to generate plants expressing the Pro_{REC8}*:REC8-S377A:GFP* construct, but this site was

phosphorylated in vitro, it is advisable to repeat this experiment. I could show that S406A and T561A are not necessary for normal REC8 function since the *Pro$_{REC8}$:REC8-S406A:GFP* and *Pro$_{REC8}$:REC8-T561A:GFP* could fully rescue the *rec8* mutant phenotype. If we exclude technical problems, the result would indicate that phosphorylation of this site is not necessary for full REC8 function, since in one case I apparently get full rescue. However, it is advisable to generate further independent lines and to investigate the existing lines more closely. T446A is the best candidate observed in this study for an amino acid with a role in cleavage control. I found that 67% of meiocytes from line#1 and 50% of line#2 exhibit a wild-type prophase I, while problems seem to appear from meta-anaphase I onwards. However, so far I could not capture enough cells in anaphase I to draw clear conclusions from line #2 and #4. Thus further chromosome spread analyses of PMCs need to be performed. In addition, I need to analyse line #10 more closely that had a longer persistance of *Pro$_{REC8}$:REC8-T446A:GFP* on meiotic chromosomes. For this line chromosome spread data are missing.

Since the expression of *Pro$_{REC8}$:REC8-T446A:GFP* lead to entangled chromosomes and fragments it would be interesting to perform a Fluorescence-in situ hybridization (FISH) analysis to get detailed informations about the presence of bivalents in anaphase I, revealing separase resistance of the mutated REC8.

Since REC8 is involved in many other processes like homologous pairing, thus *rec8* mutants display a very complex phenotype. This makes the identification of phosphorylation sites responsible for the stepwise loss of cohesion difficult, since an over-cohesive phenotype might be masked by other *rec8* phenotypes. It could for example be possible that specific phosphorylation sites within REC8 could influence other processes such as homologous pairing as it was reported for yeast. Important to mention is that I can not exclude the possibility that the phosphorylation site mutations lead to conformational changes of the protein structure, leading to a nonfunctional REC8 protein per se.

However, to get a better understanding if the CDKA;1 phosphorylation sites of REC8 identified in vitro are also used in vivo we performed a GFP-pulldown experiments from flowerbuds of *35S:AP1-GR ap1cal* Pro_{REC8}*:REC8:GFP* plants. So far, the identification of phosphorylation sites by mass spectrometry failed in my hands but the experiment should be repeated since it will give a better insight into the REC8 phosphoproteome *in vivo*. Furthermore, the localization of the functional Pro_{REC8}*:REC8:GFP* reporter should be analyzed in *cdka;1* weak loss of function mutants. If CDKA;1 is indeed relevant for a REC8 phosphorylation that leads to a cleavage by separase, I would expect that REC8 is only partially removed if the CDKA;1 level is reduced.

Taken together, it was not possible to unequivocally identify a single phosphorylation site within REC8 that is required for a separase-mediated cleavage. However, we showed that the exchange of seven phosphorylation sites in REC8 as well as the single T446A mutation resulted in meiotic defects and a prolonged binding of the mutant forms of REC8 to meiotic chromosomes.

4. Material and methods

4.1 General

All chemicals and enzymes that were obtained from following companies: AppliChem (Darmstadt), Invitrogen (Karlsruhe), Merck (Darmstadt), Milipore (Billerica, USA), New England Biolabs (Frankfurt am Main), Qiagen (Hilden), Roche Diagnostics (Mannheim), Roth (Karlsruhe), Sigma Aldrich (Munich), TAKARA BIO INC (Kusato, Japan) and Thermo Fischer Scientific (Dreieich). Commercially available kits and prepared buffers that were used are described in Appendix 6.1.

4.2 Plant material

In this study, the *Arabidopsis thaliana* accession Columbia (Col-0) was used as a wild-type reference. The used T-DNA insertion lines SALK_044851 (*rad21.1*), SALK_053140 (*rad21.2*), SALK_076116 (*rad21.3*), SAIL_807_B08 (*rec8*), CS16082 (*ttn8-1; smc1*), SALK_076791 (*wapl1-1*) and SALK_127445 (*wapl2*) were obtained from the Nottingham Arabidopsis Stock Center (http://arabidopsis.info/). Corresponding geneses are depicted in the table below.

Table 3: T-DNA insertion lines and the corresponding genes that were used in this thesis.

Name of T-DNA insertion line	mutagenized gene	Background
SALK_044851	AT5G40840 (RAD21.1)	*Col-0*
SALKseq_053140.1	AT3G59550 (RAD21.2)	*Col-0*
SALK_076116	AT5G16270 (RAD21.3)	*Col-0*
SAIL_807_B08	AT5G05490 (REC8)	*Col-0*
TTN8-1	AT3G54670 (SMC1)	*Col-0*
SALK_076791	AT1G11060 (WAPL1)	*Col-0*
SALK_127445	AT1G61030 (WAPL2)	*Col-0*

The *35S:AP1-GR ap1 cal* line was kindly provided by Frank Wellmer (Wellmer et al., 2006). PRO_{REC8}*:REC8:GFP* (Prusicki et al., 2019), $PRO_{H2A.W.6}$*:H2A.W.6:RFP (*Yelagandula et al., 2014) Pro_{HTR5}*:MBD6:GFP*

(Ingouff et al., 2017), *Pro$_{SMC1}$:SMC1:GFP* (Master Thesis VK) and *PRO$_{RPS5}$:RFP:TUA5* (Komaki and Schnittger, 2017) reporters were previously generated.

4.3 Plant growth conditions

Seeds were surface-sterilized with chlorine gas and sown on 1% (w/v) agar plates containing half-strength Murashige and Skoog (MS) media (Appendix 6.1 table 8). Antibiotics were added for seed selection when required. For stratification, plates were stored for 2 days at 4°C in the dark, thereafter plates were transferred for 10 days to a growth chamber with long day conditions (16h of light; 21°C/ 8h of dark; 18°C and 60% humidity) for seed germination. Seedlings were transferred to soil and grown under long day conditions until seed production.

4.4 Genotyping

First genomic DNA was extracted from 2-3 weeks old *Arabidopsis thaliana* leaves: Leaves were removed with sterile forceps and added to 300 µl of Magic Buffer (Appendix 6.1 table 8) into a 96-er well plate. Finally two steel beads were added and the plate was shaken in a rocker mill for 2 min with a frequency of 25/s. Plates were centrifuged at 4500 rpm for 2 minutes. Extracted DNA was diluted 1:10 in PCR water and stored at -20 °C. Genotypes were determined by PCR using primers listed in Appendix 6.4 table 17. Reactions were performed in the following Thermocycler: Biometra TProfessional Basic Thermocycler or Biometra TAdvanced Thermal Cycler (Analytik Jena, Jena). For the used PCR reactions and program see Appendix V.

4.5 Agarose gel electrophoresis

PCR products were analyzed by agarose gel electrophoresis. The size dependent separation of DNA molecules was performed by horizontal gel electrophoresis in 1% agarose gel (1% (w/v) agar in 1x TAE (Appendix 6.1

table 10) with 100 ng/ml ethidium bromide. DNA samples were mixed with 10x Loading Dye (Appendix 6.1 Tabl. 10) if that was necessary. Gels were run at 120 V for 30-40 minutes.

4.6 Plasmid constructions and plant transformation

The used and generated plasmids are summarized in Appendix III. The plasmid construction primers are listed in Appendix 6.4 table 18 and 19. Furthermore, used bacteria strains are listed in Appendix 6.2.

For generating the different single REC8 phosphomutants, the serine residues were mutated to alanine (GCT). The reporter construct *Pro$_{REC8}$:REC8:GFP* was used as template. Specific forward primers were designed and phosphorylated at the 5´end. The mutagenesis was constructed by Primestar max polymerase PCR. PCR products were extracted from the agarose gel according to manufacturers instruction of NucleoSpin Gel and PCR Clean-up kit (Appendix 6.1 table 4) and were purified. Subsequently, the generated plasmids were ligated according to the TAKARA Ligation mix manual (Appendix 6.1 table 4) and transformed into *E.coli DH5a* cells.

To create the *Pro$_{RAD21s}$:RAD21s:GFP* and *Pro$_{RAD21.2}$:GFP:RAD21.2* constructs, a fragment covering the genomic region of each gene together with an upstream region of the start codon of 2 Kb, 1 Kb and 2.5 Kb, respectively, along with 1 Kb downstream of the stop codon of each gene was amplified by PCR and cloned into pENTR2B by SLiCE. For the SLiCE reaction 50- 200 ng of linearized vector was mixed with the insert in a molar ratio of 1:1-1:10 (vector: insert). 1 µl of 10x SLiCE buffer (Appendix 6.1 table 10) and 1 µl of SLiCE extract were added. Finally, the SLiCE reaction was filled up to 10 µl with ddH_2O and incubated for 1 hour at 37 °C. Resulting plasmids were used for transformation of *E.coli TOP10* cells. Next, a restriction enzyme site (*Sma*I for *RAD21.1* and *RAD21.2*, and *Nae*I for *RAD21.3*) was inserted in front of the stop codon (C-terminal GFP fusion) or behind the start codon (N-terminal GFP fusion) of the RAD21s constructs. The resulting construct was linearized by the restriction enzyme digestion and was ligated to the *GFP* gene, followed by LR recombination reactions with the destination vector

pGWB501. 100- 300 ng of entry vector was mixed with 150 ng of the destination vector. 1 µl TE buffer (Appendix 6.1 table 10) and 1 µl LR Clonase™ enzyme mix (Appendix I Tabl. 3) were added. The reaction was incubated for 1-2 h at RT. Plasmids were stored at -20 °C or were immediately transformed into *E.coli TOP10*.

For the exchange of the native RAD21.2 promoter with the ASK1 promoter (1 kb upstream of the start codon), the promoter sequence was amplified by PCR and cloned into the *pENTR2B* $Pro_{RAD21.2}$*:GFP:RAD21.2* by SLiCE, followed by LR recombination reaction (Appendix 6.1 table 4) with the destination vector *pGWB501*.

To generate the Pro_{FIB2}*:FIB2:mTurquoise,* the genomic FIB2 sequence and 1kb upstream of the start codon and 800 bp downstream of the stop codon was amplified by PCR and cloned into the *pENTR2B* vector by SLiCE. A *SmaI* restriction enzyme site was inserted in front of the stop codon. The resulting construct was linearized by *SmaI* digestion and was ligated to the *mTurquoise* gene.

To generate the *RAD21.2 RNAi* construct, a 400 bp fragment of the *RAD21.2* CDS was amplified by PCR with attB flanking primers and cloned into the *pDONR221* vector by gateway BP reaction (Appendix 6.1 table 4). The resulting construct was integrated into the *pK7GWIWG2* vector by gateway LR reaction (Appendix 6.1 table 4).

All DNA samples were analyzed for their correct sequences at Eurofins Genomics (Hamburg) and sequencing primers are listed in Appendix 6.4 table 20. For this, 800 ng DNA per 15 µl reaction solution were mixed with 2 µl of primers and were sent in for sequence analysis. Finally, constructs were transformed into *Arabidopsis thaliana* plants by floral dipping (Clough and Bent, 1998). Plants were grown under long day conditions until bolting. Before transformation, plants were watered and siliques were cut off. Transformed *A. tumefaciens GV3101* were cultivated in 3 ml of LB $gent^{30}$/$spec^{100}$ for 2 days at 28 °C. 3 ml of bacterial suspension was centrifuged at full speed for 2 min, the supernatant was removed and the pellet was dissolved in 3 ml of transformation medium (Appendix 6.1 table 8). Closed flowers were coated

with *Agrobacterium* suspension by using a pipette. Excess liquid was removed with filter paper. Transformed plants were covered in plastic bags and incubated for 2 days in the dark. Finally plants were grown under standard condition until seeds were collected and T_1 screening was performed. For the selection of transformed T_1 plants, seeds were sterilized and sowed on selective 0.5x MS $Carb^{50}$/AB (depending on the final vector) medium. Seedlings that were resistant as determined by root development were transferred to soil after 2 weeks. Furthermore, fluorescence expression of transformed plants was analyzed by microscopy.

4.7 Phenotypic evaluation

Peterson staining was used to analyze the pollen viability (Peterson et al., 2010). Three flower buds containing either dehiscent or indehiscent (for whole anther staining) pollen were collected and dipped in 25 μl Peterson staining solution (Appendix 6.1 table 9) for 15 s on a microscope slide that was covered by a coverslip. Slides were incubated at 80°C for 10 min (for pollen counting) or 30 min (for whole anther staining) and aborted and non-aborted pollen grains were observed using a light microscope. Seed sets were determined by quantifying viable and aborted seeds of mature siliques; 3 siliques per plant were analyzed.

4.8 Cytogenetic analysis

The preparation of pollen mother cells DAPI spreads was performed as previously described (Ross et al., 1996). Flower buds were fixed in 3:1 ethanol/ acetic acid (fixative) overnight and washed once with fresh fixative solution and stored in 70% ethanol at 4°C. The flower buds were staged by size and washed once with ddH_20 and once with 10mM citrate buffer. The digestion of flower buds was performed in 10 mM citrate buffer (Appendix 6.1 table 9) for 2.5 hours at 37 °C. For the chromosome spreading, single flower buds were transferred to a drop of 45% acetic acid on a glass slide and squashed with a bended needle for 1 min. The spreading was performed for 1

min on a 46°C hot plate. The slide was washed with fixative solution and dried for at least 2 hours. The chromosome spreads were stained by 18 µl of Vectashield Antifade Mounting medium with DAPI (vector laboratories) and sealed with a cover slip.

4.9 FISH

The DAPI slides selected for fluorescence *in situ* hybridization (FISH) were washed in 100% ethanol until the coverslips could easily be removed (5-10 min) and subsequently washed in 4T (4X SCC and 0.05% v/v Tween20) for at least 1 h in order to remove the mounting medium.

After washing the slides in 2X SCC for 10 min they were placed in pre-warmed 0.01 M HCl with 250 µl of 10 mg/ml Pepsin for 90 seconds at 37 °C. The slides were then washed in 2X SCC for 10 min at room temperature. 15 µl of 4% paraformaldehyde (PFA) were added onto the slides, covered with a strip of autoclave bag and placed for 10 min in the dark at RT. The slides were then washed with deionized water for 1 minute and dehydrated by passing through an alcohol series of 70, 90, 100 %, for 2 minutes each. Slides were left to air-dry for 30 min.

Meanwhile, the probe mix was prepared by diluting 1 µl of probe (2-3 µg of DNA) in a total of 20 µl of hybridization mix (10% dextran sulphate MW 50,000, 50% formamide in 2x SSC).

Only 50 pmols (final concentration) of the LNA probes were used per slide. The probe mix was denatured at 95 °C for 10 min and then placed on ice for 5 min. Afterwards, the probe mix was added to the slide, covered with a glass coverslip, sealed and placed on a hot plate for 4 min in the dark at 75 °C. Finally, the slides were placed in a humidity chamber overnight at 37 °C. After hybridization, the coverslips were carefully removed and the slides were treated with 50% formamide in 2X SCC for 5 min in the dark at 42 °C. The slides were then washed twice with 2X SCC for 5 min in the dark at room temperature. Finally, 15 µl of DAPI-Vectashield solution were added to the slide and sealed with a coverslip. Images were taken on a Zeiss Axioplan

microscope (Carl Zeiss) equipped with a mono cool-view CCD camera. For all repetitive regions analyzed we used specific LNA probes.

4.10 Immuno-FISH

Immuno-FISH was performed using the TACE method (Sims et al., 2019). Immunofluorescence (IF) antibodies were used as follows: anti-ASY1 raised in guinea pig 1:10,000, anti-RAD51 raised in rat 1:300, anti-guinea pig Alexa488 1:400, anti-rat Alexa568 1:400. 45 rDNA was detected by using an LNA probe directed against the *Sal*I repeats (Sims et al., 2019). Slides were mounted in 2 *µ*g/ml DAPI diluted in Vectashield (Vectorlabs), imaged on an Axioplan 2 microscope (Carl Zeiss) and acquired with a mono cool view CCD camera. Z-stacks at 100 nm intervals were recorded, deconvolved (AutoQuantX software), slice aligned and Z-projected (HeliconFocus software). RAD51 foci were quantified by manually counting colocalizing signals with the DAPI only. Colocalization with the 45S rDNA probe was scored if the RAD51 focus overlapped by at least 50 % with the labelled probe. Global RAD51 detection was performed as described.

4.11 Protein localization analysis by confocal laser scanning microscopy

Anthers expressing the respective fluorescence reporter construct were dissected, transferred onto a slide with a drop of water and sealed with a cover slip. Images were acquired by using a Leica TCS SP8 inverted confocal microscope or a Zeiss LSM 880 upright microscope immediately. The fluorescent protein mTurquoise was excited at λ 458 nm and detected at λ 460–510 nm, GFP was excited at 488 nm and detected at 495–560 nm and TagRFP was excited at 561 nm and detected at 570–650 nm.

4.12 RAD21.2/ H2A.W.6 accumulation analysis

To analyze the chromatic features of RAD21.2 accumulations, we performed confocal microscope analysis of meiocytes expressing *PRO$_{ASK1}$GFP:RAD21.2*

and *PRO$_{H2A.W.6}$:H2A.W.6:RFP* at pachytene. For 20 meiocytes, 3 areas with no accumulation and 3 areas with accumulations of RAD21.2 were determined. The fluorescence intensity was measured by plot profile in Fiji. For the accumulation evaluation, the maximum intensity of RAD21.2 fluorescence in each of 3 areas was averaged, and relative intensity was calculated as the ratio of the averaged intensity in the RAD21.2 accumulated area to the relative intensity of the non-accumulated area.

4.13 Live cell imaging

Live cell imaging of flower buds was performed according to Pursicki et al., 2019. In brief, a single flower bud was dissected and the stem was embedded into Arabidopsis Apex Culture Medium (APCM) in a petri dish. The sepal was removed to expose two anthers that were covered by a drop of APCM with 2% w/v agarose and the petri dish was filled with autoclaved water and placed under a W-plan Apochromat 40X/1.0 DIC objective. The Zeiss LSM 880 upright confocal microscope and the ZEN 2.3 SP1 software (Carl Zeiss) were used for the acquisition of time lapses. For the analysis of the WAPL-dependent removal of RAD21.2, a series of Z-stacks (7 planes, 28 μm distance) were acquired at 15 min time intervals. For the analysis of the RAD21.2 dynamics from pre-meiosis to pachytene, a series of Z-stacks (10 planes, 45 μm) at 15 min time intervals were acquired.

4.14 Image processing

The time lapses were converted to sequential images and a focal plane was selected for each time point using the function “Review Multi Dimensional Data” of the software Metamorph, version 7.8. Sample drift was corrected by using the Stack Reg plugin of Fiji (version 1.52p) (Schindelin et al., 2012).

For the calculation of the relative intensity of RAD21.2 over the time, time lapses were acquired from leptotene to metaphase I that was denoted as 0 h. We measured the fluorescence intensity of nuclei cross sections from 9-20 meiocytes by using the image processing software Fiji. From the calculated

intensity the background intensity was subtracted. The highest measured intensity was marked as 100% and used as reference for the calculation of the RAD21.2 relative intensity for every time point.

4.15 Yeast two-hybrid assay

The *SMC1*, *SCC3, ASY1* and ASY3 constructs were generated as described previously (Yang et al., 2019). Furthermore the *ASY4* and *SPO11-1* and *SPO11-4* constructs were kindly provided by Dr. Chao Yang. To generate the RAD21.2 construct, the coding sequence was amplified by PCR with primers (Appendix 6.4 table 19) flanking *NdeI* and *NhoI* restriction sites and was subcloned into the *pGADT7* vector by using the T4 Ligase. To generate the *REC8* construct, the coding sequence was amplified by PCR with primers flanked by *attB* sites and subcloned into the *pDONR221* vector by BP clonase reaction. The resulting construct was integrated into the *pGADT7-GW* vector by gateway LR reaction. Primers used for generating the constructs are listed in Appendix IV Tabl.18. The yeast two-hybrid assays were performed according to the Matchmaker Gold Yeast two-hybrid system manual from Clontech (Appendix 6.1 table 4). Different variations of the constructs were co-transformed by the polyethylene glycol/ lithium acetate method into the *AH109 yeast* strain and selected on SD/-Leu-Trp plates. The interactions were tested on SD/-Leu-Trp-His plates. For Buffer recipe see Appendix 6.1 table 11.

4.16 Plant material collection for protein extraction

2 week old seedlings expressing PRO_{35S}*:GFP* or PRO_{ASK1}*:GFP:RAD21.2* were grown on ½ MS plates. Around 0.1 g seedlings were collected in a precooled tube and immediately frozen in liquid nitrogen.

4 weeks old *35S:AP1-GR ap1cal* plants expressing either PRO_{REC8}*:REC8-GFP* or $PRO_{RAD21.2}$*:GFP:RAD21.2* were induced by dexamethasone induction solution (Appendix 6.1 table 8). 5 g flower buds were harvested 7-10 days after induction and collected in a precooled tube and frozen in liquid nitrogen.

To determine the correct collection time point, flower buds were analyzed with confocal microscopy.

4.17 Protein Sample preparation, Western Blot analysis and LC-MS/MS data acquisition

Plant material was ground to a fine powder and covered by protein extraction buffer (Appendix 6.1 table 12). The extraction was performed for 1 hour on ice with mixing the solution in between. The solution was centrifuged for 30 min at 4°C. The supernatant was collected in a new tube and the centrifugation step was repeated until no pellet was left. For the enrichment, 50 µl of GFP-Trap Magnetic beads (Appendix 6.1 table 5) were equilibrated with ice-cold wash buffer (Appendix 6.1 table 12) according to the manual. Total protein and magnetic beads were mixed and incubated overnight at 4°C on a rolling wheel. The followed wash steps were performed according to the manual. The elution step was performed when a Western Blot analysis followed or the magnetic beads were frozen at -20°C until on-bead digestion was performed.

For Western Blot analysis, the Electrophoresis System Mini-PROTEAN® (Appendix 6.1 table 4) was used. Protein samples were diluted with 5x SDS-Laemmli sample buffer (Appendix 6.1 table 12) and boiled for 5 min at 95 °C. Proteins were separated on Mini-PROTEAN®TGX Stain-Free 4-15 % (Appendix 6.1 table 6) gradient gels in 1x SDS-PAGE running buffer (Appendix 6.1 table 12) at 30 mA per gel.

The protein transfer from polyacrylamide gels to Roti®-PVDF membrane (Appendix I table 6) was performed according to the western blot Protocol from R&D Systems. The PVDF membrane was activated for 15 s in methanol and soaked for 5 min in Anode Buffer II (Appendix 6.1 table 12). For the discontinuous buffer transfer system two pieces of filter paper were wetted in Anode Buffer I (Appendix 6.1 table 12) and placed on anode plate of Trans-Blot® Turbo™ Transfer System (Bio-Rad, Munich). One filter paper was soaked in Anode Buffer I and was placed on the other filter papers. The PVDF membrane and the polyacrylamide gel were placed on top of each other.

Three pieces of filter paper were wetted in Cathode Buffer (Appendix 6.1 table 12) and were placed on top of the stack. The electrophoretic separated proteins were transferred for 1 hour and with constant current of 2 mA per cm^2 of gel area. The PVDF membrane was blocked for 1 hour in blocking solution (Appendix 6.1 table 12) and was washed three times for 5 min with 1x TBS-T (Appendix 6.1 table 12). The membrane was incubated with Anti-GFP mouse (Appendix 6.1 table 5) diluted in a blocking buffer (1: 1000) for 1 hour at RT or overnight at 4 °C on a shaker. The PVDF membrane was washed three times with TBS-T for 5- 10 min and was incubated with an HRP-conjugated Goat anti-Mouse IgG (H+L) (Appendix I table 5) at a 1:2000 dilution in blocking buffer for 1 hour and washed 4 times with 10 ml TBS-T. For the detection of bound antibodies the Clarity™ Western ECL Substrate (Appendix 6.1 table 4) was used. The PVDF membrane was incubated for 5 min in 1 ml of Clarity™ Western ECL-Luminol Reagent and 1 ml of Peroxidase Reagent. The membrane was finally covered with foil and signals were detected with the ChemiDoc™ Touch Imaging System (Bio-Rad, Munich). Western blots were analyzed with Image™ Lab software 5.2.1 from Bio-Rad, Munich.

For the on-bead digestion, dry beads were re-dissolved in 25 µL digestion buffer 1 (50 mM Tris, pH 7.5, 2M urea, 1mM DTT, 5 ng/µL trypsin) and incubated for 30 min at 30 °C in a Thermomixer with 400 rpm. Next, beads were pelleted and the supernatant was transferred to a fresh tube. Digestion buffer 2 (50 mM Tris, pH 7.5, 2M urea, 5 mM CAA) was added to the beads, after mixing the beads were pelleted, the supernatant was collected and combined with the previous one. The combined supernatants were then incubated o/n at 32 °C in a Thermomixer with 400 rpm; samples were protected from light during incubation. The digestion was stopped by adding 1 µL TFA and desalted with C18 Empore disk membranes according to the StageTip protocol{Rappsilber et al., 2003, #63164}. Dried peptides were re-dissolved in 2% ACN, 0.1% TFA (10 µL) for analysis and measured without dilution. In the case of the RAD21.2-GFP vs REC8-GFP experiment, samples from the RAD21.2-GFP vs 35S-YFP experiment were diluted to 0.2 µg/µL.

Samples were analyzed using an EASY-nLC 1000 (Thermo Fisher) coupled to a Q Exactive mass spectrometer (Thermo Fisher). Peptides were separated on 16 cm frit-less silica emitters (New Objective, 0.75 μm inner diameter), packed in-house with reversed-phase ReproSil-Pur C18 AQ 1.9 μm resin (Dr. Maisch). Peptides were loaded on the column and eluted for 115 min using a segmented linear gradient of 5% to 95% solvent B (0 min : 5%B; 0-5 min -> 5%B; 5-65 min -> 20%B; 65-90 min ->35%B; 90-100 min -> 55%; 100-105 min ->95%, 105-115 min ->95%) (solvent A 0% ACN, 0.1% FA; solvent B 80% ACN, 0.1%FA) at a flow rate of 300 nL/min. Mass spectra were acquired in data-dependent acquisition mode with a TOP15 method. MS spectra were acquired in the Orbitrap analyzer with a mass range of 300–1750 m/z at a resolution of 70,000 FWHM and a target value of 3×10^6 ions. Precursors were selected with an isolation window of 2.0 m/z (Q Exactive). HCD fragmentation was performed at a normalized collision energy of 25. MS/MS spectra were acquired with a target value of 10^5 ions at a resolution of 17,500 FWHM, a maximum injection time (max.) of 120 ms and a fixed first mass of m/z 100. Peptides with a charge of +1, greater than 6, or with unassigned charge state were excluded from fragmentation for MS2, dynamic exclusion for 30s prevented repeated selection of precursors.

Raw data were processed using MaxQuant software (version 1.5.7.4) with label-free quantification (LFQ) and iBAQ enabled (Cox and Mann, 2008). MS/MS spectra were searched by the Andromeda search engine against a combined database containing the sequences from *A. thaliana* (TAIR10_pep_20101214) and sequences of 248 common contaminant proteins and decoy sequences (Tyanova et al., 2016). Trypsin specificity was required and a maximum of two missed cleavages allowed. Minimal peptide length was set to seven amino acids. Carbamidomethylation of cysteine residues was set as fixed, oxidation of methionine and protein N-terminal acetylation as variable modifications. Peptide-spectrum-matches and proteins were retained if they were below a false discovery rate of 1%.

Statistical analysis of the MaxLFQ values was carried out using Perseus (version 1.5.8.5). Quantified proteins were filtered for reverse hits and hits

“identified by site” and MaxLFQ values were log2 transformed. After grouping samples by condition only those proteins were retained for the subsequent analysis that had two valid values in one of the conditions. Missing values were imputed from a normal distribution (1.8 downshift, separately for each column). Volcano plots were generated in Perseus using an FDR of 6% and an *S0*=1. Perseus output was exported and further processed using Excel.

4.18 qRT-PCR

Expression analysis of *RAD21.2* in seedlings and flower buds was performed by qRT-PCR. Plant material was collected and ground to fine powder by using liquid N_2. RNA extraction was performed according to the manual of the RNeasy Plant Mini kit (Appendix 6.1 table 4). A DNase treatment (Appendix 6.1 table 4) was added before the first washing step. Finally, the RNA concentration was determined and 1 μg RNA was used for the cDNA synthesis according to the Transcriptor First Strand cDNA Synthesis kit (Appendix I table 4). The expression of the following genes *FTSH7* (AT3G47060), *COX11* (AT1G02410) and AT2G41960 was used as reference. The expression of each gene was analyzed using the primers listed in Appendix 6.4 table 22) The qRT-PCR was performed using the Light Cycler 480 SYBR Green I Master (Appendix 6.1 table 4) in triplicates. PCR conditions that were used are listed in Appendix 6.5. The experiment was performed in a Light Cycler 480 System.

4.19 qPCR

4-week-old leaves of T_2 *RAD21.2 RNAi* #1 were collected and grinded to fine powder. DNA was extracted by using the DNeasy Plant Pro kit (Appendix 6.1 table 4). The qPCR was performed in triplicates and 1.5 ng DNA was used. To quantify the relative *18S* gene number primers, previously described, were used (Sims et al., 2019). To calculate the relative 18S quantity the *HXK1* (AT4G29130) and *UEV1C* (AT2G36060) genes were used for normalization.

PCR conditions are listed in Appendix 6.5. The experiment was performed in a Light Cycler 480 System.

4.20 Statistical analysis

Student's t-test (two-tailed) was used to evaluate the significance of the difference between two groups. For the analysis of variance, two samples F-test was performed. The numbers of samples are indicated in the figure legend. The strength of significance is presented by the p-values. *,$P< 0.05$; **,$P< 0.01$; and ***,$P< 0.001$. Unpaired, two-tailed Mann-Whitney tests were performed, since D'Agostino Pearson omnibus K2 normality testing revealed that most data were not sampled from a Gaussian population, and nonparametric tests were therefore required.

5. References

Armstrong, Susan J., et al. "Asy1, a protein required for meiotic chromosome synapsis, localizes to axis-associated chromatin in Arabidopsis and Brassica." *Journal of cell science* 115.18 (2002): 3645-3655.

Attner, Michelle A., et al. "Polo kinase Cdc5 is a central regulator of meiosis I." *Proceedings of the National Academy of Sciences* 110.35 (2013): 14278-14283.

Bai, Xuefang, et al. "Isolation and characterization of SYN1, a RAD21-like gene essential for meiosis in Arabidopsis." *The Plant Cell* 11.3 (1999): 417-430.

Baker, Katie, et al. "The low-recombining pericentromeric region of barley restricts gene diversity and evolution but not gene expression." *The Plant Journal* 79.6 (2014): 981-992.

Barakate, Abdellah, et al. "The synaptonemal complex protein ZYP1 is required for imposition of meiotic crossovers in barley." *The Plant Cell* 26.2 (2014): 729-740.

Barrington, Christopher, Ronald Finn, and Suzana Hadjur. "cohesin biology meets the loop extrusion model." *Chromosome research* 25.1 (2017): 51-60.

Berg, Anita, et al. "Ten members of the Arabidopsis gene family encoding methyl-CpG-binding domain proteins are transcriptionally active and at least one, AtMBD11, is crucial for normal development." *Nucleic acids research* 31.18 (2003): 5291-5304.

Berger, Shelley L. "Histone modifications in transcriptional regulation." *Current opinion in genetics & development* 12.2 (2002): 142-148.

Birkenbihl, Rainer P., and Suresh Subramani. "The rad21 gene product of Schizosaccharomyces pombe is a nuclear, cell cycle-regulated phosphoprotein." *Journal of Biological Chemistry* 270.13 (1995): 7703-7711.

Blackwell, Alexander R., et al. "MSH 2 shapes the meiotic crossover landscape in relation to interhomolog polymorphism in Arabidopsis." *The EMBO journal* 39.21 (2020): e104858.

Bolaños-Villegas, Pablo, et al. "In favor of establishment: regulation of chromatid cohesion in plants." *Frontiers in plant science* 8 (2017): 846.

Bolaños-Villegas, Pablo, et al. "Arabidopsis CHROMOSOME TRANSMISSION FIDELITY 7 (AtCTF7/ECO1) is required for DNA repair, mitosis and meiosis." *The Plant Journal* 75.6 (2013): 927-940.

Bose, Tania, et al. "Cohesin proteins promote ribosomal RNA production and protein translation in yeast and human cells." *PLoS Genet* 8.6 (2012): e1002749.

Brar, Gloria A et al. “Rec8 phosphorylation and recombination promote the stepwise loss of cohesins in meiosis.” *Nature* vol. 441,7092 (2006): 532-6. doi:10.1038/nature04794

Brieño-Enríquez, Miguel A., et al. "cohesin removal along the chromosome arms during the first meiotic division depends on a NEK1-PP1γ-WAPL axis in the mouse." *Cell reports* 17.4 (2016): 977-986.

Castellano-Pozo, Maikel, et al. "Surveillance of cohesin-supported chromosome structure controls meiotic progression." *Nature communications* 11.1 (2020): 1-16.

Challa, Kiran, et al. "Rad61/Wpl1 (Wapl), a cohesin regulator, controls chromosome compaction during meiosis." *Nucleic acids research* 44.7 (2016): 3190-3203.

Challa, Kiran, Miki Shinohara, and Akira Shinohara. "Meiotic prophase-like pathway for cleavage-independent removal of cohesin for chromosome morphogenesis." *Current genetics* 65.4 (2019): 817-827.

Chambon, Aurélie, et al. "Identification of ASYNAPTIC4, a component of the meiotic chromosome axis." *Plant Physiology*178.1 (2018): 233-246.

Chan, Kok-Lung, et al. "Pds5 promotes and protects cohesin acetylation." *Proceedings of the National Academy of Sciences*110.32 (2013): 13020-13025.

Che, Lixiao, et al. "OsAM1 is required for leptotene-zygotene transition in rice." *Cell research* 21.4 (2011): 654-665.

Chelysheva, Liudmila et al. “AtREC8 and AtSCC3 are essential to the monopolar orientation of the kinetochores during meiosis.” *Journal of cell science* vol. 118,Pt 20 (2005): 4621-32. doi:10.1242/jcs.02583.

Chen, Yu-Fan, Chia-Ching Chou, and Marc R. Gartenberg. "Determinants of Sir2-mediated, silent chromatin cohesion." *Molecular and cellular biology* 36.15 (2016): 2039-2050.

Chen, Wenliang, and Sue Jinks-Robertson. "The role of the mismatch repair machinery in regulating mitotic and meiotic recombination between diverged sequences in yeast." *Genetics*151.4 (1999): 1299-1313.

Choi, Kyuha, and Ian R. Henderson. "Meiotic recombination hotspots–a comparative view." *The Plant Journal* 83.1 (2015): 52-61.

Choi, Kyuha, et al. "Arabidopsis meiotic crossover hot spots overlap with H2A. Z nucleosomes at gene promoters." *Nature genetics* 45.11 (2013): 1327-1336.

Choi, Kyuha, et al. "Nucleosomes and DNA methylation shape meiotic DSB frequency in Arabidopsis thaliana transposons and gene regulatory regions." *Genome Research* 28.4 (2018): 532-546.

Clift, D., and A. L. Marston. "The role of shugoshin in meiotic chromosome segregation." *Cytogenetic and genome research*133.2-4 (2011): 234-242.

Clough, S J, and A F Bent. “Floral dip: a simplified method for Agrobacterium-mediated transformation of Arabidopsis thaliana.” *The Plant journal : for cell and molecular biology* vol. 16,6 (1998): 735-43. doi:10.1046/j.1365-313x.1998.00343.

Clyne, Rosemary K., et al. "Polo-like kinase Cdc5 promotes chiasmata formation and cosegregation of sister centromeres at meiosis I." *Nature cell biology* 5.5 (2003): 480-485.

Cole, Francesca, et al. "Homeostatic control of recombination is implemented progressively in mouse meiosis." *Nature cell biology* 14.4 (2012): 424-430.

Cox, Jürgen, and Matthias Mann. "MaxQuant enables high peptide identification rates, individualized ppb-range mass accuracies and proteome-wide protein quantification." *Nature biotechnology* 26.12 (2008): 1367-1372.

Crawley, Oliver, et al. "cohesin-interacting protein WAPL-1 regulates meiotic chromosome structure and cohesion by antagonizing specific cohesin complexes." *Elife* 5 (2016): e10851.

Cromer, Laurence, et al. "Centromeric cohesion is protected twice at meiosis, by SHUGOSHINs at anaphase I and by PATRONUS at interkinesis." *Current Biology* 23.21 (2013): 2090-2099.

Cromer, Laurence, et al. "Patronus is the elusive plant securin, preventing chromosome separation by antagonizing separase." *Proceedings of the National Academy of Sciences* 116.32 (2019): 16018-16027.

da Costa-Nunes, J. A., et al. "Characterization of the three Arabidopsis thaliana RAD21 cohesins reveals differential responses to ionizing radiation." *Journal of experimental botany*57.4 (2006): 971-983.

da Costa-Nunes, José A., et al. "The AtRAD21. 1 and AtRAD21. 3 Arabidopsis cohesins play a synergistic role in somatic DNA double strand break damage repair." *BMC plant biology* 14.1 (2014): 1-14.

De, Kuntal, et al. "Arabidopsis thaliana WAPL is essential for the prophase removal of cohesin during meiosis." *PLoS Genet* 10.7 (2014): e1004497.

De, Kuntal, et al. "The opposing actions of Arabidopsis CHROMOSOME TRANSMISSION FIDELITY7 and WINGS APART-LIKE1 and 2 differ in mitotic and meiotic cells." *The Plant Cell* 28.2 (2016): 521-536.

Dheur, Sonia, et al. "Role for cohesin in the formation of a heterochromatic domain at fission yeast subtelomeres." *Molecular and cellular biology* 31.5 (2011): 1088-1097.

Dissmeyer, Nico, et al. "Control of cell proliferation, organ growth, and DNA damage response operate independently of dephosphorylation of the Arabidopsis Cdk1 homolog CDKA; 1." *The Plant Cell* 21.11 (2009): 3641-3654.

Dreier, Megan R., Michael E. Bekier, and William R. Taylor. "Regulation of sororin by Cdk1-mediated phosphorylation." *Journal of cell science* 124.17 (2011): 2976-2987.

Eckhardt, Florian, et al. "DNA methylation profiling of human chromosomes 6, 20 and 22." *Nature genetics* 38.12 (2006): 1378-1385.

Eijpe, M., et al. "Association of mammalian SMC1 and SMC3 proteins with meiotic chromosomes and synaptonemal complexes." *Journal of cell science* 113.4 (2000): 673-682.

Emmanuel, Eyal, et al. "The role of AtMSH2 in homologous recombination in Arabidopsis thaliana." *EMBO reports* 7.1 (2006): 100-105.

Ferdous, Maheen, et al. "Inter-homolog crossing-over and synapsis in Arabidopsis meiosis are dependent on the chromosome axis protein AtASY3." *PLoS Genet* 8.2 (2012): e1002507.

Fischer, Tamás, et al. "Diverse roles of HP1 proteins in heterochromatin assembly and functions in fission yeast." *Proceedings of the National Academy of Sciences* 106.22 (2009): 8998-9003.

Folco, H. Diego, et al. "cohesin impedes heterochromatin assembly in fission yeast cells lacking Pds5." *Genetics* 213.1 (2019): 127-141.

Gartenberg, Marc. "Heterochromatin and the cohesion of sister chromatids." *Chromosome research* 17.2 (2009): 229-238.

Giraut, Laurène, et al. "Genome-wide crossover distribution in Arabidopsis thaliana meiosis reveals sex-specific patterns along chromosomes." *PLoS Genet* 7.11 (2011): e1002354.

Gligoris, Thomas, and Jan Löwe. "Structural insights into ring formation of cohesin and related Smc complexes." *Trends in cell biology* 26.9 (2016): 680-693.

Golubovskaya, Inna, Nadezhda Avalkina, and William F. Sheridan. "New insights into the role of the maize ameiotic1 locus." *Genetics* 147.3 (1997): 1339-1350.

Golubovskaya, Inna N., et al. "Alleles of afd1 dissect REC8 functions during meiotic prophase I." *Journal of cell science*119.16 (2006): 3306-3315.

Gong, Chunyan, et al. "Rice OsRAD21-2 is Expressed in Actively Dividing Tissues and its Ectopic Expression in Yeast Results in Aberrant Cell Division and Growth." *Journal of integrative plant biology* 53.1 (2011): 14-24.

Gottlieb, Shoshanna, and Rochelle Easton Esposito. "A new role for a yeast transcriptional silencer gene, SIR2, in regulation of recombination in ribosomal DNA." *Cell* 56.5 (1989): 771-776.

Grafi, Gideon, Assaf Zemach, and Letizia Pitto. "Methyl-CpG-binding domain (MBD) proteins in plants." *Biochimica et Biophysica Acta (BBA)-Gene Structure and Expression* 1769.5-6 (2007): 287-294.

Gutiérrez-Caballero, Cristina, et al. "Identification and molecular characterization of the mammalian α-kleisin RAD21L." *Cell cycle*10.9 (2011): 1477-1487.

Gutiérrez-Caballero, Cristina, Luis R. Cebollero, and Alberto M. Pendás. "Shugoshins: from protectors of cohesion to versatile adaptors at the centromere." *Trends in Genetics* 28.7 (2012): 351-360.

Gutierrez, Crisanto. “The Arabidopsis cell division cycle.” *The arabidopsis book* vol. 7 (2009): e0120. doi:10.1199/tab.0120.

Gyuricza, Mercedes R., et al. "Dynamic and stable cohesins regulate synaptonemal complex assembly and chromosome segregation." *Current Biology* 26.13 (2016): 1688-1698.

Haering, Christian H et al. “Molecular architecture of SMC proteins and the yeast cohesin complex.” *Molecular cell* vol. 9,4 (2002): 773-88. doi:10.1016/s1097-2765(02)00515-4.

Haering, Christian H et al. “The cohesin ring concatenates sister DNA molecules.” *Nature*vol. 454,7202 (2008): 297-301. doi:10.1038/nature07098.

Hamant, Olivier, et al. "A REC8-dependent plant Shugoshin is required for maintenance of centromeric cohesion during meiosis and has no mitotic functions." *Current Biology* 15.10 (2005): 948-954.

Harashima, Hirofumi, et al. "Modulation of plant growth in vivo and identification of kinase substrates using an analog-sensitive variant of CYCLIN-DEPENDENT KINASE A; 1." *BMC plant biology* 16.1 (2016): 1-19.

Harrison, C Jill et al. “Meiosis in flowering plants and other green organisms.” *Journal of experimental botany* vol. 61,11 (2010): 2863-75. doi:10.1093/jxb/erq191

Hartl, Markus, et al. "Lysine acetylome profiling uncovers novel histone deacetylase substrate proteins in Arabidopsis." *Molecular systems biology* 13.10 (2017): 949.

He, Yonghui, et al. "Maize Dek15 encodes the cohesin-loading complex subunit SCC4 and is essential for chromosome segregation and kernel development." *The Plant Cell* 31.2 (2019): 465-485.

Heidmann, Doris, et al. "The Drosophila meiotic kleisin C (2) M functions before the meiotic divisions." *Chromosoma* 113.4 (2004): 177-187.

Herrán, Yurema, et al. "The cohesin subunit RAD21L functions in meiotic synapsis and exhibits sexual dimorphism in fertility." *The EMBO journal* 30.15 (2011): 3091-3105.

Higgins, James D., et al. "The Arabidopsis synaptonemal complex protein ZYP1 is required for chromosome synapsis and normal fidelity of crossing over." *Genes & development* 19.20 (2005): 2488-2500.

Huang, Julie, et al. "Inhibition of homologous recombination by a cohesin-associated clamp complex recruited to the rDNA recombination enhancer." *Genes & development* 20.20 (2006): 2887-2901.

Huisinga, Kathryn L., Brent Brower-Toland, and Sarah CR Elgin. "The contradictory definitions of heterochromatin: transcription and silencing." *Chromosoma* 115.2 (2006): 110-122.

Ingouff, Mathieu, et al. "Live-cell analysis of DNA methylation during sexual reproduction in Arabidopsis reveals context and sex-specific dynamics controlled by noncanonical RdDM." *Genes & development* 31.1 (2017): 72-83.

Ishiguro, Kei-ichiro, et al. "A new meiosis-specific cohesin complex implicated in the cohesin code for homologous pairing." *EMBO reports* 12.3 (2011): 267-275.

Ishiguro, Kei-ichiro. "The cohesin complex in mammalian meiosis." *Genes to Cells* 24.1 (2019): 6-30.

Ishiguro, Tadashi, et al. "Shugoshin–PP2A counteracts casein-kinase-1-dependent cleavage of Rec8 by separase." *Nature cell biology* 12.5 (2010): 500-506.

Ito, Masaru, et al. "Meiotic recombination cold spots in chromosomal cohesion sites." *Genes to Cells* 19.5 (2014): 359-373.

Jiang, Ling, et al. "Proper levels of the Arabidopsis cohesion establishment factor CTF7 are essential for embryo and megagametophyte, but not endosperm, development." *Plant physiology* 154.2 (2010): 820-832.

Jiang, Ling, et al. "The Arabidopsis cohesin protein SYN3 localizes to the nucleolus and is essential for gametogenesis." *The Plant Journal* 50.6 (2007): 1020-1034.

Jonassen, Else Müller, et al. "Protein phosphatase 2A regulatory subunits are starting to reveal their functions in plant metabolism and development." *Plant signaling & behavior* 6.8 (2011): 1216-1218.

Jones, Susan, and John Sgouros. "The cohesin complex: sequence homologies, interaction networks and shared motifs." *Genome biology* 2.3 (2001): 1-12.

Katis, Vittorio L., et al. "Rec8 phosphorylation by casein kinase 1 and Cdc7-Dbf4 kinase regulates cohesin cleavage by separase during meiosis." *Developmental cell* 18.3 (2010): 397-409.

Khoo, Kelvin HP, Amanda J. Able, and Jason A. Able. "The isolation and characterisation of the wheat molecular ZIPper I homologue, Ta ZYP1." *BMC research notes* 5.1 (2012): 1-13.

Kirik, Angela, et al. "The chromatin assembly factor subunit FASCIATA1 is involved in homologous recombination in plants." *The Plant Cell* 18.10 (2006): 2431-2442.

Kobayashi, Takehiko, et al. "SIR2 regulates recombination between different rDNA repeats, but not recombination within individual rRNA genes in yeast." *Cell* 117.4 (2004): 441-453.

Komaki, Shinichiro, and Arp Schnittger. "The spindle assembly checkpoint in Arabidopsis is rapidly shut off during severe stress." *Developmental cell* 43.2 (2017): 172-185.

König, Ann-Christine, et al. "The Arabidopsis class II sirtuin is a lysine deacetylase and interacts with mitochondrial energy metabolism." *Plant physiology* 164.3 (2014): 1401-1414.

Kugou, Kazuto, et al. "Rec8 guides canonical Spo11 distribution along yeast meiotic chromosomes." *Molecular biology of the cell* 20.13 (2009): 3064-3076.

Lam, Wing See, Xiaohui Yang, and Christopher A. Makaroff. "Characterization of Arabidopsis thaliana SMC1 and SMC3: evidence that AtSMC3 may function beyond chromosome cohesion." *Journal of cell science* 118.14 (2005): 3037-3048.

Lambing, Christophe, et al. "ASY1 acts as a dosage-dependent antagonist of telomere-led recombination and mediates crossover interference in Arabidopsis." *Proceedings of the National Academy of Sciences* 117.24 (2020): 13647-13658.

Lambing, Christophe, et al. "Interacting genomic landscapes of REC8-cohesin, chromatin, and meiotic recombination in Arabidopsis." *The plant cell* 32.4 (2020): 1218-1239.

Lambing, Christophe, F. Chris H. Franklin, and Chung-Ju Rachel Wang. "Understanding and manipulating meiotic recombination in plants." *Plant physiology* 173.3 (2017): 1530-1542.

Lambing, Christophe, et al. "Arabidopsis PCH2 mediates meiotic chromosome remodeling and maturation of crossovers." *PLoS Genet* 11.7 (2015): e1005372.

Lee, Brian H., and Angelika Amon. "Role of Polo-like kinase CDC5 in programming meiosis I chromosome segregation." *Science* 300.5618 (2003): 482-486.

Lee, Jibak, and Tatsuya Hirano. "RAD21L, a novel cohesin subunit implicated in linking homologous chromosomes in mammalian meiosis." *Journal of Cell Biology* 192.2 (2011): 263-276.

Lee, Ding Hua, et al. "The axial element protein DESYNAPTIC2 mediates meiotic double-strand break formation and synaptonemal complex assembly in maize." *The Plant Cell* 27.9 (2015): 2516-2529.

Lhuissier, Franck GP, et al. "The mismatch repair protein MLH1 marks a subset of strongly interfering crossovers in tomato." *The Plant Cell* 19.3 (2007): 862-876.

Lin, Zhonghui, Xuelian Luo, and Hongtao Yu. "Structural basis of cohesin cleavage by separase." *Nature* 532.7597 (2016): 131-134.

Liu, Chun-ming, et al. "Condensin and cohesin knockouts in Arabidopsis exhibit a titan seed phenotype." *The Plant Journal* 29.4 (2002): 405-415.

Liu, Xiaoyun, et al. "Histone deacetylase AtSRT1 links metabolic flux and stress response in Arabidopsis." *Molecular plant* 10.12 (2017): 1510-1522.

Liu, Xuncheng, et al. "HDA6 directly interacts with DNA methyltransferase MET1 and maintains transposable element silencing in Arabidopsis." *Plant physiology* 158.1 (2012): 119-129.

Liu, Xuncheng, et al. "Transcriptional repression by histone deacetylases in plants." *Molecular plant* 7.5 (2014): 764-772.

Liu, Zhe, and Christopher A. Makaroff. "Arabidopsis separase AESP is essential for embryo development and the release of cohesin during meiosis." *The Plant Cell* 18.5 (2006): 1213-1225.

Llano, Elena, et al. "Meiotic cohesin complexes are essential for the formation of the axial element in mice." *Journal of Cell Biology* 197.7 (2012): 877-885.

Lopez-Serra, Lidia, et al. "The Scc2–Scc4 complex acts in sister chromatid cohesion and transcriptional regulation by maintaining nucleosome-free regions." *Nature genetics* 46.10 (2014): 1147-1151.

Luhua, Song, et al. "Linking genes of unknown function with abiotic stress responses by high-throughput phenotype screening." *Physiologia plantarum* 148.3 (2013): 322-333.

Luo, Ming, et al. "Regulation of flowering time by the histone deacetylase HDA 5 in A rabidopsis." *The Plant Journal* 82.6 (2015): 925-936.

Luo, Shukun, and Liang Tong. "Structural biology of the separase–securin complex with crucial roles in chromosome segregation." *Current opinion in structural biology* 49 (2018): 114-122.

Manheim, Elizabeth A., and Kim S. McKim. "The synaptonemal complex component C (2) M regulates meiotic crossing over in Drosophila." *Current Biology* 13.4 (2003): 276-285.

Mercier, Raphael, et al. "The meiotic protein SWI1 is required for axial element formation and recombination initiation in Arabidopsis." *Development* 130.14 (2003): 3309-3318.

Mercier, Raphaël, et al. "The molecular biology of meiosis in plants." *Annual review of plant biology* 66 (2015): 297-327.

Mercier, Raphaël, et al. "Two meiotic crossover classes cohabit in Arabidopsis: one is dependent on MER3, whereas the other one is not." *Current Biology* 15.8 (2005): 692-701.

Miao, Chunbo, et al. "Central region component1, a novel synaptonemal complex component, is essential for meiotic recombination initiation in rice." *The Plant Cell* 25.8 (2013): 2998-3009.

Michan, Shaday, and David Sinclair. "Sirtuins in mammals: insights into their biological function." *Biochemical Journal* 404.1 (2007): 1-13.

Minina, Elena A., et al. "The Arabidopsis homolog of Scc4/MAU2 is essential for embryogenesis." *Journal of cell science* 130.6 (2017): 1051-1063.

Mishra, Ajay, et al. "Both interaction surfaces within cohesin's hinge domain are essential for its stable chromosomal association." *Current biology* 20.4 (2010): 279-289.

Nakajima, Masato, et al. "The complete removal of cohesin from chromosome arms depends on separase." *Journal of cell science* 120.23 (2007): 4188-4196.

Nasmyth, Kim, and Christian H. Haering. "cohesin: its roles and mechanisms." *Annual review of genetics* 43 (2009).

Nonaka, Nobuhiro, et al. "Recruitment of cohesin to heterochromatic regions by Swi6/HP1 in fission yeast." *Nature cell biology* 4.1 (2002): 89-93.

Nonomura, K-I., et al. "An insertional mutation in the rice PAIR2 gene, the ortholog of Arabidopsis ASY1, results in a defect in homologous chromosome pairing during meiosis." *Molecular Genetics and Genomics* 271.2 (2004): 121-129.

Osman, Kim, et al. "Pathways to meiotic recombination in Arabidopsis thaliana." *New Phytologist* 190.3 (2011): 523-544.

Osman, Kim, et al. "Affinity proteomics reveals extensive phosphorylation of the Brassica chromosome axis protein ASY 1 and a network of associated proteins at prophase I of meiosis." *The Plant Journal* 93.1 (2018): 17-33.

Oya, Eriko, et al. "H3K14 ubiquitylation promotes H3K9 methylation for heterochromatin assembly." *EMBO reports* 20.10 (2019): e48111.

Pan, Guangjin, et al. "Whole-genome analysis of histone H3 lysine 4 and lysine 27 methylation in human embryonic stem cells." *Cell stem cell* 1.3 (2007): 299-312.

Panizza, Silvia, et al. "Spo11-accessory proteins link double-strand break sites to the chromosome axis in early meiotic recombination." *Cell* 146.3 (2011): 372-383.

Parvanov, Emil D., et al. "PRDM9 interactions with other proteins provide a link between recombination hotspots and the chromosomal axis in meiosis." *Molecular biology of the cell* 28.3 (2017): 488-499.

Pawlowski, Wojciech P., et al. "Maize AMEIOTIC1 is essential for multiple early meiotic processes and likely required for the initiation of meiosis." *Proceedings of the National Academy of Sciences* 106.9 (2009): 3603-3608.

Peterson, Ross, Janet P. Slovin, and Changbin Chen. "A simplified method for differential staining of aborted and non-aborted pollen grains." *International Journal of Plant Biology*1.2 (2010): e13-e13.

Pradillo, Mónica, et al. "Involvement of the cohesin cofactor PDS5 (SPO76) during meiosis and DNA repair in Arabidopsis thaliana." *Frontiers in plant science* 6 (2015): 1034.

Prusicki, Maria A., et al. "Live cell imaging of meiosis in Arabidopsis thaliana." *Elife* 8 (2019): e42834.

Rabanal, Fernando A., et al. "Unstable inheritance of 45S rRNA genes in Arabidopsis thaliana." *G3: Genes, Genomes, Genetics*7.4 (2017): 1201-1209.

Rankin, Susannah. "Complex elaboration: making sense of meiotic cohesin dynamics." *The FEBS journal* 282.13 (2015): 2426-2443.

Ravi, Maruthachalam, et al. "The rapidly evolving centromere-specific histone has stringent functional requirements in Arabidopsis thaliana." *Genetics* 186.2 (2010): 461-471.

Riddle, Nicole C., and Eric J. Richards. "Genetic variation in epigenetic inheritance of ribosomal RNA gene methylation in Arabidopsis." *The Plant Journal* 41.4 (2005): 524-532.

Rong, Mei, et al. "Meiotic cohesin subunits RAD21L and REC8 are positioned at distinct regions between lateral elements and transverse filaments in the synaptonemal complex of mouse spermatocytes." *Journal of Reproduction and Development* (2016).

Roig, Maurici B., et al. "Structure and function of cohesin's Scc3/SA regulatory subunit." *FEBS letters* 588.20 (2014): 3692-3702.

Ross, K. J., P. Fransz, and G. H. Jones. "A light microscopic atlas of meiosis in Arabidopsis thaliana." *Chromosome research* 4.7 (1996): 507-516.

Šamanić, Ivica, et al. "Evidence for distinct functions of MRE11 in Arabidopsis meiosis." *PLoS One* 8.10 (2013): e78760.

Schindelin, Johannes, et al. "Fiji: an open-source platform for biological-image analysis." *Nature methods* 9.7 (2012): 676-682.

Schubert, V. “SMC proteins and their multiple functions in higher plants.” *Cytogenetic and genome research* vol. 124,3-4 (2009): 202-14. doi:10.1159/000218126

Schubert, Veit, Inna Lermontova, and Ingo Schubert. "The Arabidopsis CAP-D proteins are required for correct chromatin organisation, growth and fertility." *Chromosoma* 122.6 (2013): 517-533.

Schwarzacher, Trude. "Meiosis, recombination and chromosomes: a review of gene isolation and fluorescent in situ hybridization data in plants." *Journal of Experimental Botany*54.380 (2003): 11-23.

Severson, Aaron F., and Barbara J. Meyer. "Divergent kleisin subunits of cohesin specify mechanisms to tether and release meiotic chromosomes." *Elife* 3 (2014): e03467.

Severson, Aaron F., et al. "The axial element protein HTP-3 promotes cohesin loading and meiotic axis assembly in C. elegans to implement the meiotic program of chromosome segregation." *Genes & development* 23.15 (2009): 1763-1778.
Shao, Tian, et al. "OsREC8 is essential for chromatid cohesion and metaphase I monopolar orientation in rice meiosis." *Plant Physiology* 156.3 (2011): 1386-1396.

Sims, Jason, Gregory P. Copenhaver, and Peter Schlögelhofer. "Meiotic DNA repair in the nucleolus employs a nonhomologous end-joining mechanism." *The Plant Cell* 31.9 (2019): 2259-2275.

Singh, Dipesh K., et al. "AtCTF7 is required for establishment of sister chromatid cohesion and association of cohesin with chromatin during meiosis in Arabidopsis." *BMC plant biology*13.1 (2013): 1-10.

Skibbens, Robert V. "Condensins and cohesins–one of these things is not like the other!." *Journal of cell science* 132.3 (2019).

Smagulova, Fatima, et al. "The evolutionary turnover of recombination hot spots contributes to speciation in mice." *Genes & development* 30.3 (2016): 266-280.

Stacey, Nicola J., et al. "Arabidopsis SPO11-2 functions with SPO11-1 in meiotic recombination." *The Plant Journal* 48.2 (2006): 206-216.

Stanvitch, Gerald, and Landon L. Moore. "cin-4, a gene with homology to topoisomerase II, is required for centromere resolution by cohesin removal from sister kinetochores during mitosis." *Genetics* 178.1 (2008): 83-97.

Strunnikov, Alexander V., Vladimir L. Larionov, and Douglas Koshland. "SMC1: an essential yeast gene encoding a putative head-rod-tail protein is required for nuclear division and defines a new ubiquitous protein family." *The Journal of cell biology*123.6 (1993): 1635-1648.

Sun, Xiaoji, et al. "Transcription dynamically patterns the meiotic chromosome-axis interface." *Elife* 4 (2015): e07424.

Tang, Yu, et al. "MTOPVIB interacts with AtPRD1 and plays important roles in formation of meiotic DNA double-strand breaks in Arabidopsis." *Scientific reports* 7.1 (2017): 1-13.

Tao, Jiayi, et al. "OsRAD21-3, an orthologue of yeast RAD21, is required for pollen development in Oryza sativa." *The Plant Journal* 51.5 (2007): 919-930.

Tiang, Choon Lin. *The role of SYN1 in early Arabidopsis meiosis*. Diss. University of Birmingham, 2011.

Tran, Hue T., et al. "Arabidopsis thaliana histone deacetylase 14 (HDA14) is an α-tubulin deacetylase that associates with PP2A and enriches in the microtubule fraction with the putative histone acetyltransferase ELP3." *The Plant Journal* 71.2 (2012): 263-272.

Turck, Franziska, et al. "Arabidopsis TFL2/LHP1 specifically associates with genes marked by trimethylation of histone H3 lysine 27." *PLoS Genet* 3.6 (2007): e86.

Tyanova, Stefka, et al. "The Perseus computational platform for comprehensive analysis of (prote) omics data." *Nature methods* 13.9 (2016): 731.

Varas, Javier, et al. "Absence of SUN 1 and SUN 2 proteins in Arabidopsis thaliana leads to a delay in meiotic progression and defects in synapsis and recombination." *The Plant Journal* 81.2 (2015): 329-346.

Wang, Lei, Jeongsik Kim, and David E. Somers. "Transcriptional corepressor TOPLESS complexes with pseudoresponse regulator proteins and histone deacetylases to regulate circadian transcription." *Proceedings of the National Academy of Sciences*110.2 (2013): 761-766.

Wang, Mo, et al. "The central element protein ZEP1 of the synaptonemal complex regulates the number of crossovers during meiosis in rice." *The Plant Cell* 22.2 (2010): 417-430.

Wang, Mo, et al. "OsSGO1 maintains synaptonemal complex stabilization in addition to protecting centromeric cohesion during rice meiosis." *The Plant Journal* 67.4 (2011): 583-594.

Wang, Tianjiao, et al. "Smc3 is required for mouse embryonic and adult hematopoiesis." *Experimental hematology* 70 (2019): 70-84.

Waterworth, Wanda M., et al. "NBS1 is involved in DNA repair and plays a synergistic role with ATM in mediating meiotic homologous recombination in plants." *The Plant Journal* 52.1 (2007): 41-52.

Watanabe, Yoshinori. "Shugoshin: guardian spirit at the centromere." *Current opinion in cell biology* 17.6 (2005): 590-595.

Wellmer, Frank, et al. "Genome-wide analysis of gene expression during early Arabidopsis flower development." *PLoS Genet* 2.7 (2006): e117.

Wijnker, Erik, et al. "The Cdk1/Cdk2 homolog CDKA; 1 controls the recombination landscape in Arabidopsis." *Proceedings of the National Academy of Sciences* 116.25 (2019): 12534-12539.

Wijnker, Erik, et al. "The genomic landscape of meiotic crossovers and gene conversions in Arabidopsis thaliana." *Elife*2 (2013): e01426.

Wojtasz, Lukasz, et al. "Mouse HORMAD1 and HORMAD2, two conserved meiotic chromosomal proteins, are depleted from synapsed chromosome axes with the help of TRIP13 AAA-ATPase." *PLoS Genet* 5.10 (2009): e1000702.

Yan, Rihui, et al. "SOLO: a meiotic protein required for centromere cohesion, coorientation, and SMC1 localization in Drosophila melanogaster." *Journal of Cell Biology* 188.3 (2010): 335-349.

Yang, Xiaohui, et al. "The radially swollen 4 separase mutation of Arabidopsis thaliana blocks chromosome disjunction and disrupts the radial microtubule system in meiocytes." *PLoS One*6.4 (2011): e19459.

Yang, Chao, et al. "SWITCH 1/DYAD is a WINGS APART-LIKE antagonist that maintains sister chromatid cohesion in meiosis." *Nature communications* 10.1 (2019): 1-15.

Yang, Chao, et al. "The Arabidopsis Cdk1/Cdk2 homolog CDKA; 1 controls chromosome axis assembly during plant meiosis." *The EMBO journal* 39.3 (2020): e101625.

Yazdi, Parvin T., et al. "SMC1 is a downstream effector in the ATM/NBS1 branch of the human S-phase checkpoint." *Genes & development* 16.5 (2002): 571-582.

Yelagandula, Ramesh, et al. "The histone variant H2A. W defines heterochromatin and promotes chromatin condensation in Arabidopsis." *Cell* 158.1 (2014): 98-109.

Yelina, Nataliya E., et al. "DNA methylation epigenetically silences crossover hot spots and controls chromosomal domains of meiotic recombination in Arabidopsis." *Genes & development*29.20 (2015): 2183-2202.

Yuan, Guoliang, et al. "PROTEIN PHOSHATASE 2A B'α and β maintain centromeric sister chromatid cohesion during meiosis in Arabidopsis." *Plant physiology* 178.1 (2018): 317-328.

Yuan, Li, et al. "Expression of epitope-tagged SYN3 cohesin proteins can disrupt meiosis in Arabidopsis." *Journal of Genetics and Genomics* 41.3 (2014): 153-164.

Yuan, Li, et al. "The Arabidopsis SYN3 cohesin protein is important for early meiotic events." *The Plant Journal* 71.1 (2012): 147-160.

Zamariola, Linda, et al. "Chromosome segregation in plant meiosis." *Frontiers in plant science* 5 (2014): 279.

Zamariola, Linda, et al. "SHUGOSHIN s and PATRONUS protect meiotic centromere cohesion in A rabidopsis thaliana." *The Plant Journal* 77.5 (2014): 782-794.

Zemach, Assaf, et al. "DDM1 binds Arabidopsis methyl-CpG binding domain proteins and affects their subnuclear localization." *The Plant Cell* 17.5 (2005): 1549-1558.

Zhang, Fan, et al. "Histone deacetylases SRT1 and SRT2 interact with ENAP1 to mediate ethylene-induced transcriptional repression." *The Plant Cell* 30.1 (2018): 153-166.

Zhang, Huiming, Zhaobo Lang, and Jian-Kang Zhu. "Dynamics and function of DNA methylation in plants." *Nature reviews Molecular cell biology* 19.8 (2018): 489-506.

Zhang, Liang-Ran, Jia-Yi Tao, and Tai Wang. "Molecular characterization of OsRAD21-1, a rice homologue of yeast RAD21 essential for mitotic chromosome cohesion." *Journal of experimental botany* 55.399 (2004): 1149-1152.

Zhang, Liangran, et al. "The rice OsRad21-4, an orthologue of yeast Rec8 protein, is required for efficient meiosis." *Plant molecular biology* 60.4 (2006): 533-554.

Zhang, Nenggang et al. “A handcuff model for the cohesin complex.” *The Journal of cell biology* vol. 183,6 (2008): 1019-31. doi:10.1083/jcb.200801157

Zhang, Nenggang, and Debananda Pati. "Sororin is a master regulator of sister chromatid cohesion and separation." *Cell cycle*11.11 (2012): 2073-2083.

Zhang, Yu-Lan, et al. "Protein Phosphatase 2A B'α and B'β Protect Centromeric Cohesion during Meiosis I." *Plant physiology* 179.4 (2019): 1556-1568.

Zhao, Shuai, et al. "Plant HP1 protein ADCP1 links multivalent H3K9 methylation readout to heterochromatin formation." *Cell research* 29.1 (2019): 54-66.

Zhou, Yi, et al. "HISTONE DEACETYLASE19 interacts with HSL1 and participates in the repression of seed maturation genes in Arabidopsis seedlings." *The Plant Cell* 25.1 (2013): 134-148.

6. Appendix

6.1 Appendix Kits, chemical solutions and Buffer:

Table 4: Commercial kits

Gateway BP Clonase II Enzyme mix	Thermo Fisher Scientific (CAT #11789020)
Gateway LR Clonase II Enzyme mix	Thermo Fisher Scientific (CAT #11791020)
Presto TM Mini Plasmid Kit	Geneaid (CAT #PDH300)
NucleoSpin Gel and PCR Clean-up	MACEREY-NAGEL (CAT #740609.250)
PrimeSTAR Max DANN Polymerase	TAKARA BIO INC (CAT #R045A)
DreamTaq Green PCR Master Mix (2x)	Thermo Scientific (CAT #K1081)
Terra PCR Direct Red Dye Premix	TAKARA BIO INC (CAT #639286)
Ligation mix	TAKARA BIO INC (CAT #6023)
Matchmarker Gold Y2H System	TAKARA BIO INC (CAT #630489)
Clarity™ Western ECL Substrate	Bio RAD (CAT #1705061)
RNeasy Plant Mini kit (50)	Qiagen (CAT #74904)
RNase-Free DNase Set (50)	Qiagen (CAT #79254)
DNeasy Plant Pro kit (250)	Qiagen (CAT #69206)
Transcriptor First Strand cDNA Synthesis kit	Roche (CAT #04379012001)
Light Cycler 480 SYBR Green I Master	Roche (CAT #04707516001)

Table 5: Antibody list

Anti-GFP mouse $IgG_1\kappa$ monoclonal antibody, clones 7.1 and 13.1	MERCK (CAT #11814460001)
HRP-conjugated Goat anti-Mouse IgG (H+L)	Thermo Fisher Scientific (CAT #32430)
GFP Trap Magnetic beads	Chromotek (CAT #gtma-10)
anti-ASY1	Sims et al. 2019
anti-RAD51	Sims et al. 2019
anti-guinea pig Alexa488	Abcam (CAT #ab150185)
anti-rat Alexa568	Abcam (CAT #ab175476)
45S probe	Sims et al. 2019
5S probe	Sims et al. 2019
CENH3 probe	Sims et al. 2019

Table 6: Reagents for Protein analysis

Plant protease inhibitor	Sigma (CAT #P9599)
Mini-PROTEAN®TGX Stain-Free 4-15 %	Bio RAD (CAT #4568086)
Roti®-PVDF membrane	Carl Roth (CAT #T830.1)

Table 7: Buffer for Bacteria cultivation

LB	Tryptone	1%

	Yeast extract	0.5%
	NaCl	0.5%
	Milipore water	up to volume
	Agar; for plates	0.8%
SOC media	Yeast extract	0.5%
	Tryptone	2%
	NaCl	10 mM
	KCl	2.5 mM
	MgCl	10 mM
	MgSO4	10 mM
	Glucose	20 mM
	Milipore water	up to volume
Antibiotics for bacterial selection	Spectinomycin (Spec)	100 μg/ml
	Kanamycin (Kn)	50 μg/ml
	Gentamicin (Gent)	30 μg/ml
	Chloramphenicol	12.5 μg/ml
	Rifampicin (Rif)	100 μg/ml
	Carbenicillin (Carb)	50 μg/ml

Table 8: Buffer for plant cultivation, reporter selection, genotyping, transformation and induction

0.5x MS	MS BASAL powder + vitamins	0.2%
	Sucrose	1%
	Milipore water	up to volume
	Agar	1%
	pH 5.8 (adjusted with KOH)	
Antibiotics for plant selection	BASTA	12.5 μg/ml
	Hygromycin (Hyg)	25 μg/ml
	Kanamycin (Kn)	7.5 μg/ml
8(Genotyping)	Tris HCL (pH 7.5)	50 mM
	NaCl	300 mM
	Sucrose	300 mM
	Milipore water	up to volume
Plant transformation media	Sucrose	5%
	silwet-77	0.05%
	Milipore water	up to volume
Induction solution	Dexamethasone	10 μM
	Silwet-77	0.015%

Table 9: Buffer for phenotypical evaluation

Citrate Buffer	0.1M Sodium Citrate	4.45%
	0.1M Citric Acid	5.55%
	Milipore water	up to volume

	pH 4.5	
Enzyme mix	Cellulase	0.5%
	Pectolyase	0.5%
	Cytohelicase	0.5%
	0.01 M Citrate Buffer	up to volume
Peterson staining	Methanol	10%
	Malachite green	0.001%
	Glycerol	25%
	Acid fuchsin	0.005%
	Organge G	0.0005%
	Acetic acid	4%
	Milipore water	up to volume

Table 10: Buffer for Cloning and DNA analysis

1x TAE Buffer	Tris-Acetate	40 mM
	EDTA	2 mM
Loading Dye	Orange G	7.5% (w/v)
	Glycerol	50% (v/v)
	50 x TAE	30% (v/v)
	Milipore water	fill up to volume
TE Buffer	Tris-HCl pH 7.5	10 mM
	EDTA	1 mM
	Milipore water	fil up to volume
SLiCE Buffer	Tris-HCl pH 7.5	0.5 mM
	MgCl2	0.1 mM
	ATP	0.01 mM
	DTT	0.01 mM

Table 11: Buffer for Y2H assay

YPD media	Yeast extract	1%
	Peptone	2%
	Glucose	2%
	Agar for plates	2%
YPDA media	Yeast extract	1%
	Peptone	2%
	Glucose	2%
	Agar for plates	2%
	Adenine hemisulfate	0.004%
Yeast SD-Leu-Trp	Yeast without AS	0.67%
	Dropout -Leu -Trp-His	0.062%
	Histdin	0.020%
	Agar	2%
	Milipore water	up to volume

	adjust pH to 5.8 with NaOH	
40% PEG	50% PEG	6.4 ml
	10x LiAc	0.8 ml
	10 x TE	0.8 ml

Table 12: Buffer for Protein analysis

Protein extraction Buffer	Tris-HCl pH 7.5	50 mM
	NaCl	150 mM
	EDTA	2 mM
	Glycerol	10%
	Triton X-100	1%
	Complete Mini Protease Inhibitor Cocktail	10 µl/ml
Protein Wash Buffer	Tris-HCl pH 7.5	50 mM
	NaCl	150 mM
	Glycerol	10%
	EDTA	2 mM
5x SDS-Laemmli sample Buffer	Tris-HCl pH 6.8	60 mM
	SDS	2%
	Glycerol	10%
	beta-mercaptoethanol	5%
	Bromophenol blue	0.01%
1x SDS-PAGE running Buffer	Tris	25 mM
	Glycine	192 mM
	SDS	0.1%
Anoden Buffer I	Tris	300 mM
	Methanol	20% (v/v)
	Milipore water	up to volume
	pH 10.4 (adjusted with KOH)	
Anoden Buffer II	Tris	25 mM
	Methanol	20% (v/v)
	Milipore water	up to volume
	pH 10.4 (adjusted with KOH)	
Cathode Buffer	Tris	25 mM
	Methanol	20% (v/v)
	6-aminocapropic acid	40 mM
TBS-T	Tris-Hcl pH 7.5	50 mM
	NaCl	150 mM
	Tween-20	0.1% (v/v)
WB blocking solution	Tris-Hcl pH 7.5	50 mM
	NaCl	150 mM
	Tween-20	0.1% (v/v)
	non fat milk pwder	20% (v/v)

6.2 Appendix Bacteria strains:

Table 13: Bacteria Strains

E. coli TOP10	Thermo Fisher Scientific (CAT #C404010)
E. coli DH5α	Thermo Fisher Scientific (CAT #18265017)
A. tumefaciens GV3101 PMP90	DNA Cloning Service
S. cerevisiae AH109	Clontech (CAT #K1612-1)

6.3 Appendix Constructs:

Table 14: Empty vectors

pDONR221	Dr. Shinichiro Komaki
pDONR-P4P1r	Dr. Shinichiro Komaki
pENTR	Dr. Shinichiro Komaki
pENTR2B	Dr. Shinichiro Komaki
pGWB501	Dr. Shinichiro Komaki
pGWB601	Dr. Shinichiro Komaki
pK7GWIWG2	VIB gent
pGADT7	Clontech (CAT #630442)
pGBKT7	Clontech (CAT #630489)

Table 15: Plant expression constructs

pGWB501 Pro_{REC8}:REC8:GFP	Pursicki et al.
pGWB501 Pro_{REC8}:REC8:RFP	Dr. Shinichiro Komaki
pGWB501 Pro_{REC8}:REC8-7P:GFP	In this thesis
pGWB501 Pro_{REC8}:REC8-S224A:GFP	Masterthesis with Dr. Shinichiro Komaki
pGWB501 Pro_{REC8}:REC8-S239A:GFP	Masterthesis with Dr. Shinichiro Komaki
pGWB501 Pro_{REC8}:REC8-S377A:GFP	In this thesis
pGWB501 Pro_{REC8}:REC8-S406A:GFP	In this thesis
pGWB501Pro_{REC8}:REC8-T446A:GFP	In this thesis
pGWB501 Pro_{REC8}:REC8-T460A:GFP	In this thesis
pGWB501 Pro_{REC8}:REC8-T561A:GFP	In this thesis
pGWB501 Pro_{SMC1}:SMC1:GFP	Masterthesis with Dr. Shinichiro Komaki
pGWB501 Pro_{SMC1}:SMC1:mTurqoise	Masterthesis with Dr. Shinichiro Komaki
pGWB501 Pro_{RPS5}:RFP:TUA5	Dr. Shinichiro Komaki
pGWB501 $Pro_{RAD21.1}$:RAD21.1:GFP	Masterthesis with Dr. Shinichiro Komaki
pGWB501 $Pro_{RAD21.2}$:RAD21.2:GFP	Masterthesis with Dr. Shinichiro Komaki
pGWB501 $Pro_{RAD21.3}$:RAD21.3:GFP	Masterthesis with Dr. Shinichiro Komaki
pGWB501 $Pro_{RAD21.2}$:GFP:RAD21.2	In this thesis
pGWB501 ProASK1:GFP:RAD21.2	In this thesis
pGWB501 Pro_{CENH3}:CENH3:RFP	Dr. Shinichiro Komaki
pGWB504 Pro_{PCNA1}:PCNA1:RFP	Yokoyama et al., 2016

pAlli $Pro_{H2A.W.6}$:H2A.W.6:RFP	Yelagandula et al., 2014
pGWB501 Pro_{FIB2}:FIB2:mTurqoise	In this thesis
pGWB601 Pro_{ASY1}:ASY1:RFP_Pro_{HTR5}:MBD6:GFP	Frederike Schäfer; Ingouff et al. 2017
pGWB601 Pro_{REC8}:REC8:RFP_Pro_{HTR5}:MBD6:GFP	Frederike Schäfer; Ingouff et al. 2017
pGWB601 Pro_{FIB2}:FIB2:mTurq_Pro_{HTR5}:MBD6:RFP	In this thesis
pK7GWIWG2 Pro_{35S}:RAD21.2-RNAi	In this thesis

Table 16: Yeast vectors

pGBKT7 SMC1	Dr. Chao Yang
pGBKT7 SCC3	Dr. Chao Yang
pGBKT7 REC8	Dr. Chao Yang
pGBKT7 ASY1	Dr. Chao Yang
pGBKT7 ASY1 1-300	Dr. Chao Yang
pGBKT7 ASY1 309-596	Dr. Chao Yang
pGBKT7 ASY4	Dr. Chao Yang
pGBKT7 SPO11-1	Dr. Chao Yang
pGBKT7 SPO11-2	In this study
pGBKT7 MTOPIV	In this study
pGADT7 RAD21.2	In this study
pGADT7 REC8	In this study
pGADT7 ASY3	Dr. Chao Yang

6.4 Appendix Primer lists:

Table 17: Primer used for genotyping

rad21.1	SALK_044851-LP SALK_044851-RP	TGTGGTTGCCCAGTTTTTAAG CTGAAGAAGCATCCGTCAGAG
rad21.2	SALKseq_053140.1-LP SALKseq_053140.1-RP	CCTTGCTCTCCCTGTCAAAG GCTGGTTCTGAGGAAGAACG
rad21.2 w.construct	SALKseq_053140.1-LP/gRAD21.2 construct SALKseq_053140.1-RP/gRAD21.2 construct	GTGAAAGGCTTAAGGATCCTAGTGATAC CATGAAAGAAACTCGCTCGATCGATG
rad21.3	SALK_076116C-LP SALK_076116C-RP	AAGCTCACCCAAATGATTGTG CATCGGGAATAGCACTAGCAG
rec8	SAIL_807_B08-LP SAIL_807_B08-RP	CTCATATTCACGGTGCTCCC GGGGGAAAAGAGAAAGGTTC
wapl1	SALK_076791 LP SALK_076791 RP	TCCAATTTACTGAAACGTGGG ACACACTTGATTGAGAACCCG
wapl2	SALK_127445 LP SALK_127445 RP	TCCAGCAAAACAGACAGGAAG CTCAAATCTGCGAACGAAGAG
smc1;ttn8-1	ttn8-1-LP ttn8-1-RP	TCGGAGGAGTATGAGAAGGAAATC CTTGTCAATGTTGCTAGCAATGTG

Table 18: Primer used for generating fluorescene reporters and *RNAi* construct

REC8 Phosphomutants	S377A-fw	GCTCCAGGGTTTGTTCAGGAGAG
	S377 rev	TTGTTCCGCACGGAGATC
	S406A-fw	GCTCCCGCAGAAATACTCCGG
	S406 rev	ATCAAGATTTTGGGAGCTTGTG
	T446A-fw	GCTCCATTCTATTCTGGTTAAAAGC
	T446 rev	GACATTAATATCAGCAGCCTG
	T460A-fw	GCTCCATCCGCACGTGGAGCAGCTTCAATTAAC
	T460 rev	ACTAGGCATGGATCTCACATCATC
	S489A-fw	GCTCCAAGAAGAGGACTCGAACC
	S489 rev	GGAATTTGGTCTTTTTCTATTGGG
	S489A-fw	GCTCCAAGAAGAGGACTCGAACC
	S489 rev	GGAATTTGGTCTTTTTCTATTGGG
RAD21.1 reporter	gRAD21.1-F	gtcttcgaaagagaaaagtgtgtagagg
	gRAD21.1-R	tataccgcgggttaaaatctagtcctac
	pENTR2B-F for RAD21.1-F	ggactagattttaacccgcggtataGCGGCCGCACTCGAGA TATCTAGA
	pENTR2B-R for RAD21.1-R	Ctacacacttttctctttcgaagac GGATCCAGTCGACTGAATTGGTTC
	CterSmaI-gRAD21.1-F	GGGTGAaaaatggatattttcttcacttaag
	CterSmaI-gRAD21.1-R	GGGACAAGCTTTTTGTGGTCTGGAAACA
RAD21.1 reporter	gRAD21.2-F	GGAGGAAGAGACTGCTTCAACTTATCGG
	gRAD21.2-R	GAGTGAGAAGATGCATACGCACAGCCAT
	pENTR2B-F for RAD21.2-F	GCTGTGCGTATGCATCTTCTCACTCGCGGCCGCA CTCGAGATATCTAGA
	pENTR2B-R for RAD21.2-R	ATAAGTTGAAGCAGTCTCTTCCTCCGGATCCAGT CGACTGAATTGGTTC
	CterSmaI-gRAD21.2-F	GGGTGAataaacaatgcttaataaacttac
	CterSmaI-gRAD21.2-R	GGGCGTTTGAACCTTAGAAAAAAGGGCAG
	NterSmaI-gRAD21.2-F	GGGATGTTTTATTCACATACGCTTTTGGC
	NterSmaI-gRAD21.2-R	GGGtttaattccttcgaacaaggagc
ASK1:RAD21.2 reporter	SLiCE-ASK1promoter-F	CTCACCATGCCACCCCCGGGgttatggaaacgaagag agaag
	SLiCE-ASK1promoter-F	CAATTCAGTCGACTGGATCCagcaaagaatcaaacaaa ac
	SLiCE-RAD21.2promoter-F	ctcttcgtttccataaccCCCGGGGGGTGGCATGGTGAGCA AG
	SLiCE-RAD21.2promoter-R	gtttgattctttgctGGATCCAGTCGACTGAATTG
RAD21.3 reporter	gRAD21.3-F	AAGGTCGAGCAAAAGTTGCTTGGATGGG
	gRAD21.3-R	tgtgtcagtcattgtcctctgtgaattc
	pENTR2B-F for RAD21.3-F	ttcacagaggacaatgactgacacaGCGGCCGCACTCGAG ATATCTAGA
	pENTR2B-R for RAD21.3-R	ATCCAAGCAACTTTTGCTCGACCTTGGATCCAGT CGACTGAATTGGTTC
	CterNaeI-gRAD21.3-F	GGCTAGatggagaagatcagtcatatag
	CterNaeI-gRAD21.3-R	GGCGAAGATGGATTTGGTGAGCTTTGGT
FIB2 reporter	gFIB2-F	CCAACATCCCACATGCACACTTCCCTCTC
	gFIB2-R	GTGGAGGAGACGATGGAACGTATGAAG
	pENTR2B-F for FIB2-F	ATCGTCTCCTCCACGCGGCCGCACTCGAGATATC TAG
	pENTR2B-F for FIB2-R	GTGGGATGTTGGGGATCCAGTCGACTGAATTGG TTC

	CterSmaI-gFlB2-F	GGGAGCAGCAGTAGCAGCCTTTGGCTTC
	CterSmaI-gFlB2-R	GGGTAGAAGTTTTCTACTCTACGCTCTTCCCAGTACC
RAD21.2 *RNAi*	attB1-RAD21.2_2-F	AAAAAGCAGGCTCCACCATTGAGAACGTCAAGTCAC
	attB2-RAD21.2_2-R	AGAAAGCTGGGTCCTCCGGTATGCCTACTCACAGG
	attB1-F	GGGGACAAGTTTGTACAAAAAAGCAGGCT
	attB2-R	GGGGACCACTTTGTACAAGAAAGCTGGGT

Table 19: Primer used for Y2H contructs

RAD21.2	RAD21.2-NcoI-F	GGAATTCCATATGATGTTTTATTCACATACGCTTTTGG
	RAD21.2-NcoI-R	CATGCCATGGTCACGTTTGAACCTTAGAAAAAAGG
REC8	attB1-REC8-F	CAAAAAAGCAGGCTCCACCATGTTGAGACTGGAGAG
	attB1-REC8-R	CAAGAAAGCTGGGTTCATGTTGGGTCCTCTTGC

Table 20: Primer for sequencing analysis

REC8	AT5G05490-seq1F	ATCTAACCAGAGGTGCAAATTAGC
	AT5G05490-seq2F	CGTAGAAGATGAGGGTGACATTGA
	AT5G05490-seq3F	AGTGTGAAGAAGAACTTAACGGCG
	AT5G05490-seq4F	ACTCAGATTCAGCTTCTTCTCCAC
	AT5G05490-seq5F	GGTGTTCCTGCCATGAAAACGAAC
	AT5G05490-seq6F	TCTGTTCCGGATCCCACTTTACTA
	AT5G05490-seq7F	AGCATGTGGTTTATGAGTAGCCTC
	AT5G05490-seq8F	CAATCCCACTATCTATCTTCAGTC
	AT5G05490-seq9F	TTAGCCATCTGCAGGAGTCAACCC
	AT5G05490-seq10F	CTTCAAACCTCATCATCTGGTCTC
	AT5G05490-seq10.2F	tggatttatgcagCATGAGCGCAG
	AT5G05490-seq11F	CAGGAGATGATGTGAGATCCATGC
	AT5G05490-seq12F	CAGTCACCTGAAGACACACTTTGA
	REC8-GFP-fw	TCGCGGAGTCATCAAGGTAAAC
	REC8-GFP-rev	gaaatcaaaccTTACCCGGGTC
RAD21.1	gRAD21.1-seqF1	aagaatattaacgaccagtttggg
	gRAD21.1-seqF2	ccattcgcaacgtaatgccacgtc
	gRAD21.1-seqF3	gaaggtgtgattttctggtcaccg
	gRAD21.1-seqF4	gagtgaaactttgcagctttagtg
	gRAD21.1-seqF5	AAAGGAACAGAGAAAAGACAGGTG
	gRAD21.1-seqF6	GTTATGAAGGAAATGATAGAGGAC
	gRAD21.1-seqF7	tgtaggtctcatgagtgctcaggc
RAD21.2	gRAD21.2 F1	TCCTAGTCGTGAGAACAGATAATC
	gRAD21.2 F2	GTATCTCCATCTCTGCTTCTTTAG
	gRAD21.2 F3	AGTCTGTTACTTTGCCTCAAGCAC
	gRAD21.2 F4	AACAGAACCTGTGAGTAGGCATAC
	gRAD21.2 F5	TGTAGCAACAGAAGCACAATCTCC
	gRAD21.2 F6	GAGCGAGATCTTGGCAGGAAAGAC

RAD21.3	gRAD21.3-seqF1	tttatttaggtcagtggccattgc
	gRAD21.3-seqF2	GGATCGGAGAGATGCACAGAAATG
	gRAD21.3-seqF3	gtttttgtgtgacaccatcacatg
	gRAD21.3-seqF4	ctgagaattagggtttccgcgagg
	gRAD21.3-seqF5	gttatgtggctaaacaagttcatc
	gRAD21.3-seqF6	cgctacttcagattgttatcatag
	gRAD21.3-seqF7	atgtacattgcagttacagactcc
	gRAD21.3-seqF8	ttgctctttgagctagctttatgg
	gRAD21.3-seqF9	CGTGCGAAAGAAGGCACCTTGCAC
	gRAD21.3-seqF10	actctggtcatcatatcctggttc
FIB2	gFIB2 F1	CCAACATCCCACATGCACAC
	gFIB2 F2	CCACATATTTAGCAGCCCAG
	gFIB2 F3	AGCCGCCTCTTCTCTTTTCT
	gFIB2 F4	GAAGATGCCCTTGTTACCAAG
	gFIB2 F5	GATCTGATAGGAGGGGTGTG
	gFIB2 F6	CATTCAGCTTGTGGGTTGCT
	gFIB2 F7	TGTTCACTTGGCTTCCAGCG
General primers	M13_FW	GTAAAACGACGGCCAG
	M13_RV	CAGGAAACAGCTATGAC
	GFP_300F	GAAGGGCATCGACTTCAAGG
	GFP_300R	TTGAAGTCGATGCCCTTCAG

Table 21: Primer used for quantitative analysis (qPCR)

18S	18S-F	CGGCTACCACATCCAAGGAA
	18S-R	GCTGGAATTACCGCGGCT
HXK1	HXK1-F	AGGAGCTCGTCTCTCTGCTG
	HXK1-R	GCTCAAACAATCCACCATCC
UEV1C	UEV1C-F	GGTGACTGAAATGTGAATTTGC
	UEV1C-R	ATGCAGCCATCTCCTTCTTC

Table 22: Primer used for expression analysis by qRT-PCR

RAD21.2	qRT-RAD21.2-F	GGATGTCGACCAATCAACAGAACC
	qRT-RAD21.2-R	CTGTGACGTTACGAGGACTATAG
FTSH7	FTSH7-F	GGCTTGGTGCTCAACTTGAAGAG
	FTSH7-R	TGGTGCAACCACCATGCTTAAC
COX11	AT1G02410 qRT-F	ATCTGGTACCGTCACTGAAAGGG
	AT1G02410 qRT-R	TGCATCCCATCTGCAACATCAGC
AT2G41960	AT2G41960 qRT-F	TTTGGTCTGAGGACGACGATG
	AT2G41960 qRT-R	ACAGCTCACTCCAGAACTGGTC

6.5 Appendix PCR reactions and programs:

Table 23: PCR programs

plasmid construction	PrimeSTAR Max Premix	25 µl
	Primer FW (100 mM)	1.5 µl
	Primer REV (100 mM)	1.5 µl
	Nuclease Free Water	21 µl

Genotyping (8 reactions)	Dreamtaq Green or TerraRed Polymerase MM	50 µl
	Primer FW (100 mM)	3 µl
	Primer REV (100 mM)	3 µl
	Nuclease Free Water	44 µl

Genotyping PCR program (Dreamtaq green):

5 min	95 °C Initial denaturation	
30 s	95 °C Denaturation	x 35 cycles
30 s	Annealing temperature; dependent on primer	
1 min/kb	72 °C Elongation	
5 min	72 °C Final Extension	

Genotyping PCR program (TerraRed)

2 min	98 °C Initial denaturation	
10 s	98 °C Denaturation	x 35 cycles
15 s	60°C Annealing temperature	
1 min/kb	68 °C Elongation	
5 min	72 °C Final Extension	

Plasmid construction PCR:

30 s	98 °C Initial denaturation	
10 s	98 °C Denaturation	x 30 cycles
5 s	Annealing temperature; dependent on primer	
5 s/kb	72 °C Elongation	
2 min	72 °C Final Extension	

qRT-PCR:

5 min	95 °C Pre-Incubation	
10 s	95 °C Denaturation	x 45 cycles
5 s	58 °C Annealing	
10 s	72 °C Elongation	

qPCR:

7 min	95 °C Pre-Incubation	
30 s	95 °C Denaturation	⎫
30 s	56 °C Annealing	⎬ x 40 cycles
30 s	72 °C Elongation	⎭

7. Eidesstattliche Versicherung/ Declaration On Oath

Hiermit erkläre ich an Eides statt, dass ich die vorliegende Dissertationsschrift selbst verfasst und keine anderen als die angegebenen Quellen und Hilfsmittel benutzt habe.

I hereby declare, on oath, that I have written the present dissertation by my own and have not used other than the acknowledged resources and aids.

Hamburg, den 19.05.2021 **Unterschrift**

8. Confirmation of correct English

EMMA BANCK

embanck@gmail.com
0163 90 23 425
Keplerstraße 32, Hamburg

May 18, 2021

To whom it may concern,

I am writing to confirm that the thesis submitted by Viola Kuttig has been written in correct English throughout the full text.

Warm Regards,

Emma Banck

9. Acknowledgements

First I would like to thank Prof. Arp Schnittger. I am deeply impressed by your passion for science and your knowledge. Thank you for the guidance and the support in my scientific career but also in personal life circumstances. I really appreciate that you gave me the opportunity to join Monicas lab in Madrid. This was such a great experience that led me develop myself further.

I would like to thank Prof. Stefan Hoth to kindly agree to be my second supervisor and to examine my final dissertation.

I like to say thanks to Dr. Peter Schlögelhofer and Dr. Jason Sims for their contribution to shed further insights in the functions of RAD21.2. I am very happy for sharing your knowledge and passion with me.

Thanks to Dr. Maren Heese for proofreading my thesis and beeing tortured by my mistakes. This thesis would not exists in this form without your help. Furthermore, I am very thankful for your will to discuss and giving opinions during the last five years.

I further acknowledge Emma Banck, who kindly proofread this thesis.

I would like to acknowledge all the present and past Schnittger group members. Keep your open-minded and supportive team spirit!
Special thanks to Joke, who is an important person to me in the lab. I really appreciate your support with reading this thesis and your daily emotinal support. I hope we keep our „Joke friday walks“ since Polly and I really enjoy our frisbee times.
I would like to thank Kosti, Yuki, Marti, Maria and Poyu for everyday life support, fun experiences and scientific support. Special thanks to Yuki, I really appreciate your microscopic support but I will never forget our trip to London. I am looking forward to more trips like this.

Shini, Chao and Max, I would like to thank for many fruitful discussions and guidance throughout this thesis.
I will be always thankful for having Maren Röper in the Schnittger group since she supported me in my hardest time with advices going beyond her duties.
Thanks to Katja, Dagmar, Jantje, Dave and Jara for having the best lunch breaks, sharing jokes, emotions and sheering me up. Especially, Katja was a great support during hard times in the lab and in private. Also Rheinhold was also part of the lunch breaks but he also need to be mentioned as the person who brought me to work in the Schnittger group. Through all the past years he was also a mentor in my scientific life. Thank you for that!

Without my friends and family it would have never been possible to finish this thesis. I am so happy to have you all in my life since you always supported and encouraged me. A special thanks to my sisters Ulrike and Wiebke, who never hesitated to let me know about her opinions and helped me to continue when I was stucked and frustrated.

Last but not least I would like to thank the most important person in my life, Alexander. You thought me to see the things from a different perspective and helped me to fight against setbacks. Thank you for all the support and love over the past years. I am so much looking forward to spend my life with you and Polly.

I would like to dedicate my thesis to my mother who made me to the person I am. I know you will be always by my side, believing in me no matter where you are.